2020

# Bias and Sensitivity of Nonlinear Models for Seismic Response of Ordinary Standard Bridges

Andres Rodriguez Caballero
*University of Central Florida*

University of Central Florida

STARS
Showcase of Text, Archives, Research & Scholarship

BIAS AND SENSITIVITY OF NONLINEAR MODELS FOR SEISMIC RESPONSE OF
ORDINARY STANDARD BRIDGES.

by

ANDRES F. RODRIGUEZ
B.S. Universidad del Norte, 2004

A thesis submitted in partial fulfilment of the requirements
for the degree of Master of Science
in the Department of Civil, Environmental, and Construction Engineering
in the College of Engineering and Computer Science
at the University of Central Florida
Orlando, Florida

Fall Term
2020

Major Professor: Kevin Mackie

# ABSTRACT

The implementation of nonlinear structural analysis under large deformation demands has enabled more realistic response prediction in comparison with the classical linear approaches. However, the sensitivity to modeling assumptions, element and material formulations, implementations, and parameter selection may lead to unreliable results. While previous works have led to a better understanding of how to best model nonlinear static responses of bridge components and systems, the introduction of dynamic loads and the corresponding material hysteresis presents an additional source of variability in the nonlinear responses. The current research involves the analysis of two ordinary standard bridges in California under seismic load in SAP2000 and OpenSees after a calibration phase to standardize the material, section, and element-level nonlinear static responses. The bridges were defined using simplified steel and concrete constitutive models in concentrated plasticity elements, with common unloading-reloading rules, damping, and mass. Analyses showed that minor differences in the material constitutive models did not impact agreement of drift, base shear, and curvature time histories. The column hinge and abutment nonlinear characterization clearly dominated the dynamic response variability of the bridge models. The bias analysis of the nonlinear model concluded that both software agreed after improving the hinge length and the inclusion of gaps in the abutments. The same SAP2000 models were used to analyze the sensitivity of the most representative nonlinear parameters in the columns, superstructure, and abutments, as well as sensitivity to the hysteresis behavior of the concrete and the reinforcement steel. The prediction of the sensitivity was obtained applying the finite difference method, perturbing each parameter forward and backward by a coefficient of variation. The results obtained indicate that the selected bridges have a strong sensitivity in the longitudinal direction to the hysteretic assumptions and to small variations in parameters such as steel yield strength, superstructure Young's modulus, and abutment strength, while the displacement response in the transversal direction seems to be insensitive.

# ACKNOWLEDGMENTS

# TABLE OF CONTENTS

# LIST OF FIGURES

# LIST OF TABLES

# CHAPTER 1: INTRODUCTION

Poor seismic performance of older bridges is often attributable to the design philosophy at the time of construction. Numerous historical events have led to improvements in design criteria and evolution of codes and guidelines. In the United States, many design philosophy changes occurred after damage during the 1971 San Fernando earthquake where, for example, the Newhall Pass interchange collapsed (Fung et al., 1971). The 1989 Loma Prieta earthquake caused nearly $6.5 billion damage in bridge structures, including the signature 50 ft span of San Francisco - Oakland bridge and more than a mile of elevated road way on I-880 (EERI, 1989). Two bridges retrofitted after 1971 San Fernando collapsed and 39 highway bridges experienced structural damage in the 1994 Northridge earthquake. The most important collapses occurred in the Gavin Canyon Bridge and an elevated portion of the Los Angeles I-10 (Bolin & Stanford, 2006).

After the Hyogoken-Nanbu (Kobe) 1995 earthquake in Japan, several lessons were learned about shear detailing and longitudinal bar continuity. Design criteria and assumptions about recorded seismic coefficients were improved, particularly given the similarity between several Japanese and central-southeastern US bridges (steel girders and concrete columns) (NIST, 1996, pp. 163-191). Recent earthquakes such as Maule (Chile) in 2010 illustrated performance of retrofits for foundation bearing capacity, anchors and stopper mechanisms at bearings, seat support length and the strength of the prestressed concrete girder (Kawashima et al., 2011). As a result, important changes were incorporated into the bridge design criteria, such as reductions to overpass skew, increases in seat width, the use of multi-rotational instead of rocker-type bearings, distance to hinges from columns, the use of spiral reinforcement to confine the longitudinal rebars, and the increase of reinforcement in the column-deck connection (Khan, 2015).

While bridges are often treated as simple structural systems for analysis and design, complex responses may occur in the two primary load paths (bents and abutments) under large seismic loads. In addition, the structural simplicity that they possess seems to generate a greater sensitivity

to errors during design and construction process (Priestly et al., 1996). The implementation of nonlinear methods in the analysis of bridges exposed to dynamic loads has provided more accurate response in comparison with the traditional linear approaches. A summary of common element formulations and implementations in nonlinear static analysis of typical reinforced concrete bridges was recently reported by Mackie and Scott (2019). Beyond standard concentrated and distributed plasticity approaches for columns, recommendations were made on making sure response differences were due to the formulation and not the software-specific implementation - two items that are commonly confused.

The study further develops previous models of two Caltrans ordinary bridges evaluating different kinds of responses, such as nonlinear time history analysis and moment-rotation column reactions, when seismic loads are applied (Mackie et al., 2017), and the sensitivity of the nonlinear time history response after a slightly perturbation of the basic nonlinear constitutive materials and the hysteresis behavior. The calibration of the nonlinear static responses of the constitutive models for abutments and columns between two different software (SAP2000 and OpenSees) was an important step to reduce sources of uncertainty when comparing dynamic responses. A simple boundary condition, which consisted of a roller abutment at the end of the superstructure, was used to concentrate nonlinear response in the columns. After obtaining an adequate agreement in the column nonlinear behavior, the abutment impact on hysteresis was studied by replacing the roller abutment with an abutment model comprised of gap-link elements. The numerical models presented in the current study are based on SAP2000 (version 21.0.2 Build 1491) and OpenSees (version 2.6.4), employing the same finite element formulations for the column and abutment nonlinearities to better identify the sources of discrepancies in the responses.

## 1.1 Background

Nonlinear time history studies on bridges have been evolving alongside the nonlinear analysis tools. Modeling of bridge collapse mechanisms and retrofit for bridges after the 1994 Northridge used DRAIN-3DX (Fenves & Ellery, 1998). A bridge in the Egnatia motorway in northern Greece was seismically analyzed to study the responses using Ruaumoko 3D for nonlinear analysis (Kappos & Dimitrakopoulos, 2005). Follow up studies on other as-built structures were conducted as nonlinear analysis tools for bridges matured in OpenSees (Kunnath, 2007) that started to identify component vulnerabilities through nonlinear dynamic modeling (Nielson & DesRoches, 2007). Explicit soil-structure-interaction modeling was included in bridge models of the Humboldt Bay bridge by Zhang, et al. (2004) and the I-880 viaduct (Jeremić et al., 2004), concluding that the SSI effects can be detrimental depending on the seismic loading. The link between nonlinear behavior in bridges after seismic events and damage and decision making in a performance-based context was conducted by Mackie and Stojadinovic (2003). A seismic analysis of the Meloland road overcrossing was conducted using a multiplatform approach that analyzed the structural model of the bridge built in Zeus-NL and the soil-structure interaction modeled in OpenSees (Kwon & Elnashai, 2008).

The link between nonlinear behavior in concrete bridges after seismic events and damage and decision making in a performance-based context was conducted by (Mackie, 2008) and (Nielson & DesRoches, 2007), amongst others. Although many studies followed on the seismic performance of typical concrete bridges that included distributions of parameters and the corresponding component/system fragilities, few formal model sensitivity studies have been conducted the impact of modeling parameters on seismic response prediction. However, recent studies have established guidelines for modeling the nonlinear time history response of ordinary standard bridges and investigated variability of peak responses to modeling parameters and software implementations. In addition, recommendations for modeling were made in different commercially or freely available

software that aimed to eliminate or quantify differences that arose from software implementations (Aviram et al., 2008; Mackie & Scott, 2019).

### 1.1.1   *Previous Research on Bridges*

The recent guidelines all investigated the role of boundary conditions on the time history responses, specifically the different assumptions for abutment models. While some studies based their analyses on the nonlinear behavior of gap-link abutments (Omrani et al., 2015), others implemented models to establish practical recommendations for the nonlinear analysis in commercial software like SAP2000 and OpenSees (Aviram et al., 2008). Mackie, et al. (2017) studied the nonlinear time history analysis (NTHA) of Caltrans bridges by separating the effects of the abutment assumptions and a simplified roller condition using OpenSees and CSiBridge software.

Realistic seismic response prediction of bridges requires the use of nonlinear analysis methods (Pinto & Franchin, 2010), which can be divided into static (using a pushover load pattern) and dynamic (hysteresis response under acceleration input) analysis. However, the degree of complexity inherent in the nonlinear models increases the computational effort necessary for the analyses, as well the difficulty in the interpretation of the results. In addition, the large number of parameters, choice of numerical methods, software implementations, and element or material formulations involved in a nonlinear analysis lead to potentially larger uncertainty in the responses. While past work has shown that nonlinear static responses can be standardized between software implementations if consistent modeling choices are made (Mackie & Scott, 2019), the causes of nonlinear dynamic response bias have not previously been isolated as due to formulation or implementation (Aviram et al., 2008).

### 1.1.2   *Bridge sensitivity analysis*

A rational method to evaluate the damages and losses in highway bridges was developed by Mackie and Stojadinovic (2005). The bridge fragilities obtained help future designers to predict

4

the amount of losses in bridges after a seismic event, based on the bridge parameters sensitivity. A finite element response sensitivity analysis was conducted by Zona, Barbato, and Conte (2006) to study the importance and the effects of different material parameters, using the direct differentiation method and forward finite difference method. Several investigations such as Pan et al. (2010) and Sullivan and Nielson (2010) have been focused to analyze the sensitivity on steel structure bridges. On the other hand, some authors addressed the sensitivity analysis in different way. This is the case of Zhao, Vasheghani-Farahani and Burdette (2011), who analyzed the sensitivity response of the bridges considering the soil-structure interaction under different backfilling conditions at the abutments and Ghotbi (2014), who studied the fragility curves sensitivity of skewed bridges under seismic loads with different types of soils. A reliable computational tool is very important to reduce time and errors during a sensitivity analysis. Thus, some studies like Haukaas and Der Kiureghian (2007) were conducted to obtain a freely library of software codes for OpenSees to analysis the response sensibility of the bridge structures.

The approach method to be used to predict the sensitivity of bridges will vary depending on the conditions, computational tool capacity, and the objective of the analysis. Therefore, several authors like Kleiber (1997) and Jurado et al (2011) dedicated their researches to explore the best method to obtain an optimal design. Regarding to the sensitivity analysis of bridges nonlinear finite element models, the most used approaches involve different theories such as the finite difference method, direct differentiation method, complex perturbation method, and the adjoint structure method. The finite difference method represents the simplest way to analyze the sensitivity in bridges under seismic loads, where after obtaining a mean response, the analysis is repeated perturbing the parameters object to study. The sensitivity is obtained by a simple differentiation between the original and the modified values response. Even though is a very simplistic method, it involves a huge computational effort and some errors could be induced due to round-off and effect of perturbation size on the nonlinear system. A more accurate result can be obtained using the direct differentiation method, which uses analytical differentiation based on the equations that

5

govern the finite element responses and the constitutive responses of the elements involved in the bridge model. On the other hand, the sensitivity analysis could be performed using the complex perturbation method by computing the responses using a complex algebra and reanalyzing each parameter in the finite element model (Mackie et al., 2017). Finally, the adjoint structure method is very useful to obtain the sensitivity response on bridges, but without a correct application in situations that involve path-dependent conditions the direct differentiation method appears to be usually more accurate (Kleiber et al., 1997).

### 1.1.3   Approximation methods in sensitivity analysis

There are a variety of theories or methods which could predict with a reasonable accurate the sensitivity of the bridge to changes in the main parameters that conform the model. The method to be chosen usually will depend on the objective of the analysis and the capacity of the computational tool. The most common approaches to establish the sensitivity for nonlinear finite element models include the finite difference method (FDM), the direct differentiation method (DDM), complex perturbation method (CPM), and adjoint structure method (ASM). Because the computational tools to be used in the current research only require the FDM and DDM to achieve the research objectives, the other methods will not be described.

#### 1.1.3.1   Finite difference method (FDM)

The FDM probably represents the simplest technique to estimate the bridge sensitivity. In the method, it is necessary to obtain the value u(x) as the original response without perturbation and then repeat the entire calculation for a perturbed value x+$\Delta$x to obtain u(x+$\Delta$x). Therefore, the first-order forward-difference approximation $\Delta$u/$\Delta$x to the derivative $du/dx$ can be expressed as

$$\Delta u/\Delta x = (u(x + \Delta x) - u(x))/\Delta x \tag{1.1}$$

where $du/dx = \Delta u/\Delta x + 0(\Delta x)$, and considering $0(\Delta x)$ as the truncation error of the approximation Kleiber et al., 1997. If the calculation is done perturbing backward the value x-$\Delta$x to obtain $u(x - \Delta x)$, the second-order central difference approximation can be obtained as

$$\Delta u/\Delta x = (u(x + \Delta x) - u(x - \Delta x))/2\Delta x + \mathcal{O}(\Delta x^2) \tag{1.2}$$

The same analysis can be done employing higher order approximations, but the increase in the computation effort could drastically reduce the efficiency of this technique (Kleiber et al., 1997). The simplicity of the method involves a few errors. The truncation error is the most common, which is produced by ignoring terms in the Taylor series and its value increases when $\Delta x$ is considerably high. On the other hand, the condition (numerical round-off) error corresponds to the difference between the exact value and the numerical evaluation of the function, which tends to be high for extremely small $\Delta x$ values (Kleiber et al., 1997). Therefore, selecting the correct $\Delta x$ for the calculation will conclude into an acceptable error for the sensitivity analysis.

### 1.1.3.2 Direct differentiation method (DDM)

The DDM is a technique that covers almost all the situation in the bridge sensitivity analysis. The method obtains the bridge sensitivity directly from the finite element response using both semi-analytical and analytical differentiation of the discretized equations that rule the original behavior of the finite elements, including the constitutive performance of them on the model response (Mackie et al., 2017). The DDM general definition can be expressed as the following equation, where the NxN stiffness matrix is represented by $K$, $N$ is the number of independent degrees of freedom, the external load vector is $Q$, and $q$ corresponds to the vector nodal displacement (Kleiber et al., 1997).

$$K(dq/dh) = (dQ/dh) - (dK/dh)q \tag{1.3}$$

This simple expression of the DDM is used to estimate the sensitivity on static linear cases and can be easily adapted to be used in a variety different cases such as nonlinear quasi-static problems, inelastic systems, and nonlinear dynamic, and others situation (Kleiber et al., 1997). The method computes the sensitivity for all the parameters while the deterministic analysis is performed achieved by considering the load vectors substituted forward and backward with the corresponding factorized dynamic tangent stiffness matrix in each calculation, contrasting with the FDM which requires to calculate the responses again after perturbing the parameters. The described process concludes in a perturbed response in the same order of accuracy than the mean response (Mackie et al., 2017), removing the condition error due to round-off and the loose of high orders terms.

## 1.2   Research Objectives

The study further wants to analyze the behavior of two Caltrans bridges under static and dynamic loads, by evaluating different kinds of responses, such as nonlinear time history analysis and moment-rotation column reactions, when seismic loads are applied, and the sensitivity of the nonlinear time history response after a slightly perturbation of the basic nonlinear constitutive materials and the hysteresis behavior. Additionally, the research will study the different hysteretic behavior and their impact in the nonlinear time history response on single degree of freedom systems. The research should achieve this objective by completing the following tasks:

- Developing and analysis of benchmark columns concrete constitutive models.

- Time history analysis of two Caltrans bridges incorporating nonlinear elements under dynamic loads using SAP2000 and OpenSees softwares.

- Elaborate modifications on the bridge models for a better agreement between softwares.

- Compare the results achieved with the improvements done.

- Establish the parameter to be perturbed to perform a sensitivity analysis.

- Using the modified bridge models, develop a nonlinear response history sensitivity analysis under static and dynamic loads.

- Develop single degree of freedom systems for linear elastic, elastoplastic, and softening backbones to construct a constant-ductility response spectrum.

- Hysteretic behaviors analysis and their impact in the nonlinear time history response on the single degree of freedom systems developed.

## 1.3   Thesis Outline

This thesis is organized into four different chapters as listed:

Chapter 1 consists of the introduction, which includes the most relevant historical events that led to improvements in the bridges design and analysis criteria, different software implementations on bridge retrofits and typical situations, materials and element formulations on bridge models, previous researches conducted to analyze the sensitivity of bridges, and the most common numerical methods employed to estimate the sensitivity of typical bridges. This chapter also includes the research objectives and the specific tasks required to achieve them.

Chapter 2 develops previous models of two Caltrans ordinary standard bridges, evaluating different kinds of responses, such as nonlinear time history analysis and moment-rotation column reactions, when seismic loads are applied (Mackie et al., 2017). The column responses were analyzed using a simplified bridge model, which consisted in a simple roller abutment at the end of the superstructure. After obtaining an adequate agreement in the column nonlinear behavior for SAP2000 and OpenSees models, the abutment hysteresis was studied by replacing the roller abutment with the original bridge consideration. The numerical models presented in the current study are based on SAP2000 (version 21.0.2 Build 1491) and OpenSees (version 2.6.4), employing

the same finite element formulations for the column and abutment nonlinearities to better identify the sources of discrepancies in the responses.

Chapter 3 evaluates the sensitivity of the nonlinear time history response using the same bridge models developed in the previous chapter. Sensitivities were obtained using the finite difference method, using a slightly perturbation of the basic nonlinear constitutive materials and the hysteresis behaviors. Using SAP2000 (version 21.0.2 Built 1491), the sensitivity analysis was performance by the implementation of the finite central difference method.

Chapter 4 studies the effects of the hysteretic considerations on the responses of different single degree of freedom (SDOF) systems under ground motions. The analysis was done by the study of a constant-ductility response spectrum under an specific ground motion, probability density functions, and fast Fourier transformation.

# CHAPTER 2: TIME HISTORY ANALYSIS OF BRIDGES INCORPORATING NONLINEAR ELEMENTS.

The content of this chapter is based on the journal paper *Time history analysis of bridges incorporating nonlinear elements* by Rodriguez A. F., Mackie K. R., and Scott M. H., which is being prepared for its final submission on 2021.

## 2.1    Benchmark column models

### 2.1.1    Reinforced concrete constitutive models

The concrete constitutive models defined in SAP2000 were Mander-Unconfined and Mander-Confined (Mander et al., 1988) with a $f'_c$ = 24.8 MPa for OSB1 and $f'_c$ = 27.60 MPa for OSB2. The parameters for unconfined and confined concrete employed in the model are shown in Table 2.1. The concrete properties were defined in OpenSees as *Concrete04* and their values are shown in Table 2.2. The values for the ultimate strain and crushing strength of the confined concrete were taken directly from SAP2000 calculation for consistency and tensile confined strength was set to zero to achieve the same backbone response. Figure 2.1 compares the behavior between OpenSees and SAP2000 (using *Concrete* and *Takeda* hysteresis rules) for OSB1 concrete under cyclic loads. Similar unloading and reloading behavior can be found for SAP2000 *Concrete* hysteresis rule and OpenSees, whereas spurious four-quadrant response can be seen with the *Takeda* hysteresis rule, as observed previously (Mackie et al., 2017).

The steel constitutive model used in SAP2000 was a table-based input, with a Young's modulus of 200 GPa, a yield stress of 413.7 MPa, and an ultimate strength of 620.5 MPa. The strain at onset of strain hardening was 0.01, while the ultimate strain capacity used was 0.09 with a final slope of -10% of the elastic modulus. In the OpenSees models, the longitudinal steel reinforcement used the same table data to identify the tension and compression backbone points. To allow for

Table 2.1: Concrete model parameters for SAP2000.

| Parameter | OSB1 | OSB2 |
|---|---|---|
| Tangent modulus of elasticity (GPa) | 23.60 | 24.80 |
| Secant modulus of elasticity (GPa) | 5.20 | 6.63 |
| Compressive strength of unconfined concrete (MPa) | 24.80 | 27.60 |
| Compressive strength of confined concrete (MPa) | 35.10 | 37.77 |
| Strain at strength of unconfined concrete (m/m) | 0.00222 | 0.002 |
| Ultimate strain capacity of unconfined concrete (m/m) | 0.005 | 0.005 |
| Strain at compressive strength of confined concrete (m/m) | 0.0067 | 0.0057 |

Table 2.2: *Concrete04* material properties employed in columns.

| Parameter | OSB1 | | OSB2 | |
|---|---|---|---|---|
| | Core | Cover | Core | Cover |
| Compressive strength (MPa) | -35.02 | -24.80 | -38.00 | -27.60 |
| Strain at maximum strength | -0.0069 | -0.0022 | -0.0056 | -0.002 |
| Crushing strength (MPa) | -32.13 | 0.00 | -33.23 | 0.00 |
| Strain at crushing strength | -0.0163 | -0.0044 | -0.0153 | -0.004 |
| Tensile strength (MPa) | 0.00 | 3.10 | 0.00 | 3.27 |
| Elastic modulus (GPa) | 28.01 | 23.60 | 29.17 | 24.80 |

hysteresis behavior, the *MultiLinear* material was used. Due to the unloading and reloading rules of the material, it was not possible to include the full softening branch. Thus, the material was wrapped in a *MinMaxMaterial* to ensure that the stress dropped to zero, in this case at a strain of 0.10 in both compression and tension. Figure 2.2 shows the behavior of the longitudinal steel models for OpenSees and SAP2000 under cyclic forces. The only distinction purposely introduced was that the OpenSees model gradually unloads to zero before being removed from the analysis (through the *MinMaxMaterial*) to eliminate spurious negative strength when unloading from the softening backbone. The cyclic results are also the same due to the assumptions of the *MultiLinear* material in OpenSees.
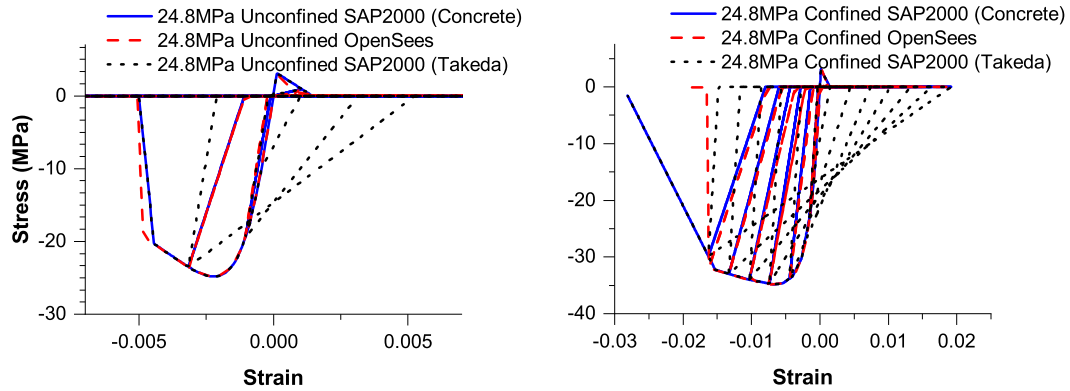
Figure 2.1: Unconfined and confined concrete cyclic stress-strain response for OSB1.
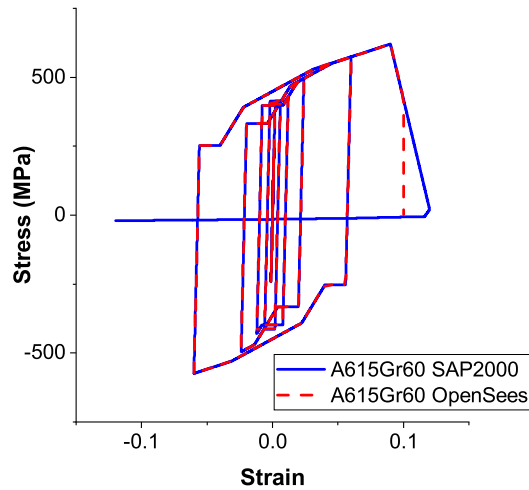


Figure 2.2: Steel cyclic stress-strain response.

### 2.1.2   Response comparison of nonlinear column models

An individual 3D, circular, cantilever column was analyzed under two lateral orthogonal components of a ground motion acceleration history to ensure the subsequent bridge models were properly calibrated. The analysis considered a plastic hinge at the base of the column, with a length $l_{ph}$ = 0.678 m, and an integration point located at the center of the hinge ($x_h$ = 0.339 m).

13

The effective moment of inertia of the column was $0.60I_g$ to assume an appropriated softening of the cracked elastic properties. The values assumed were taken according to the CP3 case (Mackie & Scott, 2019). Similar values can be obtained using ACI-318 (ACI, 2014), Caltrans Seismic Design Criteria (Caltrans, 2013), and Paulay and Priestly (1992), where the recommended effective inertias are $0.70I_g$, $0.53I_g$, and $0.50 - 0.70I_g$, respectively. The column used to calibrate the models had a diameter of 0.51 m, with 8 #8 Grade 50 longitudinal reinforcement, and #8 transverse spiral reinforcement spaced at 0.025 m (which correspond to the properties of OSB1). The circular concrete cross section was discretized into 100 and 40 fiber layers in the tangential and radial directions.

A vertical load of $P$ = -267.5 KN was applied at the top of the column. The orthogonal lateral ground motions imposed were CLAYN1N1000 and CLAYN1N1090 synthetic accelerations (Lu et al., 2015) for x-axis and z-axis respectively. No damping and P-Delta effects were considered in the dynamic analysis, and the time integration method used was Hilber-Hughes-Taylor with $\gamma = 0.5$, $\beta = 0.25$, and $\alpha = 0$. Comparisons between SAP2000 and OpenSees implementations of the CP3 benchmark column under dynamic load are shown in Figure 2.3.

The results shown in the figure concluded that SAP2000 CP3 model has a similar behavior than OpenSees, with small differences in the force peaks values. The response shapes are almost the same for both software, showing identical slopes during the ground motion.

## 2.2 Benchmark bridge models

Two previously calibrated three-dimensional (3D) bridge models under static pushover loads and and considering a concentrated plasticity (CP) approach (Mackie & Scott, 2019) are extended in this investigation to include dynamic time history response under ground motion excitation. The bridge models were originally developed by Caltrans and modeled in CSiBridge/SAP2000, denoted as ordinary standard bridges (OSBs) 1 and 2. The models represent bridge
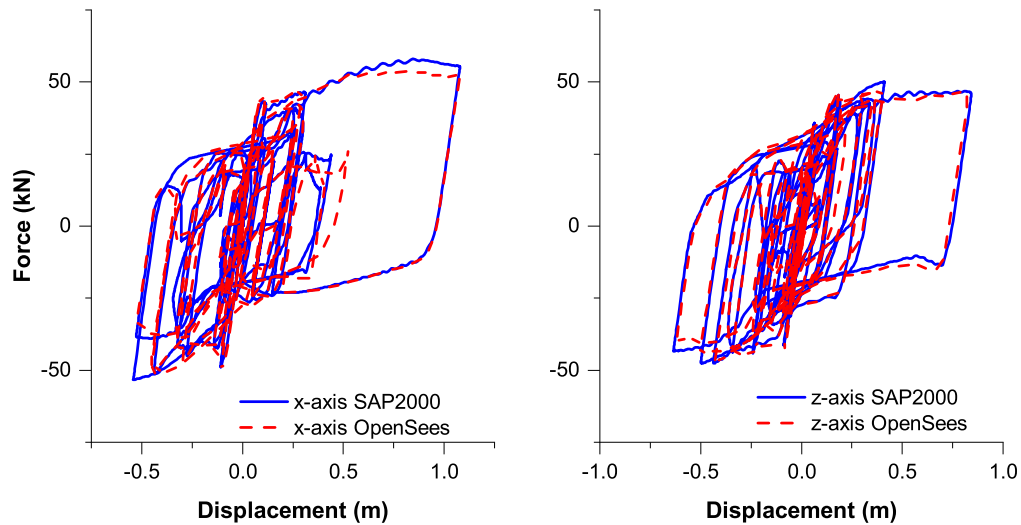
Figure 2.3: Benchmark Reinforced concrete column CP3 behavior comparison.

typical characteristics such as non-skewed, pre-stressed, monolithic, single- and two-column per bent, box girder bridges on seat-type abutments. Therefore, the results can be easily extended to common bridges under similar definitions. The CSiBridge implementations were mirrored directly in the OpenSees implementations (employing the same element formulation, material and element backbone response, and geometry) to achieve nominally identical nonlinear static responses. A plastic hinge model was used for the columns with the integration point at hinge midpoint (CP3). The analyses were developed using roller models with torsional restraint (rotation about axis of the deck) and nonlinear gap-link abutment models. The general definitions for the benchmark bridge models are described in Table 2.3.

### 2.2.1 Ordinary standard bridge description

The ordinary standard bridges (OSB) are two-span concrete bridges supported by seat-type abutments. OSB1 contains a single two-column bent, whereas OSB2 has a single one-column bent. Each span is 45.7 m long, conformed with a continuous cast-in-place post-tensioned concrete non-

Table 2.3: Benchmark bridge definitions

| Bridge Label | Columns per bent | CP case | Column Diameter (m) | Height (m) | Cap | Abutment Plastic hinge location | Gap (m) | Model |
|---|---|---|---|---|---|---|---|---|
| OSB1-S | 2 | CP3 | 1.70 | 5.60 | Offset | Top | N/A | Roller |
| OSB1-O | 2 | CP3 | 1.70 | 5.60 | Offset | Top | N/A | Link |
| OSB1-MS | 2 | CP3 | 1.70 | 5.60 | Rigid | Top | N/A | Roller |
| OSB1-MO | 2 | CP3 | 1.70 | 5.60 | Rigid | Top | 0.051 | Gap/link |
| OSB2-S | 1 | CP3 | 1.70 | 5.60 | Offset | Top and bottom | N/A | Roller |
| OSB2-O | 1 | CP3 | 1.70 | 5.60 | Offset | Top and bottom | 0.051 | Gap/link |
| OSB2-MS | 1 | CP3 | 1.70 | 5.60 | Rigid | Top and bottom | N/A | Roller |
| OSB2-MO | 1 | CP3 | 1.70 | 5.60 | Rigid | Top and bottom | 0.051 | Gap/link |

prismatic box girder superstructure. The total depth of the superstructure is 1.8 m, while the width is 14.5 m. The OSB1 superstructure is a non-prismatic cross section which contains five cells of 2.44 m width and 1.8 m depth for OSB1, while OSB2 has a standard prismatic superstructure with two cells of 3.25 m width, one cell of width 3.10 m, and the same depth as OSB1. The circular reinforced concrete columns have a diameter of 1.70 m, a clear height of 5.6 m, and are founded on pile caps. For OSB1, columns are spaced 7.30 m center-to-center and are reinforced with 36 US#11 Grade 60 longitudinal bars, #8 transversal spirals at 0.15 m, and a clear cover of 0.05 m. OSB2 has similar reinforcement distribution, but with two rows of 22 US#11 Grade 60 longitudinal bars. The top column bent cap is integral with the superstructure and has the same height, but a width of 2.64 m.

The abutments are standard seat-type abutments with 0.05 m movement rating. Each abutment is founded on a pile cap with a 7x2 and 6x2 pile group for OSB1 and OSB2, respectively. The elastomeric bearings are 0.14 m$^2$ and 0.056 m high for OSB1 bridge, while OSB2 has 0.096 m$^2$ and 0.056 m high. The backwall-to-stem wall interface contains a construction joint as does

16
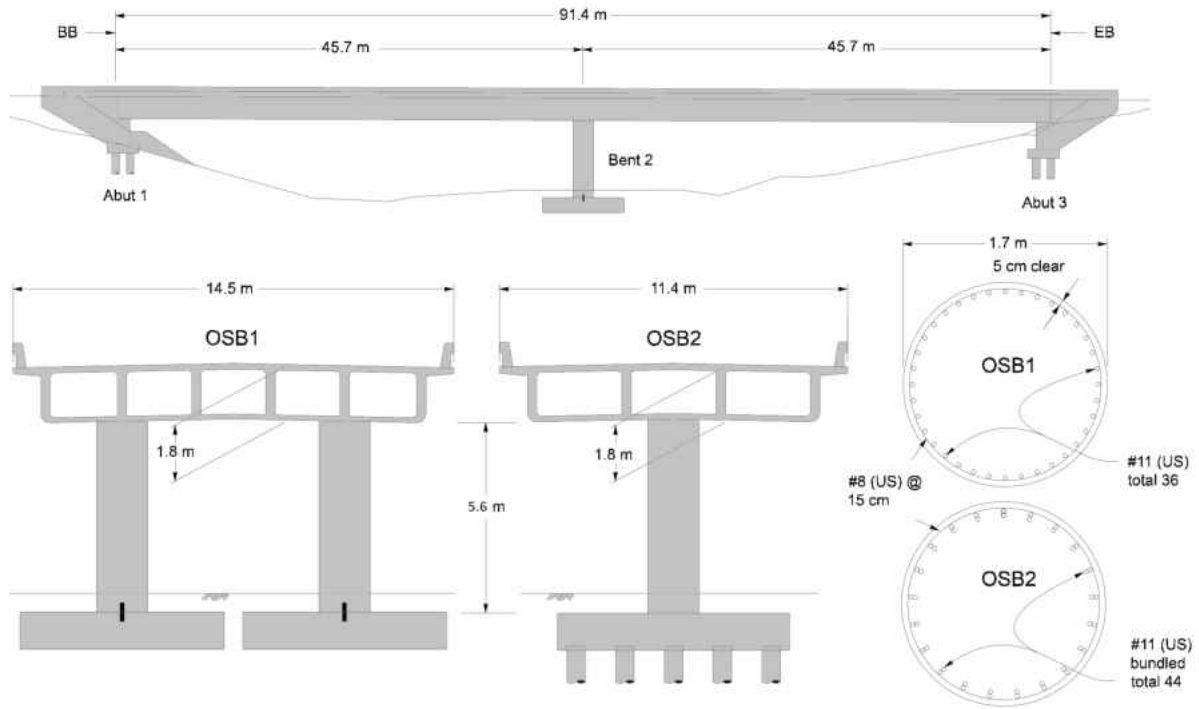
Figure 2.4: Schematic of OSB1 and OSB2 geometry and column cross section.

the exterior shear key-to-stem wall interface. The end diaphragm is also integral with the super-structure and has 0.91 m width. The material properties were $f_c' = 24.8$ MPa for the bent pile cap and $f_c' = 27.6$ MPa for the superstructure. Figure 2.4 shows a schematic representation of OSB1 geometry with its column cross section.

### 2.2.1.1 SAP2000 bridge model implementation

Previously developed by Caltrans (2013), no changes were made to the OSB1-O and OSB2-O SAP2000 models. The center of mass in these models is located 6.1 m above the column bases. A 0.85 m long rigid element was created at the top of each column, increasing its moment of inertia with a multiplier of 3. The OSB2-O model incorporated an additional rigid element at the bottom of the column, with the same characteristics as the top. The rigid element included a frame hinge

17

type Fiber P-M2-M3 (CSI, 2017) in the center and for OSB1-O model it was offset 0.45 m from the deck. The offset was modeled considering a rigid zone factor of 0.5. The moment of inertia of the remaining column was reduced in both directions by a factor of 0.35 and no frame hinge was considered. The superstructure concrete was defined with an elastic modulus of 23.60 GPa and a non-prismatic cross section. The elastic properties are described in Table 2.4.

For OSB1-O, a single multilinear plastic link element (CSI, 2017) was used to define the nonlinear properties of the longitudinal degree of freedom at each abutment. The force-deformation relation was elastic-plastic with a yield force of -6917 kN and a yield displacement of -0.0152 m, following a kinematic hysteresis rule. The effective stiffness for the linear analysis in the longitudinal and transverse directions were 453,754 kN/m and 55,165 kN/m respectively, while the vertical direction had an effective stiffness of $1.459 \times 10^7$ kN/m.

Two link elements in series defined the OSB2-O abutments. The first link element consisted of a gap link with nonlinear properties in the longitudinal axis connected to the deck end node. The effective stiffness for the linear analysis case was $3.50 \times 10^7$ kN/m, while the gap length and the stiffness for the nonlinear analysis were -0.051 m and $175.13 \times 10^4$ kN/m respectively. The deck left end node had restraints in the transverse and vertical directions, as well as all rotational degrees of freedom. However, the right end node was only restrained in the translational degrees of freedom. The second link element consisted of a multilinear plastic link with nonlinear properties in the longitudinal degree of freedom, located between the gap link and the supports. With an elastoplastic nonlinear force-deformation relation, the link had a yield displacement of -0.015 m and a yield force of -4586 kN in the longitudinal directions, but the remaining degrees of freedom were restrained. Figure 2.5 shows the resultant load-displacement relationship for OSB1-O and OSB2-O abutments.

Table 2.4: Superstructure material and section properties.

| Parameter | OSB1 | | OSB2 | |
|---|---|---|---|---|
| | Girder | Cap | Girder | Cap |
| Cross section area ($m^2$) | 7.74 | 4.83 | 6.58 | 4.83 |
| Moment of inertia $I_{22}$ ($m^4$) | 3.83 | 1.34 | 2.68 | 1.35 |
| Moment of inertia $I_{33}$ ($m^4$) | 130.21 | 2.8 | 61.26 | 2.81 |
| Torsion constant ($m^4$) | 11.70 | 3.08 | 6.71 | 3.09 |
| Young's Modulus (GPa) | 23.60 | $\infty$ | 23.60 | $\infty$ |
| Shear modulus (GPa) | 9.83 | $\infty$ | 9.83 | $\infty$ |

### 2.2.1.2  *OpenSees bridge model implementation*

The OpenSees models were developed to reproduce the OSB1-O and OSB2-O SAP2000 models. Therefore, common column and superstructure properties were utilized. Some changes were made to obtain the requirements for OSB2-O. The elements assumed to remain elastic were modeled using the *elasticBeamColumn* in OpenSees. The OpenSees hinge model incorporated an approach that consisted of a *forceBeamColumn* element with a finite length specific to the hinge length, but using only a single integration point, to match the hinge model in SAP. To accommodate the particulars of the hinge assumptions in OSB1-O, it was necessary to use the *FixedLocation* integration rule at 0.39 m from the top of the elastic portion of the column. This approach includes a fiber cross section at the single integration point, and therefore, the model accounts for axial load variations and does not require calibrating zero-length elements.

The same OSB1-O plastic hinge strategy was used for OSB2-O. According to the benchmark bridge definition, no rigid offset was assumed for OSB2-O model. The hinge element length was 0.085 m and was introduced in the middle of the two 0.85 m rigid elements at the bottom and the top of the column. The columns were pinned at the bottom and were modeled with stiff *elasticBeamColumn* elements to represent the rigid portions. The inner portion of each column was defined as an *elasticBeamColumn* with the same property modifiers as implemented in the
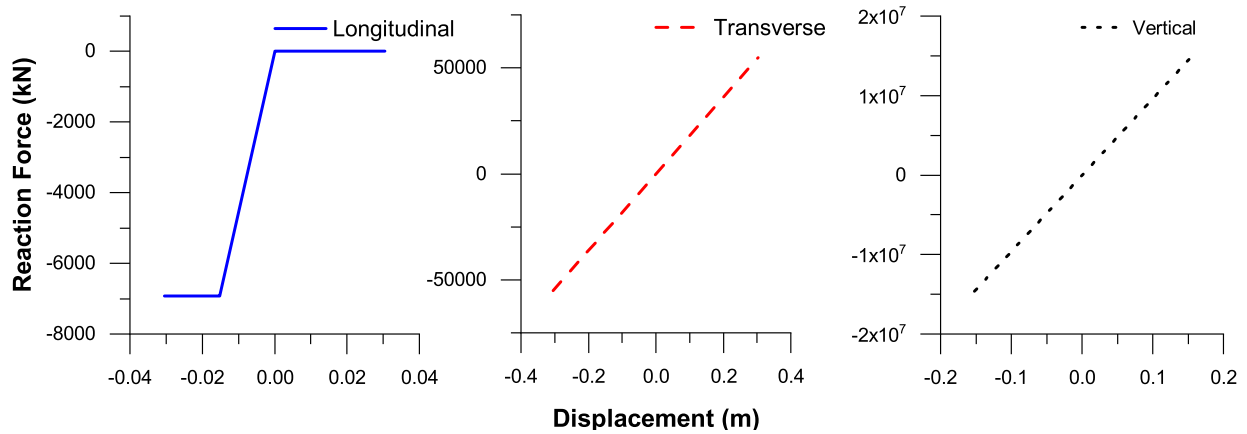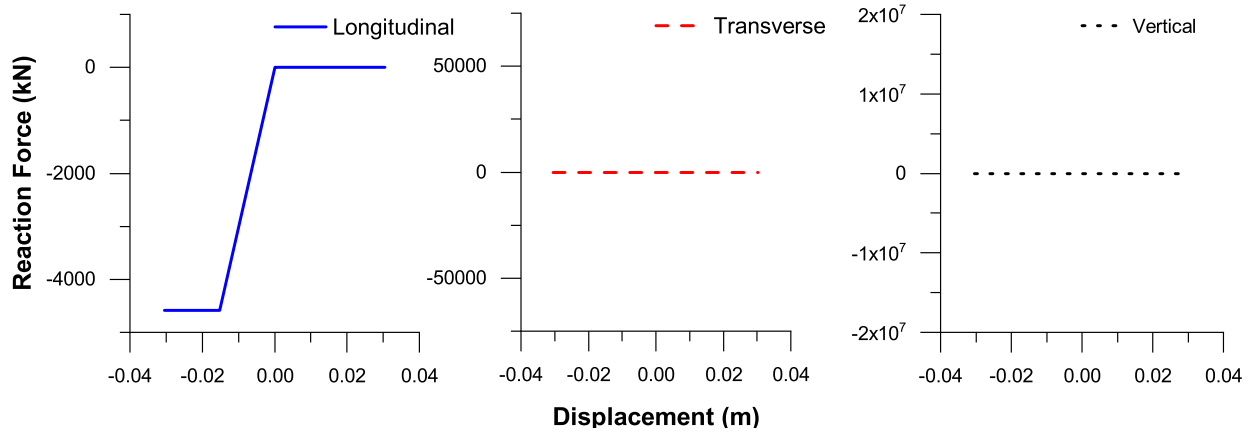
Figure 2.5: Abutment resultant load-displacement relationship in SAP2000.

SAP2000 models. The fiber cross section discretization was created to match SAP2000 with individual core concrete, cover concrete, and longitudinal reinforcing steel constitutive models. The concrete columns properties were defined with OpenSees *Concrete04* and their values are shown in Table 2.2.

The OSB1-O nonlinear properties for the abutments were defined as a compression-only *ElasticPPGap* material, with a gap of 0.0m, an effective stiffness equals to 453,754 kN/m, and a

yield force of -6917 kN/m in the longitudinal direction. A linear elastic behavior was considered for the transverse and vertical directions, with 55,168 kN/m and $1.459e^7$ kN/m respectively. The torsion of the bridge deck in the abutments was restrained. On the other hand, the OSB2-O incorporated nonlinear properties to the transverse degree of freedom of each abutment under the same definition adopted for OSB1-O. The longitudinal material used a gap of -0.05 m, an effective stiffness of 311,900 kN/m, and a yield force of -4,586 kN. By the other hand, the transverse material was defined with a gap of -0.025 m, an effective stiffness of 17,512 kN/m, and a yield force of 798 kN. The abutments were fixed in the vertical direction. The vertical and transverse direction were over-constrained with fixity, therefore do not deform, while the longitudinal direction combines two element behaviors.

### 2.2.2   *Bridge model modifications*

To achieve a better agreement between OpenSees and SAP2000 results, several simplifications and enhancements were made to the bridge models. The column hinge cross section was discretized into 50 and 40 fiber layers in the longitudinal and radial direction, respectively. In the OSB1-MO model, the hinge offset and the unusual placement of the plastic hinge within the rigid zone at the end of the column were removed. The same modification was made to OSB2-MO, in which the length of the plastic hinge was also changed from 0.085 m to 0.85 m at the top and bottom of the column. Therefore, more ductile behavior is expected to occur. In addition, a new element with high stiffness and with a length of 0.45 m was added at the top of the columns to represent the rigid offset between the superstructure center of mass and the top of the column frame element. Figure 2.6 shows the column configurations for OSB models. Boundary conditions for the OSB2-MO model in the superstructure were considered symmetric in both models, while the non-prismatic bridge cross-section in OSB1-O was replaced with a standard prismatic superstructure. Finally, a gap-link with the same nonlinear properties and length of OSB2-O gap was added between each multilinear plastic link and the deck of the OSB1-MO superstructure.
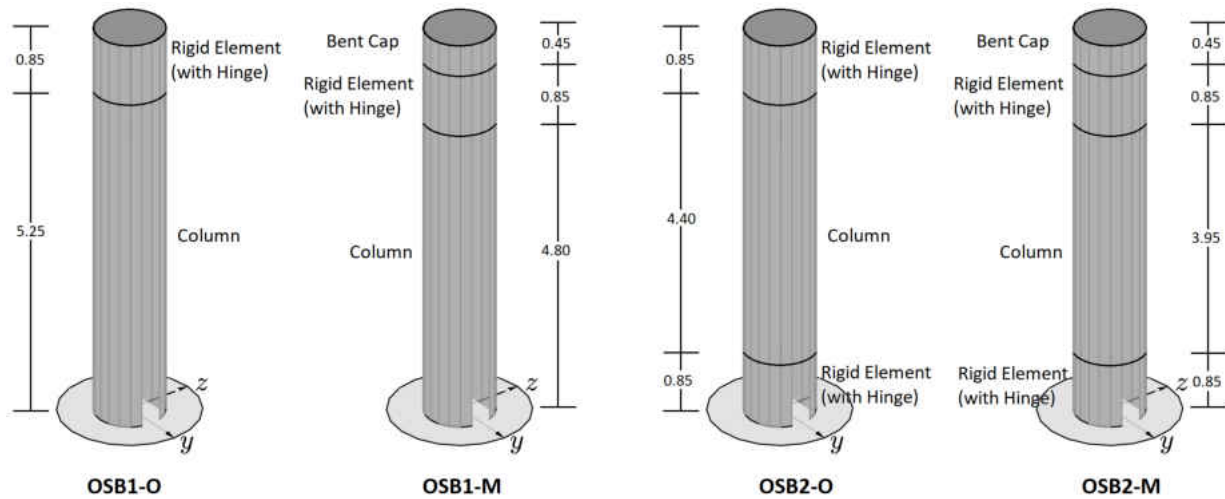
Figure 2.6: OSB reinforced concrete column.

The nonlinear static response was analyzed adopting the simple roller abutment case to isolate the bent and column from the abutment contribution. A single 445 kN lateral load was applied at the center of mass of the bridges in the longitudinal and transversal direction independently to monitor bridge responses. The comparative pushover curves obtained for the models are illustrated in Figure 2.7. Due to the roller abutments, the total base shear is the same as the column/bent shear. Similar result were obtained in previous studies for OSB1-S and OSB2-S (Mackie et al., 2017) and the differences in the responses were attributed to the non-prismatic cross section (in OSB1), hinge definition (rigid offset plus rigid zone factor), and the concrete constitutive models. The improvements done over the models concluded in more ductile responses for OSB2-MS, while OSB1-MS increased its shear resistance. Even though both SAP2000 and OpenSees models had similar initial stiffness and yield points, the pushover responses in OpenSees described a stiffer and larger yield force. The improvements done over the models had a small impact on OSB1 static response, while the changes in OSB2 hinge length affected considerably the bridge reaction to pushover loads. The early softening in the OpenSees pushover responses remained, concluding that the difference between models is produced at the material constitutive level. Another analysis was performed

using the same definition as OpenSees for the concrete constitutive model (dropping to zero stress at the end of the backbone) in the SAP2000 models, concluding that the difference is produced by the limitation on the crushing strain of the confined concrete in compression for the OpenSees constitutive model. Figure A.1 in the annex shows the pushover plot for OSB1-S using concrete constitutive model dropping to zero stress at the end of the backbone in SAP2000.

### 2.2.3   Nonlinear time history analysis

The nonlinear time history analysis was performed using CLAYN1N1, ROCKN1N1, and SANDN1N1 ground motion acceleration, which correspond to different types of soil, and were taken from a set of 50 ground motions provided by Caltrans for a previous research (Lu et al., 2015). The analysis was driven to compare the responses of the bridges after the application of two lateral orthogonal components of excitation along the longitudinal and transverse direction, therefore, only the input motions with two components were considered for this study. The strong motion duration was obtained based on the standard Arias 5-95 bounds (Mackie et al., 2017). The corresponding ground motion acceleration properties components are shown in Table 2.5. Due to the large demand presented by the ground motion CLAYN1N1, it was selected to show individual representative time history responses in the research. The dynamic analysis was done considering an equivalent viscous damping ratio of 5% at periods of 1.2 and 0.7 seconds for OSB1 and 0.889 and 0.692 for OSB2. The corresponding Rayleigh mass proportional coefficients were 0.3307 and 0.3974 for OSB1 and OSB2 respectively, while the stiffness proportional coefficients were $7.036e^{-3}$ s for OSB1 and $6.193e^{-3}$ s for OSB2. The time integration scheme employed was Hilber-Hughes-Taylor method, considering $\gamma = 0.5$, $\beta = 0.25$, and $\alpha = 0$. OpenSees used the same values directly for the analysis, with an initial stiffness used the stiffness-proportional values.

23
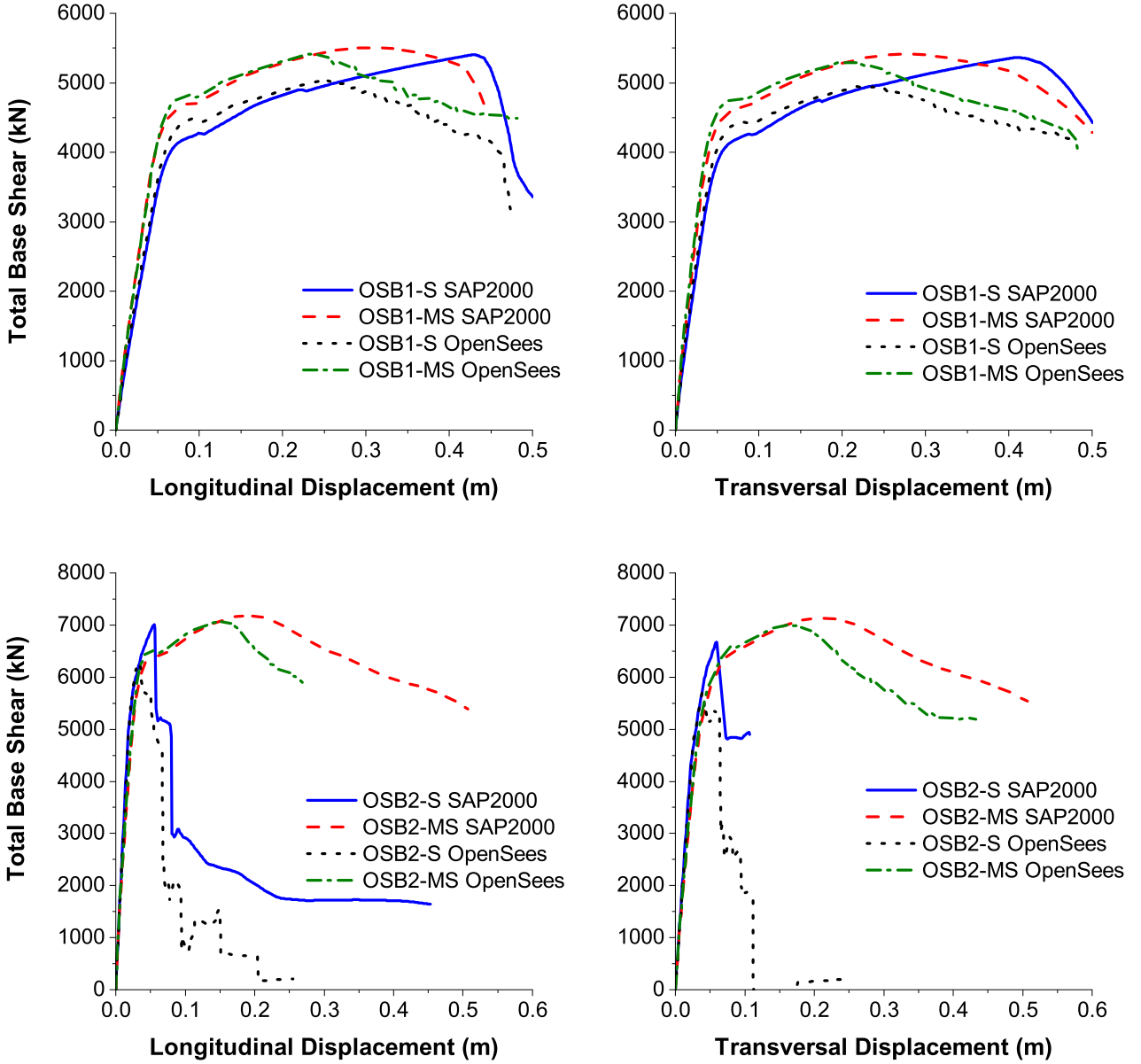
Figure 2.7: Load vs displacement pushover comparison for OSB models.

Table 2.5: Ground motion acceleration time history properties.

| Component | Direction in model | SMD (s) | PGA (g) | PGV (cm/s) | PGD (cm) |
|---|---|---|---|---|---|
| CLAYN1N1000 | Long. | 30.4 | 0.706 | 108 | 95.9 |
| CLAYN1N1090 | Tran. | 29.1 | 0.788 | 104 | 57.7 |
| ROCKN1N1000 | Long. | 15.0 | 0.399 | 59.2 | 25.7 |
| ROCKN1N1090 | Tran. | 13.2 | 0.576 | 77.9 | 44.8 |
| SANDN1N1000 | Long. | 37.0 | 0.784 | 86.3 | 33.3 |
| SANDN1N1090 | Tran. | 36.3 | 0.812 | 67.9 | 30.7 |

## 2.3    Results for Bridge models with Roller Abutments

### 2.3.1    OSB1-S

The displacement time history responses for OSB1-S at the center of mass of the bent in the longitudinal and transverse directions are shown in Figure 2.8a, respectively. The results obtained for longitudinal and transverse displacements in SAP2000 were close to the response reached by OpenSees, particularly the phasing. The peak displacement magnitudes differ by 17% and 21% for the longitudinal and transverse directions respectively, the larger values obtained in SAP2000. The variations in the inelastic peak displacement are consistent with the discrepancies found in the concrete constitutive models related to the differences in the hystertic rule considerations for both software.

In the SAP2000 responses, the changes in the elastic peaks had a larger residual displacement in both the longitudinal and transverse responses.

The moment-rotation response at the top of the two columns are shown in Figure 2.8b. The roller abutment hysteresis results illustrate an increase in the plastic curvature for both models under similar bending moments compared with original abutment models. The response obtained for the OpenSees models softens in agreement with the concrete constitutive model presented previously, while SAP2000 response showed a continued ductility near the peak. Even though both models had similar behavior, OpenSees model dissipates near 40% more energy than SAP2000's.
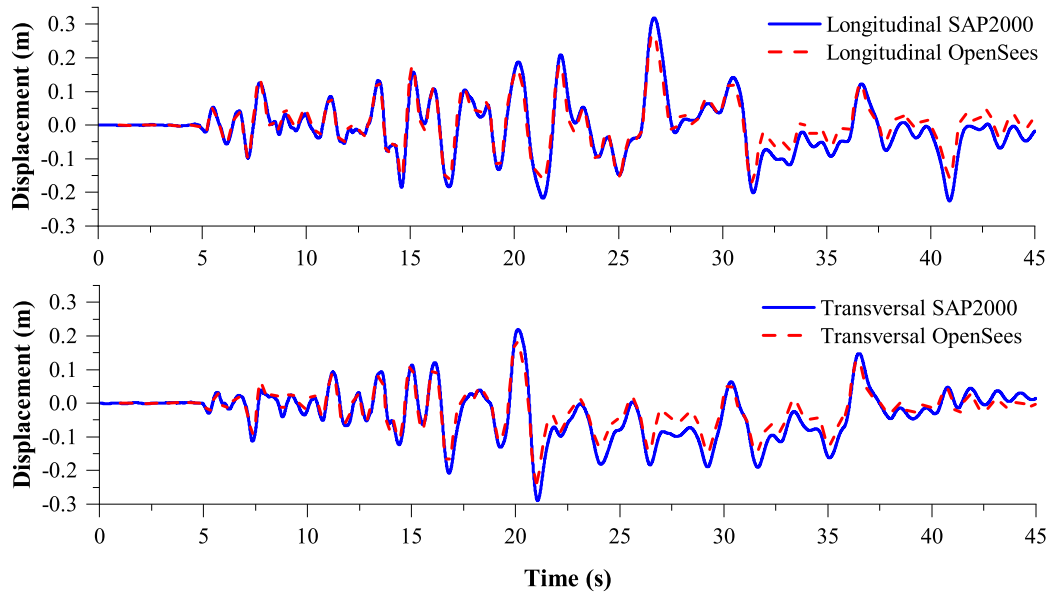
25

(a) Center of mass displacement time history.



(b) Column top moment-rotation hysteresis.

Figure 2.8: OSB1-S responses for ground motion CLAYN1N1.

### 2.3.2    *OSB2-S*

The displacement time history responses obtained for OSB2-S model at the center of mass of the bent in the bridge longitudinal and transverse directions are illustrated in Figure 2.9. Due to the small hinge length considered for this model, the response for OSB2-S should not be overly scrutinized. Its irregular behavior could be observed in the OSB2-O model and the erratic response tends to increase by using a roller model such as OSB2-S, where the highest resistance to the excitation is contributed by the columns. The results show phasing and displacement peaks very similar until the first substantial inelastic excursion (near 14 s). Beyond this peak, the displacement response tends to generate a significant period of elongation and the models tend to behave completely different.

The moment-rotation responses for the column top hinge are shown in Figure 2.11. Both models show an acceptable agreement for initial cycles in longitudinal and transverse direction, but after the peak moment is obtained, the responses became clearly different. Similar to OSB2-O, the curvature demands in SAP2000 are larger than OpenSees at a given displacement requirement.

## 2.4    Results for nonlinear link-gap abutment models

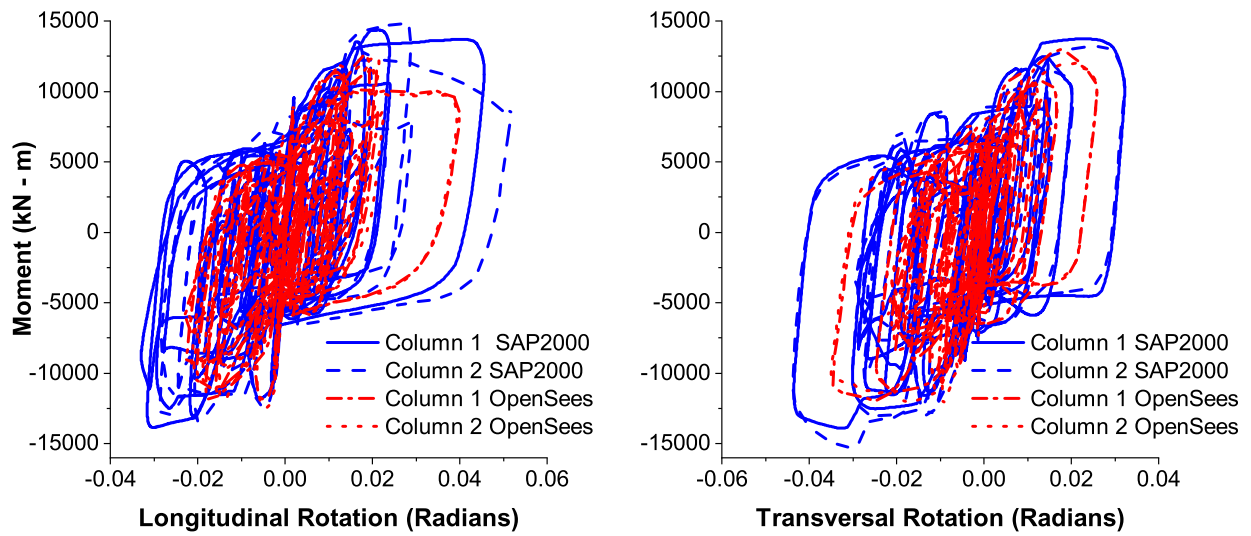### 2.4.1    *OSB1-O*

Figure 2.10a shows the displacement time history response for OSB1-O at the center of mass of the bent independently for the longitudinal and transverse direction. The phasing and agreement between the transverse response peaks are nearly identical at small amplitudes but tends to diverge after the peak response at approximately 15 s. The primary cause of this difference lays on the contribution of the longitudinal abutment, which was defined as a multilinear plastic link and seems to behave different than the OpenSees considerations. By model definition, the OSB1-O works elastic in the transverse and vertical direction; therefore, the only difference occurs in the longitudinal springs.

(a) Center of mass displacement time history.
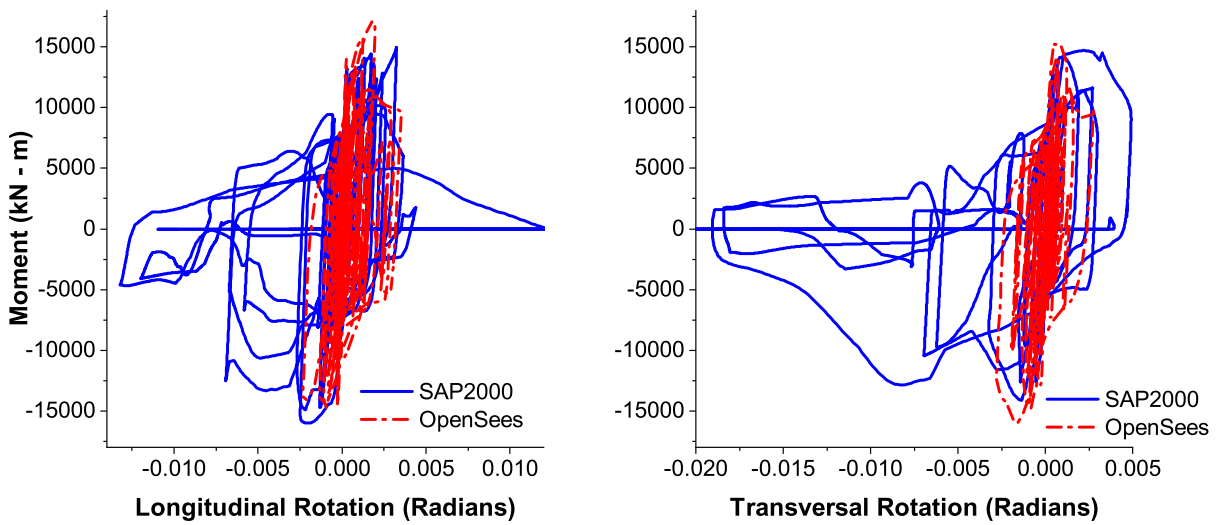


(b) Column top moment-rotation hysteresis.

Figure 2.9: OSB2-S responses for ground motion CLAYN1N1.

The moment vs rotation responses at the top of the two bent columns are shown by separately for longitudinal and transverse directions in Figure 2.10b. The sign of the moment and rotation were calibrated to be the same as the displacement, therefore, a peak positive displacement has a corresponding peak positive rotation. The results obtained show a close agreement between SAP2000 and OpenSees on the transverse displacement responses, while the longitudinal presents a substantial energy dissipation beyond the peak different than OpenSees prediction.

### 2.4.2 *OSB2-O*

The displacement time history responses for OSB2-O at the center of mass of the bent in the longitudinal and transverse directions are shown in Figure 2.9 separately. Due to the small hinge length assumed for this model, the stiffness was higher than the expected and the bridge presented a brittle behavior at displacement demands that are small. Therefore, the frequency content of the OSB2-O time history results for the ground motion was higher. This characteristic can be observed particularly in the transverse direction, where the abutments do not represent an important contribution in the resisting forces compared with the column. The results obtained for the transverse response show a significantly difference between SAP2000 and OpenSees for the peak displacement magnitude (near 50%), while the longitudinal response matches until the first substantial inelastic peak displacement. Beyond this peak the displacement response tends to generate a significant period of elongation. The reason for a change in the frequency content could be due to changes on the integrator during time history analysis or changes in the concrete constitutive models.

The moment-rotation responses obtained in the top column hinge are shown in Figure 2.11. Similar to OSB1-O, the sign of the moment and rotation were calibrated to be the same as the displacement. The shape and energy dissipated in the longitudinal response are similar for SAP2000 and OpenSees, until the peak value is obtained in about 14 seconds. After the peak is reached, the response for both models is noticeable different, with a softening in the reloading stiffness of
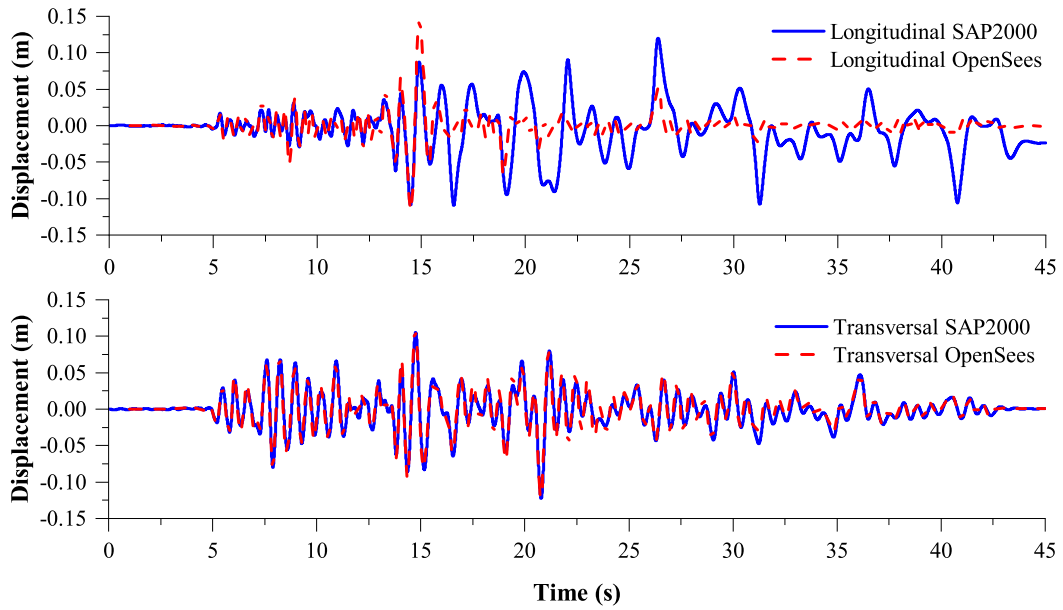
29

(a) Center of mass displacement time history.
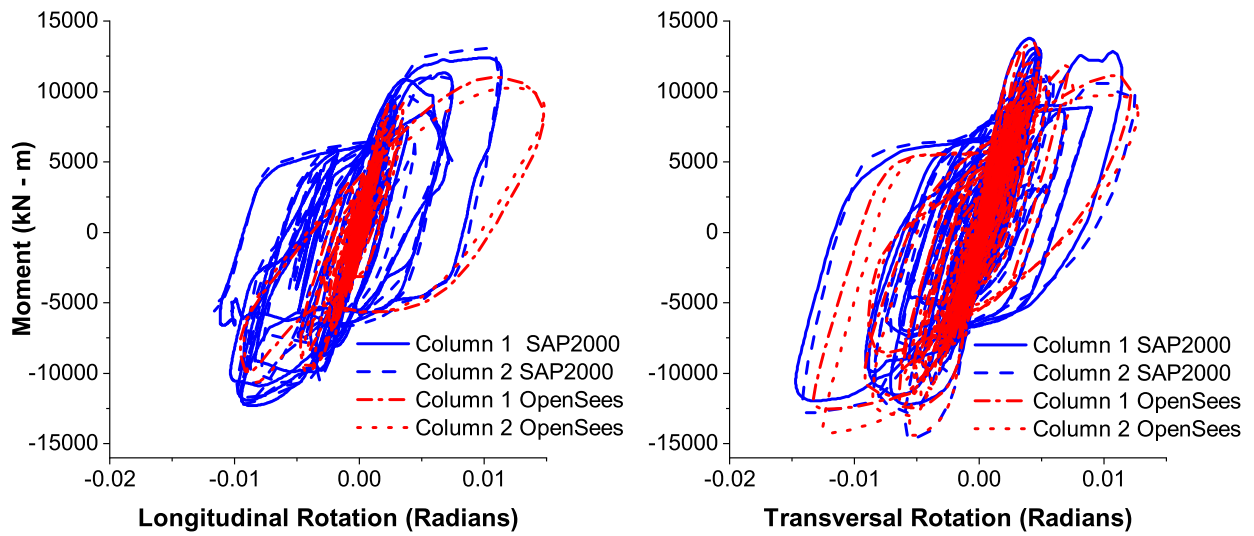


(b) Column top moment-rotation hysteresis.

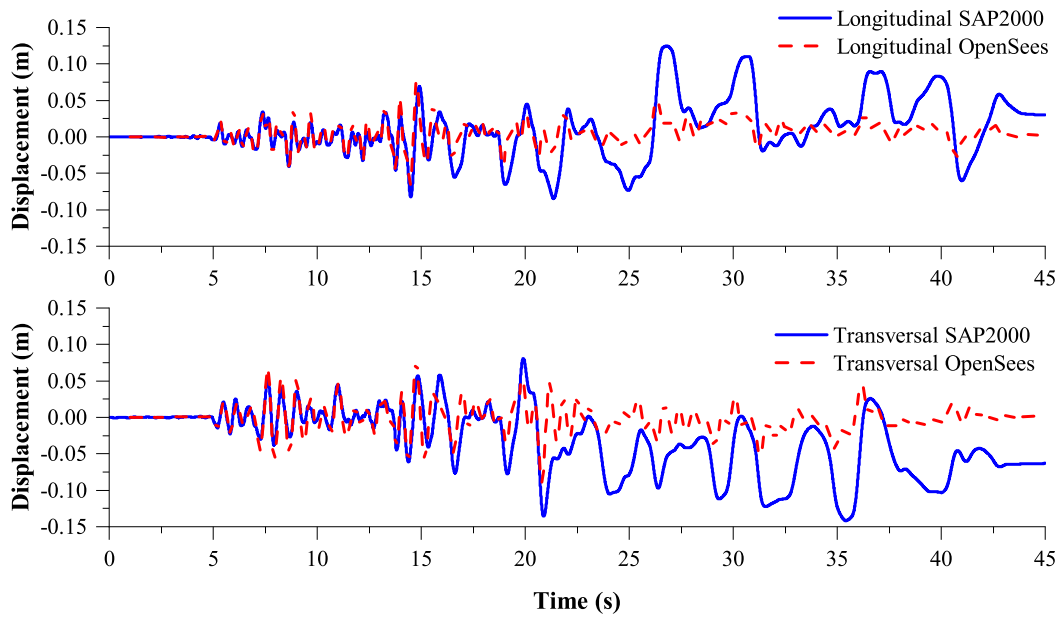Figure 2.10: OSB1-O responses for ground motion CLAYN1N1.

the SAP2000 at a smaller rotation demand than the OpenSees response. The transverse displacements, and hence rotations, remain mostly in the elastic range. The peak displacement achieved for SAP2000 is close to the first yield. Rotational inertia may contribute to slightly larger transverse curvature demands in SAP2000 than OpenSees. Because of the small hinge length in OSB2, performing numerical simulations may be extremely complex, concluding in an increase in the rotation demands for SAP2000.

### 2.4.3   OSB1-MO

The displacement time history responses generated for the OSB1-MO model at the center of mass of the bent are presented individually for the longitudinal and transverse direction in Figure 2.12. The longitudinal and transverse displacement show excellent agreement throughout the nonlinear time history analysis, specially the phasing and peaks values. The peak values difference between models is almost neglected for both directions. However, a small offset can be found in the longitudinal response after 30 s. The improvements done over the model concluded in a better nonlinear behavior and the responses were very similar in both programs.

The analysis results for the OSB-MO abutment model are illustrated in Figure 2.14. The hysteresis behavior of both models is almost identical. The overall difference between OpenSees and SAP2000 in the curvature was lower than 10%, while the bending moment was negligible. These results are in accordance with the response obtained in the displacement time history analysis and provided an excellent agreement between SAP2000 and OpenSees. A similar result can be found in the base shear vs displacement analysis done at the top of the columns, where the offset between both programs was considerable small. The maximum difference obtained in the base shear was near 10%, while the displacement was almost 0%. The results illustrated in Figure 2.13 clearly demonstrate that OpenSees and SAP2000 had an excellent agreement in the OSB1-MO abutment model. The figures show that the bias presented between OpenSees and Sap2000 in the OSB1-O responses was corrected with the use of gaps in the corners of the deck. Therefore, the
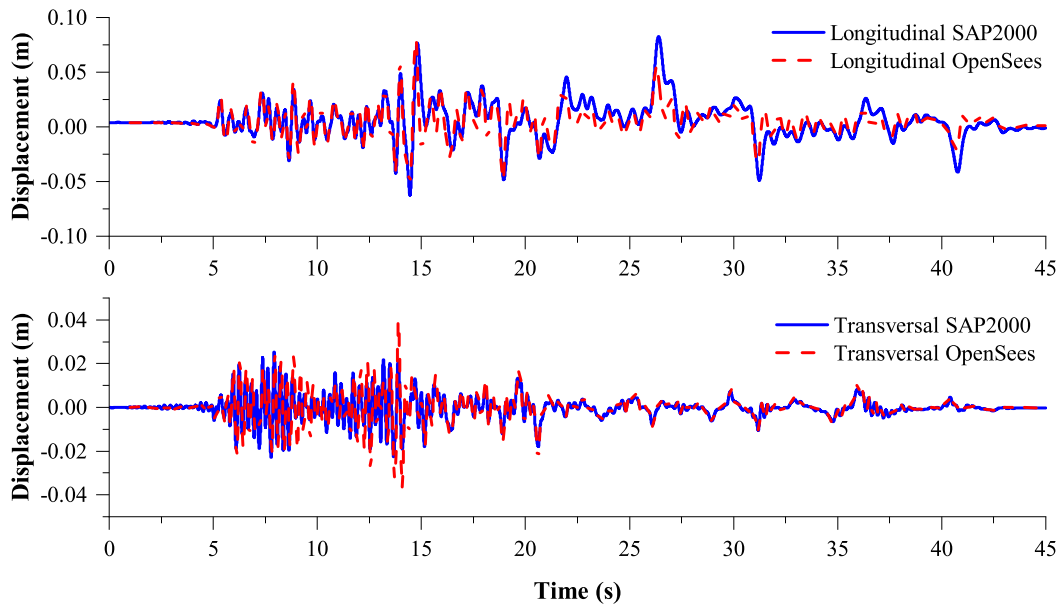
(a) Center of mass displacement time history.
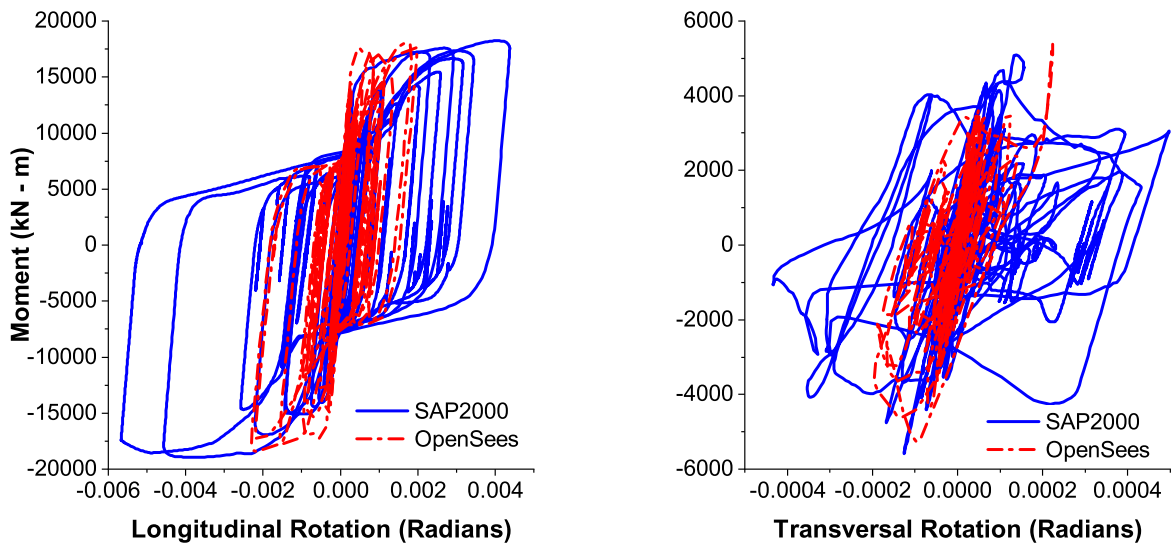


(b) Column top moment-rotation hysteresis.

Figure 2.11: OSB2-O responses for ground motion CLAYN1N1.

main cause of variance in the responses between models could be attributed to the assumptions on the abutments for both OpenSees and Sap2000, rather than the consideration of the hysteretic rule.

### *2.4.4   OSB2-MO*

The analysis done over the displacement time history of the OSB2-MO model are displayed in Figure 2.15. The phasing and peaks magnitudes for both models were almost identical, with a peak offset lower than 8% in the longitudinal direction. The difference between models for the peak value in the transverse direction was almost neglected. The modifications made over the OSB2-O models produced a better nonlinear behavior and the responses had an excellent agreement for both programs.

Similar to the other models, a moment vs rotation analysis was done over the OSB2-MO model. The analysis was performance for the top and the bottom hinges. In the longitudinal direction the results were very close, but small differences were found in the transverse response. However, the models presented an excellent agreement for phasing and peaks values. The results are illustrated in Figures 2.16 and 2.18 for OSB2-MS and OSB2-MO models, respectively.

For the OSB2-MO, the analysis was extended to the base shear vs displacement response. The results obtained were in concordance with the previous ones achieved for the displacement time history. Even small differences were found, the variation in the peak values between both models was lower than the 10%. The phasing was almost identical for both models, but a difference in the slope was registered in the transversal direction for the roller model. However, the models presented almost identical shapes, which can be observed in Figure 2.17.

## 2.5   Summary and Discussion

The Tables 2.6 and 2.7 summarize the peak values obtained in SAP2000 for all models developed in the current study after applying different ground motion combinations (Mackie et al.,
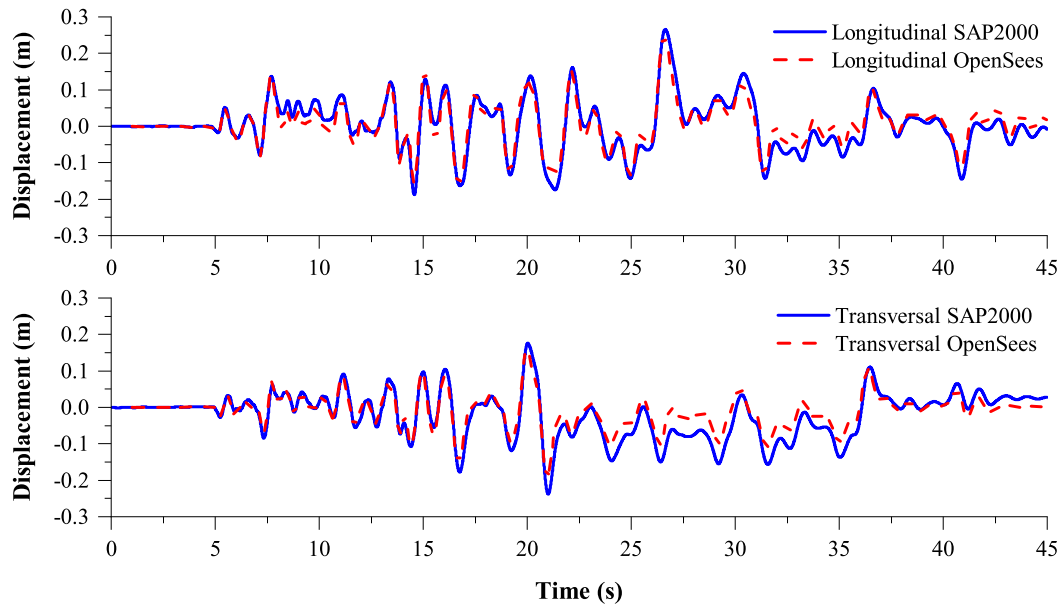
(a) Center of mass displacement time history
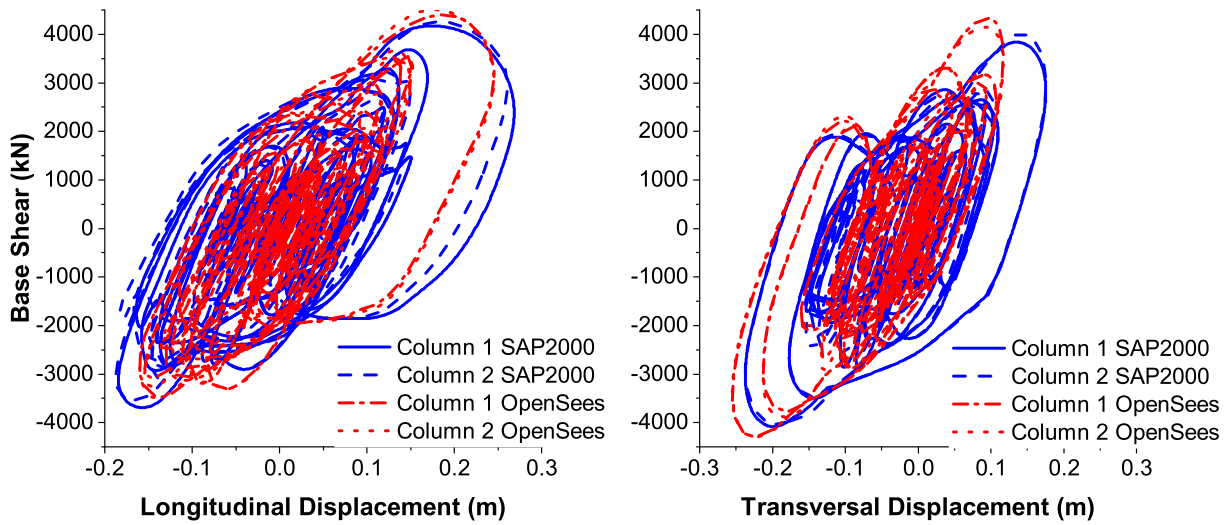


(b) Base Shear vs Displacement at the top of the column

Figure 2.12: OSB1-MS responses for ground motion CLAYN1N1.
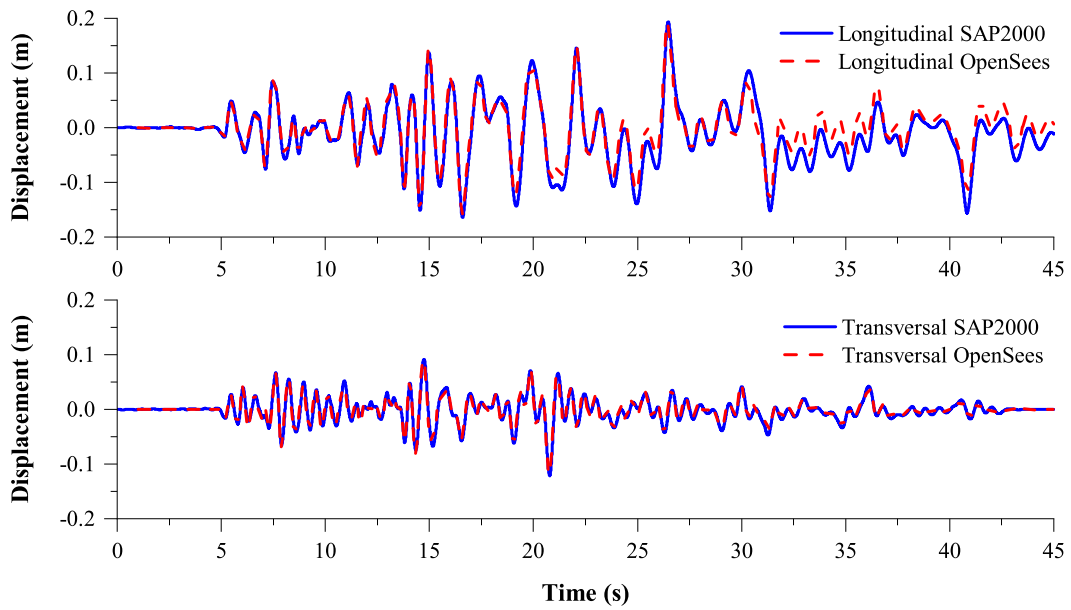
(a) Center of mass displacement time history
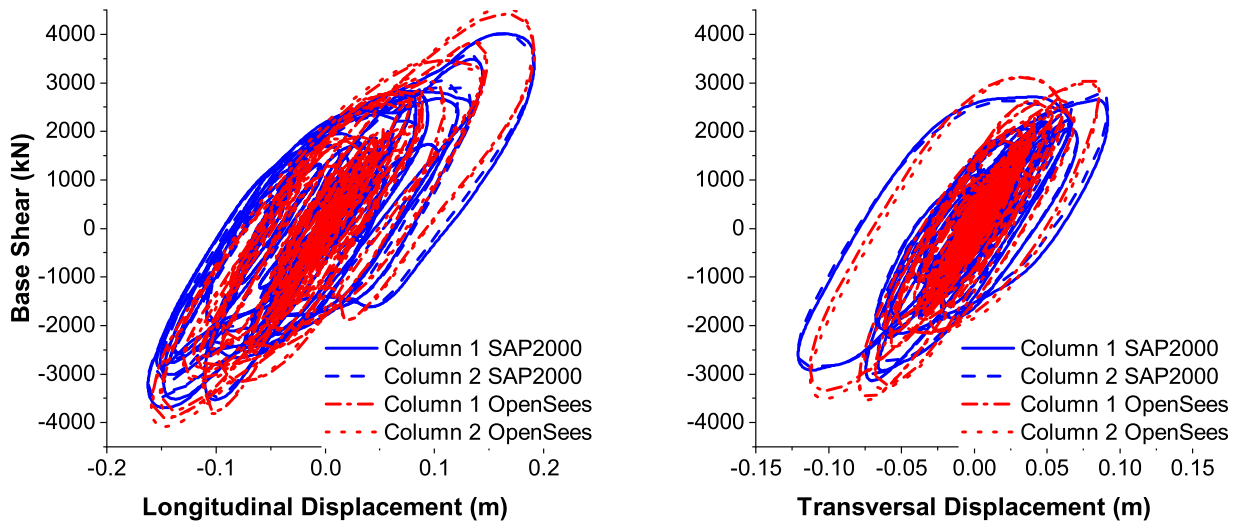


(b) Base Shear vs Displacement at the top of the column

Figure 2.13: OSB1-MO responses for ground motion CLAYN1N1.
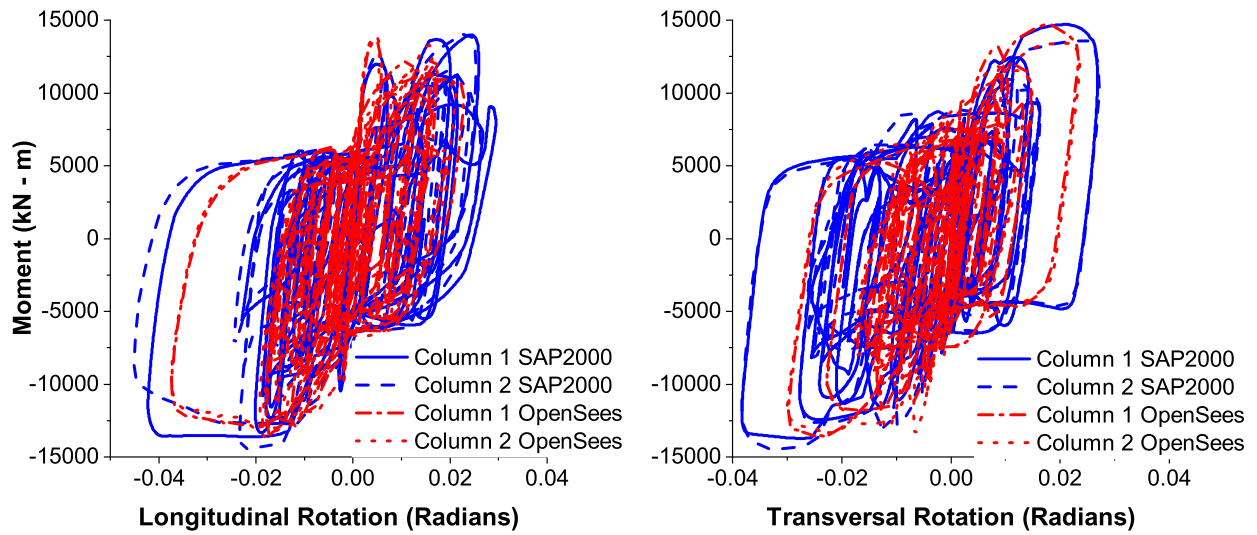
(a) OSB1-MS
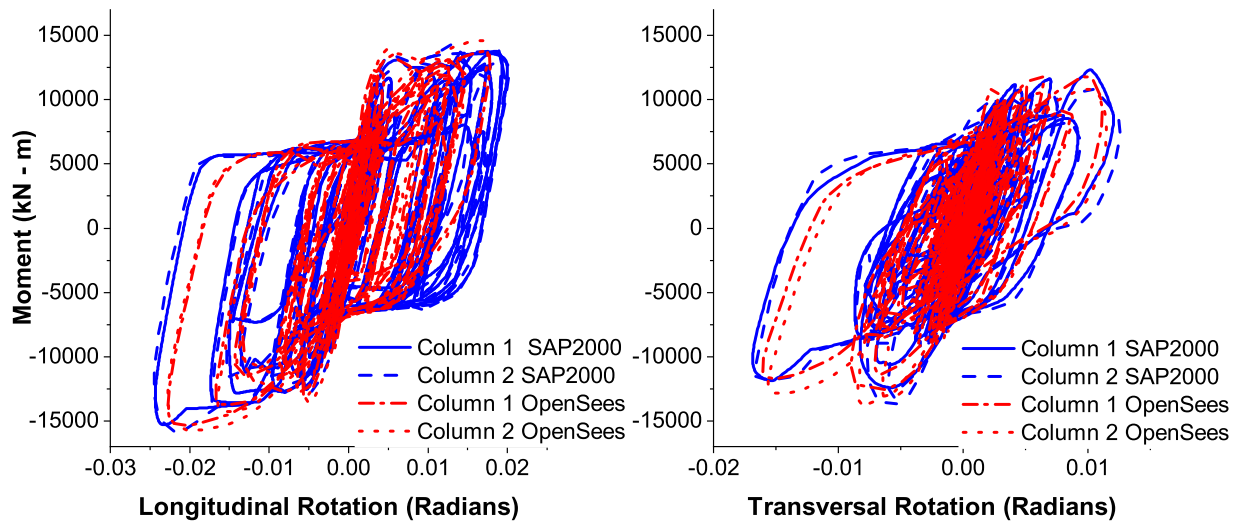


(b) OSB1-MO

Figure 2.14: OSB1-MS and OSB1-MO column top moment-rotation responses for ground motion CLAYN1N1.
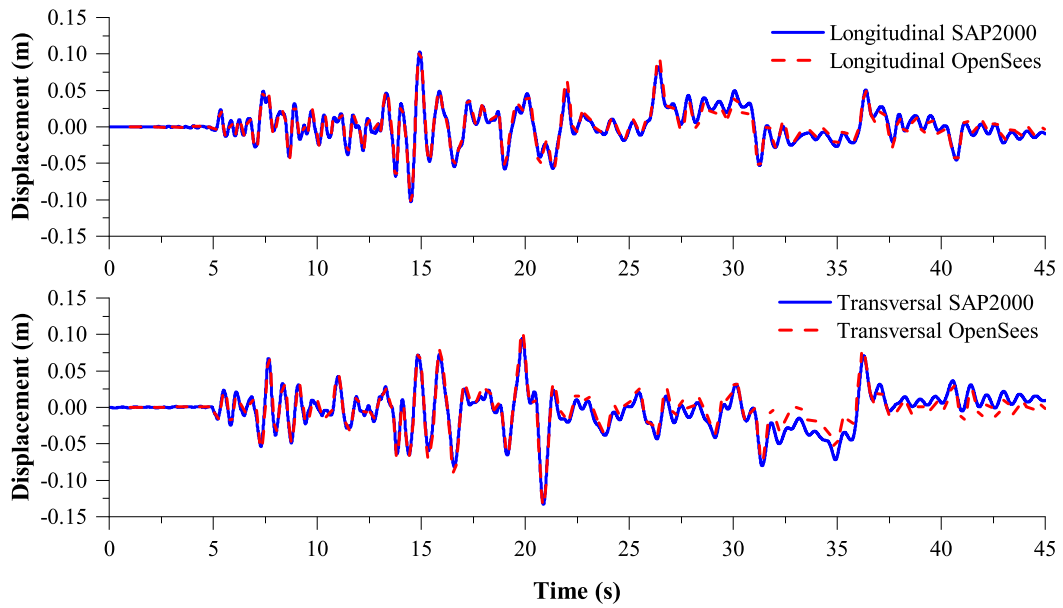
(a) Center of mass displacement time history
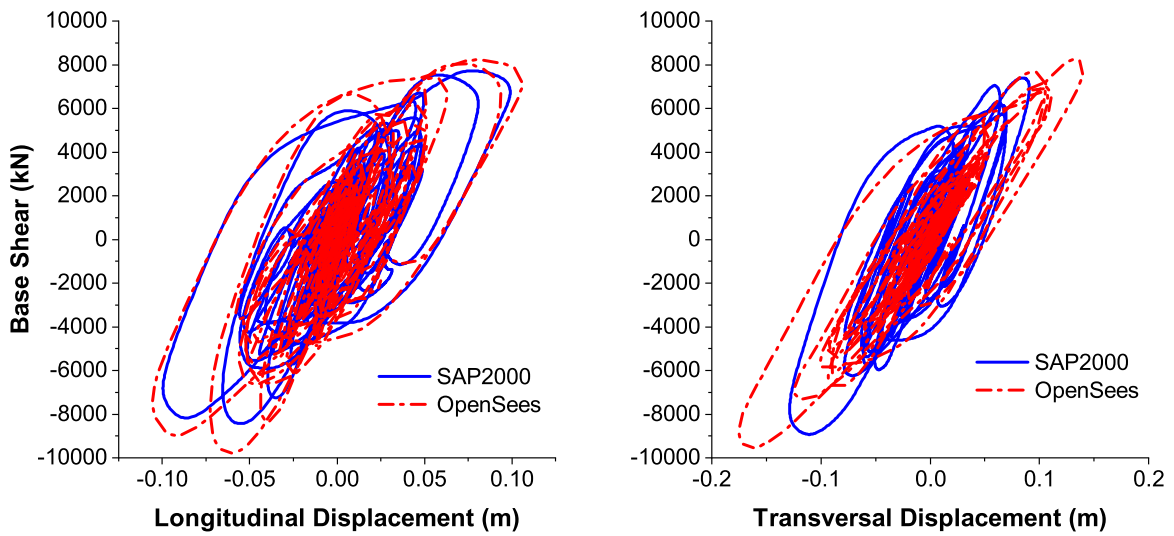


(b) Base shear vs displacement at the top of the column

Figure 2.15: OSB2-MS responses for ground motion CLAYN1N1.
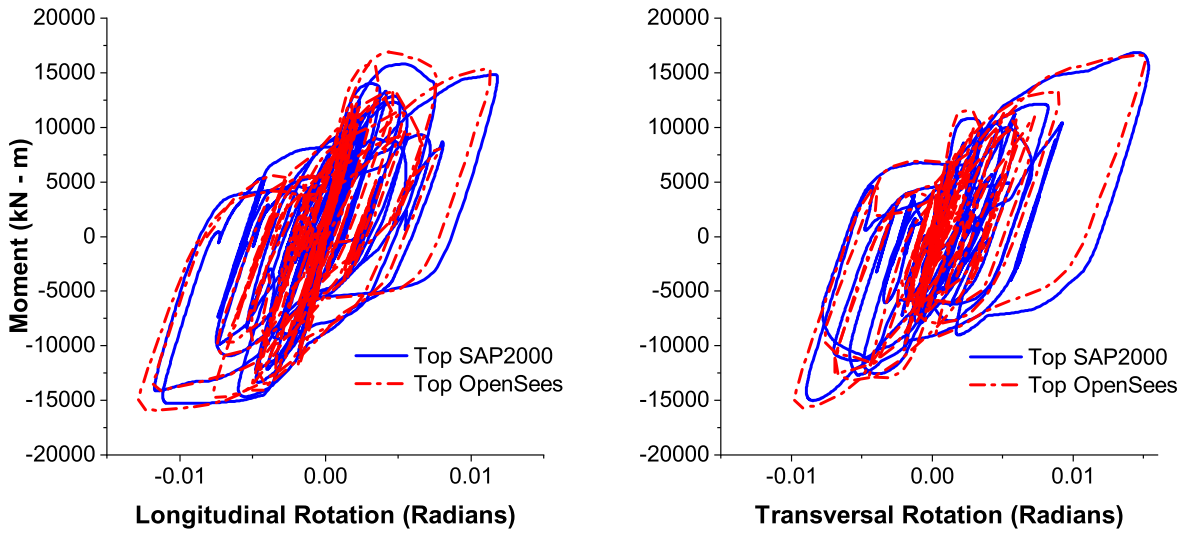
(a) Top
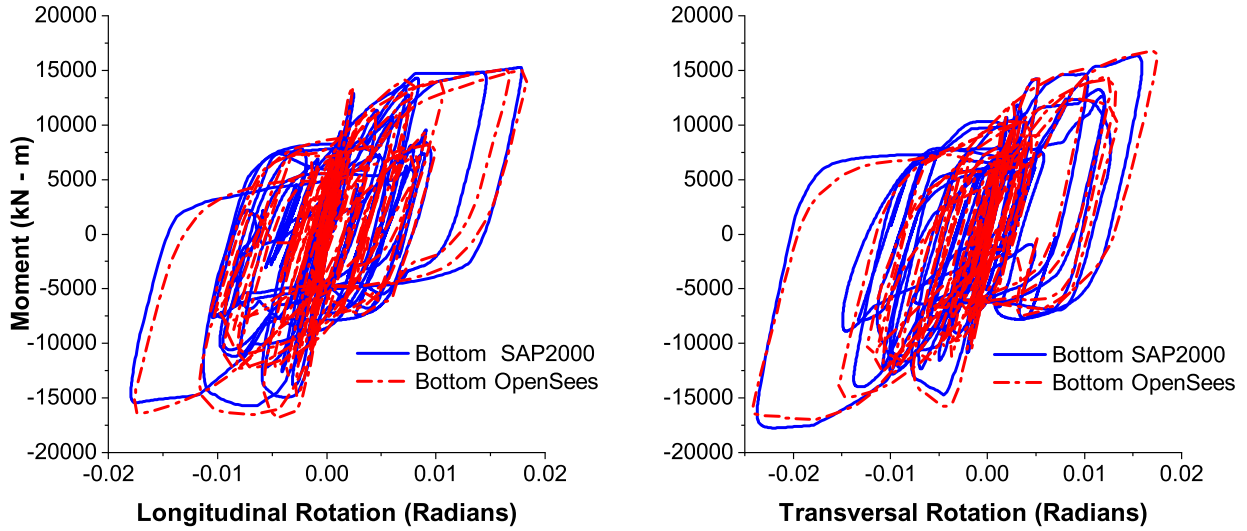


(b) Bottom

Figure 2.16: OSB2-MS column top and bottom moment-rotation responses for ground motion CLAYN1N1.
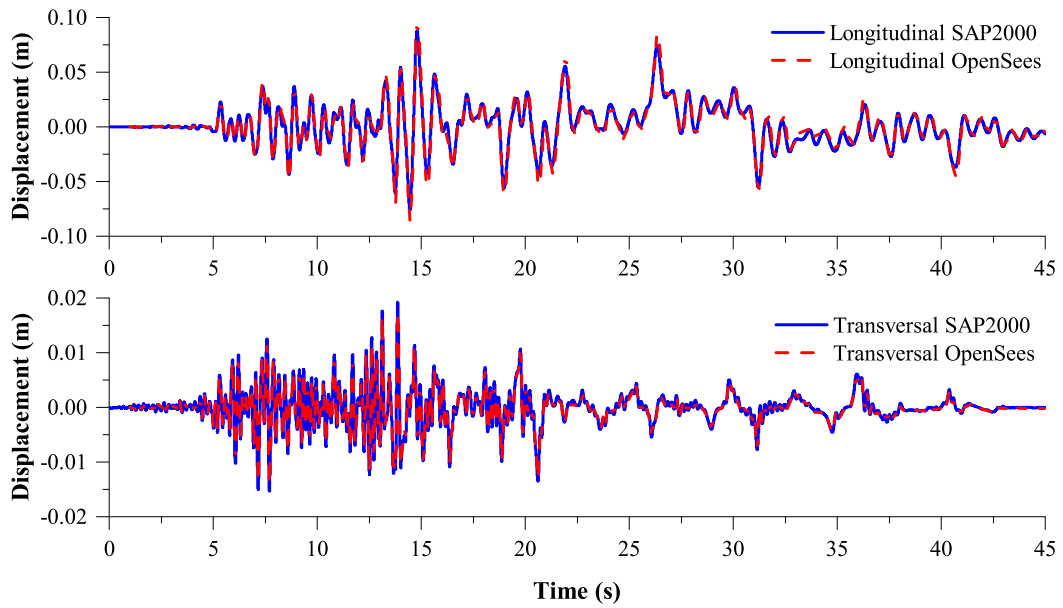
(a) Center of mass displacement time history
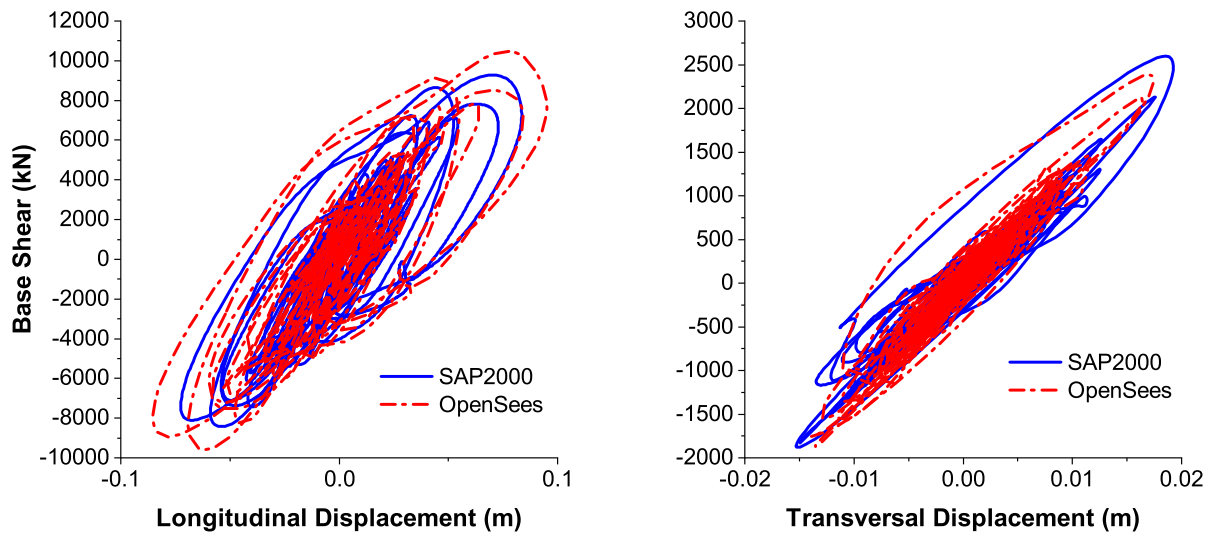


(b) Base shear vs displacement at the top of the column

Figure 2.17: OSB2-MO responses for ground motion CLAYN1N1.
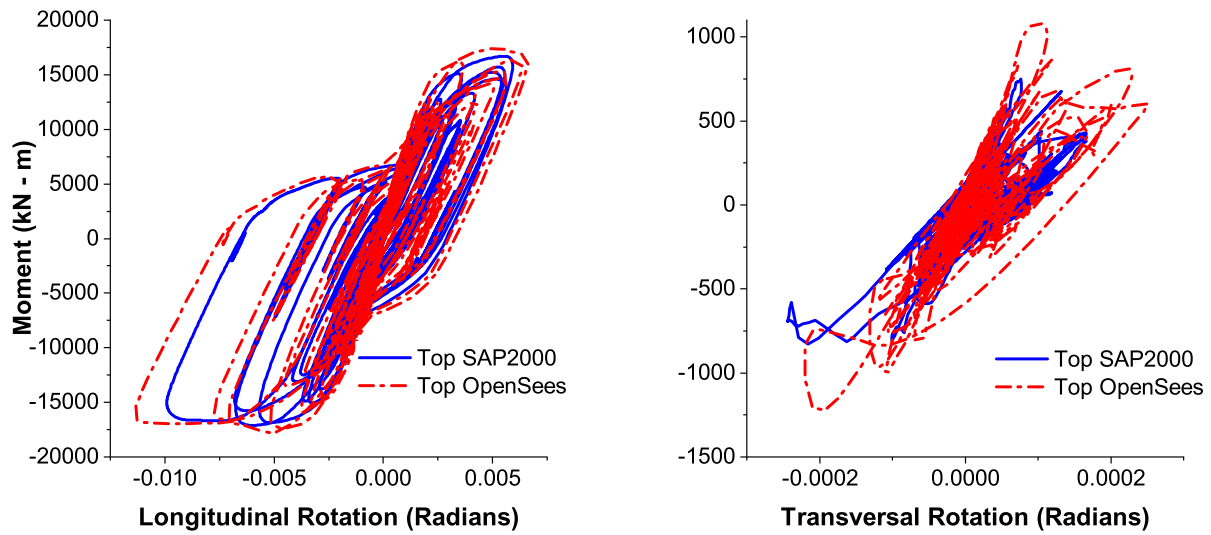
(a) Top
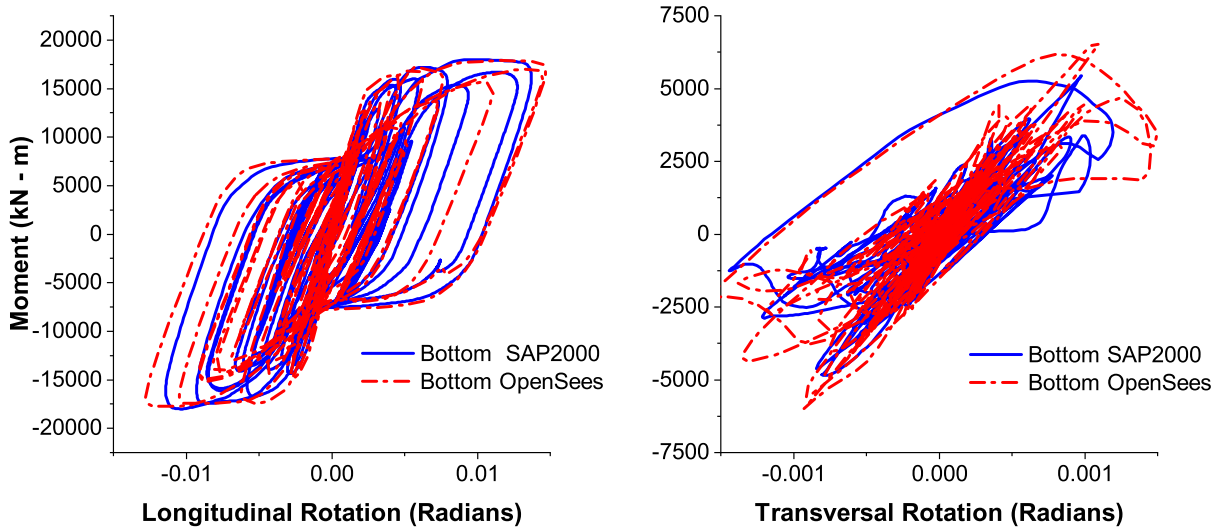


(b) Bottom

Figure 2.18: OSB2-MO column top and bottom moment-rotation responses for ground motion CLAYN1N1.

2017). The modifications done over the OSB1 models increased the columns stiffness, concluding in less deformations for OSB1-MS. However, the abutment modifications added elasticity to the model, providing more displacement to OSB1-MO. On the other hand, OSB2-MO peak displacements were very close to OSB2-O values. The results achieved after improving OSB1-O and OSB2-O models determined a better agreement between both OpenSees and SAP2000, reducing the peak response variation under different ground motions.

After analyzing and comparing the different responses obtained using the roller and the abutment models, the study shows a small bias developed by the difference in the hysteresis rule for the concrete in columns assumed for both softwares. This variance is illustrated in the results achieved by the roller models, where the abutments are not affecting the responses. While comparing the OSB1-O models, the analysis reflects a high bias which was totally removed after adding gaps in the corners of the deck for OSB1-MO models. Therefore, the link used in OpenSees has a similar behavior than the composite abutment improved in OSB1's SAP2000 model. On the other hand, OSB2-S models had a huge bias which was corrected after modifying the hinge length in the OSB2-MS models. Since both SAP2000 and OpenSees OSB2 models considered gaps in the corners of the deck, no bias was induced by the abutment considerations.

The values were compared using the bias factor formulation used by Aviram (2008) for short bridges and the ratios are illustrated in the Tables 2.8 and 2.9. The NTHA bias factors were obtained normalizing the SAP2000 peak displacement by the corresponding OpenSees values, concluding in a better agreement than Aviram's factors for bridges under high hazard seismic levels and applying a pair-wise comparison and averaging method (Aviram et al., 2008).

Table 2.6: Longitudinal peak displacement values

| Model | CLAYN1N1 | | | ROCKN1N1 | | | SANDN1N1 | | |
| | SAP Ux (m) | OpenSees Ux (m) | Δ (%) | SAP Ux (m) | OpenSees Ux (m) | Δ (%) | SAP Ux (m) | OpenSees Ux (m) | Δ (%) |
|---|---|---|---|---|---|---|---|---|---|
| OSB1-O | 0.120 | 0.145 | 20.8 | -0.032 | -0.035 | -9.2 | 0.071 | 0.096 | -36.6 |
| OSB1-S | 0.318 | 0.268 | 15.7 | -0.233 | -0.199 | 14.5 | 0.180 | 0.151 | 16.2 |
| OSB1-MO | 0.190 | 0.191 | -0.12 | 0.088 | 0.084 | 4.53 | -0.111 | -0.119 | -7.25 |
| OSB1-MS | 0.252 | 0.245 | 2.83 | -0.177 | -0.153 | 10.24 | -0.135 | -0.129 | 4.4 |
| | | | | | | | | | |
| OSB2-O | 0.082 | 0.078 | 5.0 | 0.042 | 0.050 | -18.4 | 0.067 | 0.068 | -1.1 |
| OSB2-S | 0.125 | 0.076 | 39.2 | -0.036 | -0.039 | -5.9 | 0.054 | 0.054 | -1.4 |
| OSB2-MO | 0.088 | 0.095 | -8.7 | -0.039 | -0.042 | -8.0 | 0.062 | 0.061 | -0.09 |
| OSB2-MS | 0.102 | 0.105 | -2.3 | -0.040 | -0.044 | -7.7 | 0.061 | 0.064 | -3.39 |

Table 2.7: Transversal peak displacement values

| Model | CLAYN1N1 | | | ROCKN1N1 | | | SANDN1N1 | | |
| | SAP Uy (m) | OpenSees Uy (m) | Δ (%) | SAP Uy (m) | OpenSees Uy (m) | Δ (%) | SAP Uy (m) | OpenSees Uy (m) | Δ (%) |
|---|---|---|---|---|---|---|---|---|---|
| OSB1-O | -0.122 | -0.120 | 1.7 | -0.077 | -0.082 | -7.1 | 0.137 | 0.138 | -0.85 |
| OSB1-S | -0.289 | -0.236 | 18.2 | -0.099 | -0.086 | 12.8 | 0.206 | 0.198 | 3.91 |
| OSB1-MO | -0.121 | -0.117 | 2.55 | -0.071 | -0.075 | -5.19 | 0.124 | 0.119 | 3.72 |
| OSB1-MS | -0.229 | -0.193 | 9.36 | -0.080 | -0.078 | 2.44 | 0.192 | 0.174 | 9.31 |
| | | | | | | | | | |
| OSB2-O | 0.025 | 0.039 | -55.0 | -0.030 | -0.028 | 7.8 | -0.039 | -0.048 | -23.3 |
| OSB2-S | -0.142 | -0.089 | 37.5 | -0.053 | -0.052 | 2.3 | 0.107 | 0.094 | 12.49 |
| OSB2-MO | 0.019 | 0.017 | 9.5 | -0.018 | -0.016 | 9.4 | -0.027 | -0.025 | 7.96 |
| OSB2-MS | -0.133 | -0.134 | -1.5 | -0.056 | -0.062 | -11.0 | 0.141 | 0.147 | -4.3 |

Table 2.8: Longitudinal peak displacement bias factors

| Model | NTHA Bias Factor | | | Aviram Bias Factor |
|---|---|---|---|---|
| | CLAYN1N1 | ROCKN1N1 | SANDN1N1 | High Hazard Level |
| OSB1-O | 1.21 | 1.09 | 1.37 | |
| OSB1-S | 0.84 | 0.86 | 0.84 | 1.20 |
| OSB1-MO | 1.00 | 0.95 | 1.07 | |
| OSB1-MS | 0.97 | 0.90 | 0.96 | |
| | | | | |
| OSB2-O | 0.95 | 1.18 | 1.01 | |
| OSB2-S | 0.61 | 1.06 | 1.01 | 1.20 |
| OSB2-MO | 1.09 | 1.08 | 1.00 | |
| OSB2-MS | 1.02 | 1.08 | 1.03 | |

Table 2.9: Transversal peak displacement bias factors

| Model | NTHA Bias Factor | | | Aviram Bias Factor |
|---|---|---|---|---|
| | CLAYN1N1 | ROCKN1N1 | SANDN1N1 | High Hazard Level |
| OSB1-O | 0.98 | 1.07 | 1.01 | |
| OSB1-S | 0.82 | 0.87 | 0.96 | 1.20 |
| OSB1-MO | 0.97 | 1.06 | 0.95 | |
| OSB1-MS | 0.81 | 0.96 | 0.91 | |
| | | | | |
| OSB2-O | 1.55 | 0.92 | 1.23 | |
| OSB2-S | 0.63 | 0.98 | 0.88 | 1.20 |
| OSB2-MO | 0.91 | 0.91 | 0.92 | |
| OSB2-MS | 1.02 | 1.11 | 1.04 | |

# CHAPTER 3: NONLINEAR RESPONSE HISTORY SENSITIVITY ANALYSIS OF TYPICAL HIGHWAY BRIDGES.

The content of the current chapter is based on the journal paper *Nonlinear response history sensitivity analysis of typical highway bridges* by Rodriguez A. F., Mackie K. R., and Scott M. H., which is being prepared for its submission.

## 3.1 Bridge sensitivity analysis

The models under analysis contemplated the specifications provided by Caltrans and the improvement obtained in chapter 2 (OSB1-MO and OSB2-MO). The analysis was developed using the original abutment models to reflect field real condition. The analysis was focused to the static and dynamic response of the bridges with nonlinear elements. The sensitivity analysis was developed using the FDM, which computes a deterministic bridge response and compares it with the behavior after perturbing a specific value. Therefore, the calculations were done considering the change in the responses of the properties forward and backward compared with the original value and applying the second-order central difference theory over the results obtained. On the other hand, the change in the hysteresis type assumption would represent only one final response in the nonlinear time history analysis, which means that the hysteresis type sensitivity analysis must be obtained using the first-order forward finite difference method between the original condition and the new consideration.

### 3.1.1 *Parameters*

To establish an accurate result, the sensitivity analysis included the bridges most relevant parameters, which could strongly affect the response of the nonlinear time history. Different $\Delta\theta$ were assumed as coefficient of variation of the parameters, affecting the properties forward and

Table 3.1: Parameters considered for the sensitivity analysis.

| Parameter | Unit | $\Delta\theta$ | OSB1-MO | OSB2-MO |
|---|---|---|---|---|
| Column Diameter | m | 2% | 1.68 | 1.68 |
| Concrete Strength | MPa | 15% | 24.80 | 27.60 |
| Steel Yield Strength | MPa | 10% | 413.68 | 413.68 |
| Longitudinal Abutment Effective Stiffness | MPa/m | 15% | 459827 | 311900 |
| Longitudinal Abutment Strength | kN | 15% | 6894.74 | 4586 |
| Superstructure Elastic Modulus | GPa | 20% | 23.6 | 23.6 |

backward (increasing or decreasing the property value). The bridges were analyzed with these modified properties, obtaining the maximum and minimum boundary responses. Those parameters are enlisted in the Table 3.1. The original bridge hysteresis combination type was defined as Takeda for the concrete elements and Kinematic for the A615Gr60 steel. Therefore, the hysteresis type sensitivity analysis was developed by changing the original combination to Concrete/Kinematic and Concrete/Takeda.

### 3.1.2 Static analysis

The pushover analysis was done considering the modified and simplified roller abutment boundary case OSB1-MS and OSB2-MS described in the chapter 5 to isolate the effects of the bent and the column models from the abutments. A single reference load of 444.82 kN was applied at the monitoring point for the longitudinal and transverse analysis. The nonlinear analysis was done with a displacement control monitored at 0.38 m. The longitudinal pushover curves for OSB1-MS and OSB2-MS with the corresponding forward and backward perturbed fy responses are described in the Figure 3.1. The results show no sensitivity before the yielding point for both bridges. After yielding, the models tend to generate a sensitivity response due to changes over the steel yield strength. The sensitivity analysis done over the structures parameters is described in the Figure 3.1. The figures illustrate a high sensitivity of the models to the column steel yield strength and
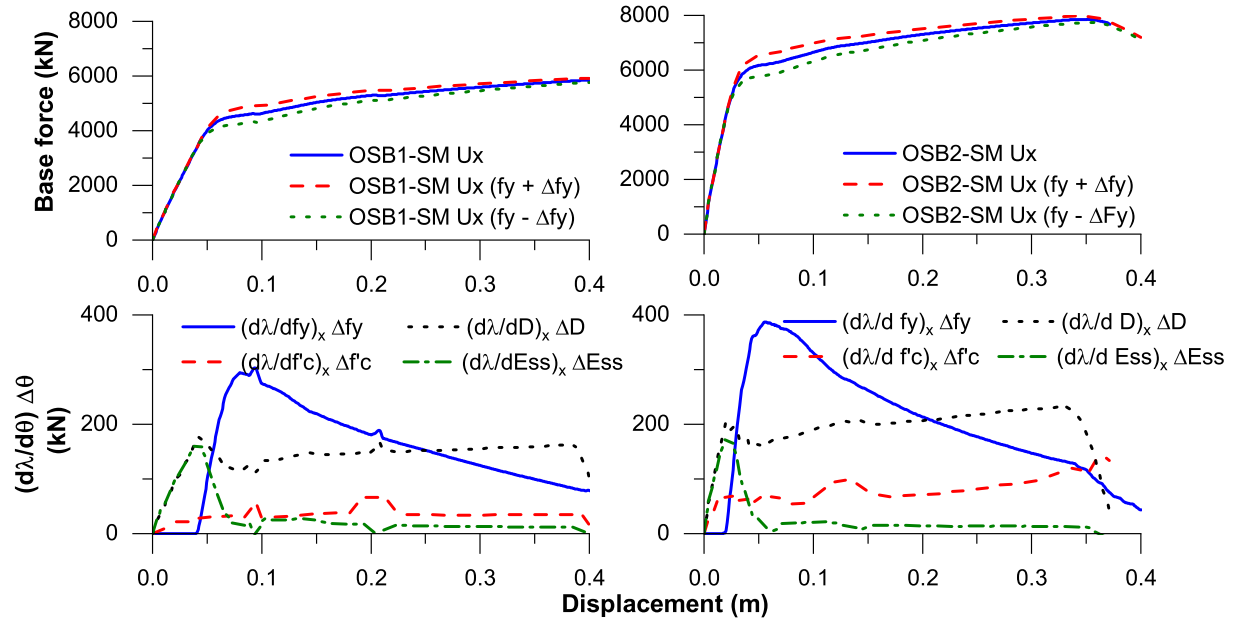
Figure 3.1: OSB-MS static sensitivity analysis for longitudinal axis.

Table 3.2: Peak sensitivity results for static analysis.

| Parameter | OSB1-MS | | | OSB2-MS | | |
|---|---|---|---|---|---|---|
| | Peak Value | | Displacement | Peak Value | | Displacement |
| | (kN) | (%) | (m) | (kN) | (%) | (m) |
| Column Diameter | 175.79 | 3.81 | 0.04 | 232.55 | 3.76 | 0.33 |
| Concrete Strength | 68.19 | 1.48 | 0.19 | 140.34 | 2.27 | 0.37 |
| Steel Yield Strength | 303.45 | 6.57 | 0.12 | 387.35 | 6.26 | 0.06 |
| Superstructure Elastic Modulus | 171.79 | 3.72 | 0.04 | 176.55 | 2.85 | 0.02 |

the superstructure Young's Modulus near to the yielding point. Even though concrete strength and column diameter reached the peak sensitivity value at the yielding point for OSB1-MS, the highest values for OSB2-MS were obtained after 0.30 m of displacement. The Table 3.2 summarizes the peak values obtained for each model normalized by a yielding strength of the undisturbed structure equals to 4618.6 kN and 6190.1 kN for OSB1-MS and OSB2-MS respectively.

### 3.1.3 Nonlinear time history analysis

The dynamic response was obtained applying two lateral orthogonal components to the bridges along the longitudinal and transverse direction. The nonlinear time history analysis was performed using the recorded ground motion acceleration CLAYN1N1 (Lu et al., 2015) , while some parameters were modified to establish the sensitivity of bridges under the same ground motion. The corresponding ground motion acceleration time history properties and ground acceleration records for CLAYN1N1 ground motion are shown in the Table 2.5. The strong motion duration was obtained based on the standard Arias 5-95 bounds (Mackie et al., 2017, p. 116).

The dynamic analysis was done considering a damping ratio of 0.05, which for OSB1-MO was defined at periods of 1.2 and 0.7 seconds. Periods of 0.889 and 0.692 were found for OSB2-MO using the same damping ratio of 0.05. The time integration scheme employed was Hilber-Hughes-Taylor method, considering $\gamma = 0.5$, $\beta = 0.25$, and $\alpha = 0$. The mass proportional coefficients were 0.3307 and 0.3974 for OSB1-MO and OSB2-MO respectively. Same values were used in the chapter 2 (Time History Analysis of Bridges Incorporating Nonlinear Elements), obtaining similar responses for both OpenSees and SAP2000.

### 3.1.4 Response sensitivity analysis of OSB1-MO

The NTHA developed for each combination of hysteresis type are described in the Figure 3.2a. The behavior of the models describes the same path, but different peaks values. In addition, the sensitivity analysis for the hysteresis type assumption is represented by the Figure 3.2b. The analysis done for the hysteresis consideration reflects a high sensitivity response of the bridges to changes in the hysteresis assumptions for the concrete and the steel. During the first 6.0 s, the model shows an insensitivity behavior to the hysteresis change, while the biggest sensitivity values are obtained between 25 and 38 s. The Concrete/Kinematic combination concluded in a peak difference value of 0.0392 m for the longitudinal direction, while the Concrete/Takeda combina-
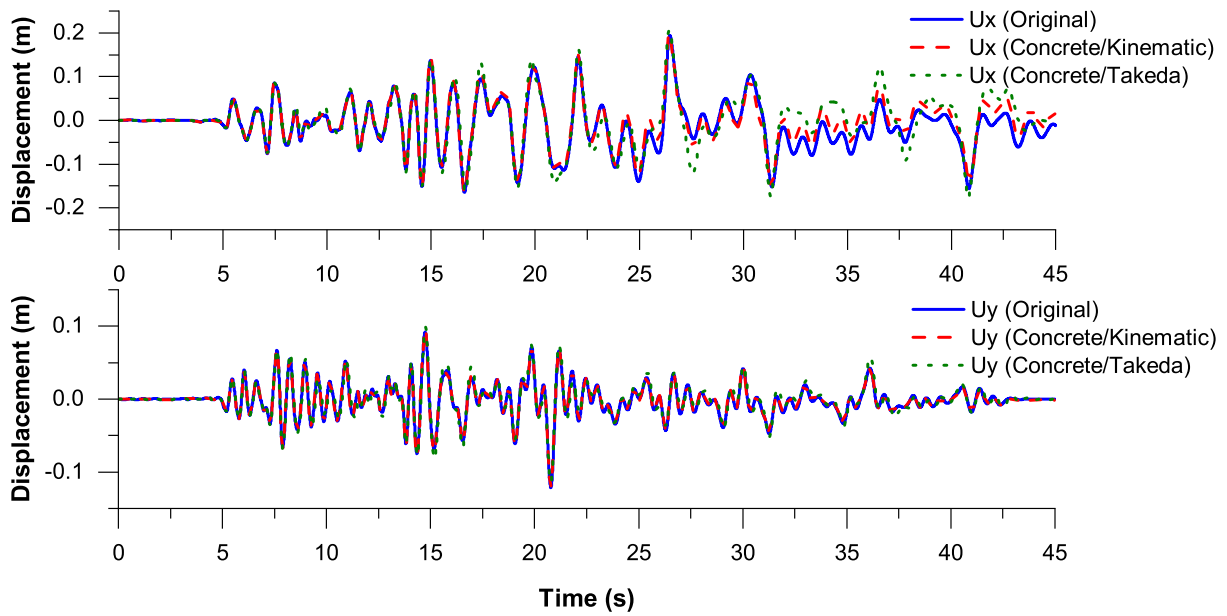
Table 3.3: OSB1-MO peak sensitivity results for hysteresis type.

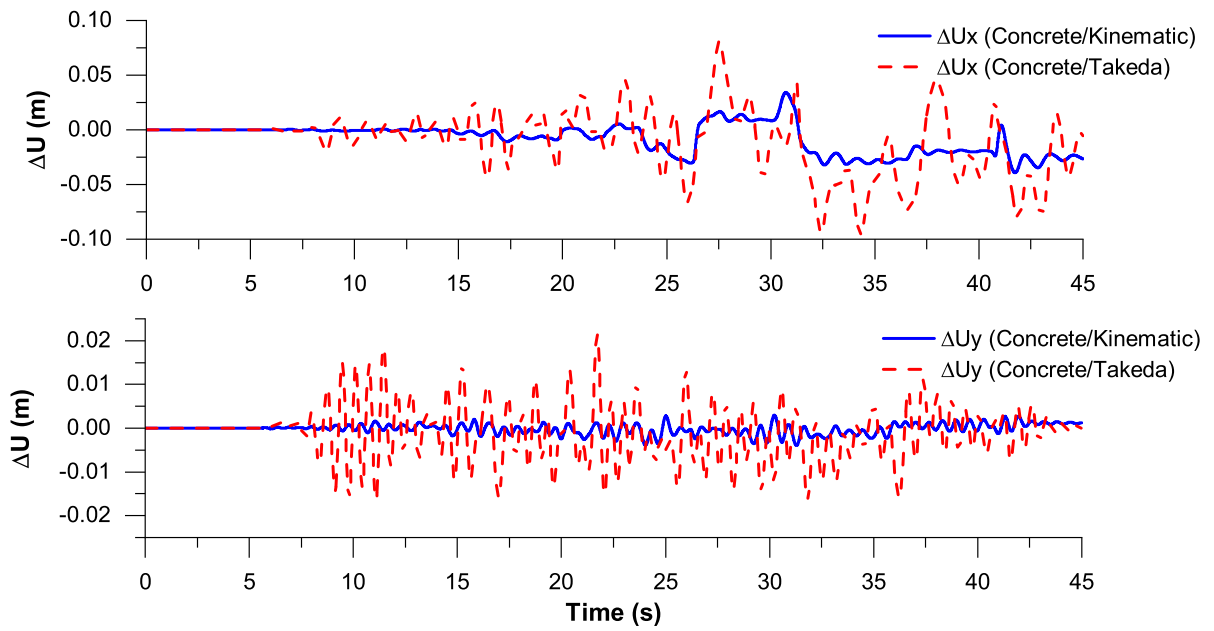| Hysteresis type | Longitudinal | | | Transversal | | |
|---|---|---|---|---|---|---|
| | $\Delta u$ (m) | $\Delta u$ (%) | t (sec) | $\Delta u$ (m) | $\Delta u$ (%) | t (sec) |
| Concrete/Kinematic | -0.0392 | 20.3 | 41.73 | -0.0039 | 3.3 | 31.28 |
| Concrete/Takeda | 0.0803 | 41.5 | 27.52 | 0.0214 | 17.7 | 21.75 |

tion had a peak difference of 0.0803 m, representing a 20.3% and 41.5% of the original NTHA peak value respectively. The sensitivity of the deck displacement to the hysteresis changes in the transversal direction is lower than the longitudinal, but still important when the changes in the steel reinforcement hysteresis behavior are considered. The peak values obtained in the sensitivity analysis for the hysteresis cases are illustrated in the Table 3.3. It is important to note that the Concrete hysteresis type was recently incorporated in the newest SAP2000 versions. Before this, the software only considered Takeda, Kinematic, and Elastic hysteresis types for the nonlinear analysis.

The sensitivity analysis done by central difference method concluded that the chosen nonlinear parameters have an important incidence in the longitudinal displacement of the superstructure. The Figure 3.3 describes the displacement sensitivity to the modification of each parameter under the seismic load by separately. The bridge response shows an unsensitive behavior to changes in the parameters during the first seconds of the seismic load. After 5 seconds, the column and superstructure parameters describe sensitive responses while the abutment considerations reflect changes after 7 seconds. The most sensitive responses are obtained between 24 and 40 seconds for the column and superstructure parameters, while the peak sensitive response for the abutment are found between 14 to 26 seconds. The perturbation done over the steel yield strength generated a peak difference of -0.0272m in the center of mass displacement, while the longitudinal abutment strength variation induced a maximum variation of -0.0146m, representing a 14.1% and 7.5% of the peak displacement of the original NTHA response respectively. In the transversal

(a) Hysteresis type NTHA.



(b) Sensitivity for hysteresis type.

Figure 3.2: OSB1-MO Sensitivity response for hysteresis type.

Table 3.4: OSB1-MO peak sensitivity results for bridge nonlinear parameters.

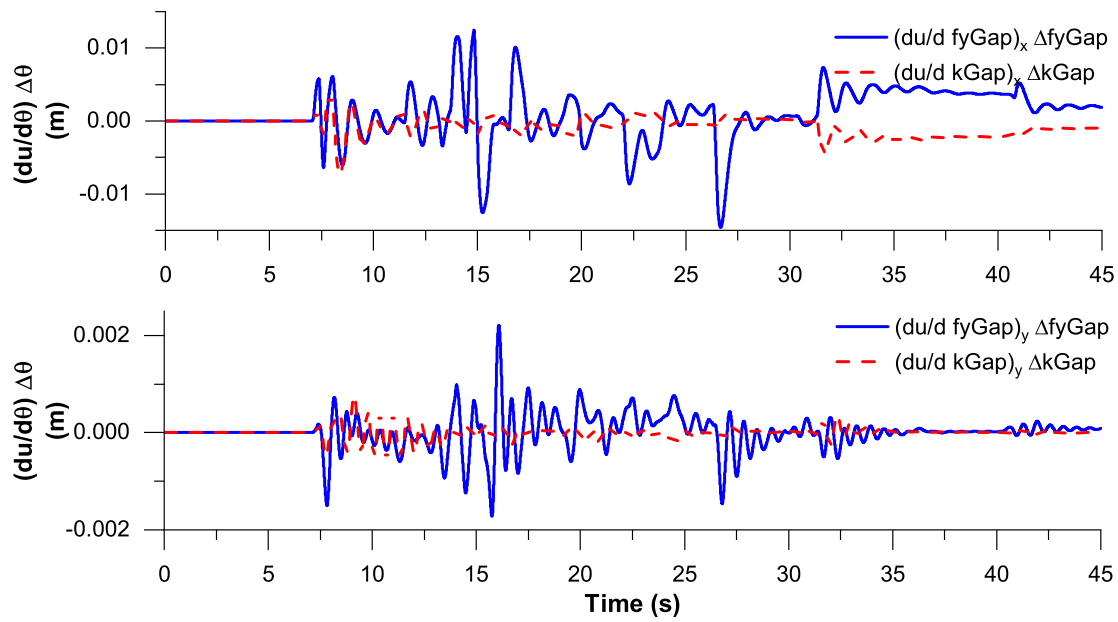| Hysteresis type | Longitudinal | | | Transversal | | |
|---|---|---|---|---|---|---|
| | $\Delta$u (m) | $\Delta$u (%) | t (sec) | $\Delta$u (m) | $\Delta$u (%) | t (sec) |
| Column Diameter | 0.0181 | 9.3 | 31.3 | -0.0073 | 6.0 | 10.98 |
| Concrete Strength | 0.0137 | 7.1 | 24.16 | 0.0038 | 3.1 | 15.25 |
| Steel Yield Strength | -0.0272 | 14.1 | 36.96 | 0.0042 | 3.4 | 15.33 |
| Longitudinal Abutment Effective Stiffness | -0.0072 | 3.7 | 8.38 | 0.0074 | 0.6 | 9.13 |
| Longitudinal Abutment Strength | -0.0146 | 7.5 | 26.67 | 0.0022 | 1.8 | 16.07 |
| Superstructure Elastic Modulus | -0.0250 | 12.9 | 31.61 | -0.0028 | 2.3 | 20.11 |

direction, the sensitivity results are very low, with a small incidence in the deck displacement. The peak values obtained in the sensitivity analysis are shown in the Table 3.4.

### 3.1.5   *Response sensitivity analysis of OSB2-MO*

OSB2-MO model was analyzed under the same criteria used for OSB1-MO. The Figure 3.4a describes the original NTHA compared with each hysteresis type combination. The Figure 3.4b illustrates the sensitivity analysis done over changes in the concrete and steel reinforcement hysteresis type assumptions. A high sensitivity response of the bridge to modifications in the hysteresis behavior was found during the analysis. The model shows an insensitive behavior during the first 7.5 seconds. The highest sensitivity values are developed between 15 to 32 seconds in the longitudinal direction. The Concrete/Kinematic combination concluded in a peak difference value of 0.0058m in the longitudinal direction representing a 6.6% of the NTHA maximum value. On the other hand, the Concrete/Takeda combination registered higher values, with a peak difference of 0.0282m and a 32.3% of the original NTHA peak displacement. The transversal direction describes fewer sensitive responses in the center of mass displacement due to changes in the hysteresis type consideration. It is noted that the bridge is very sensitive to changes in the
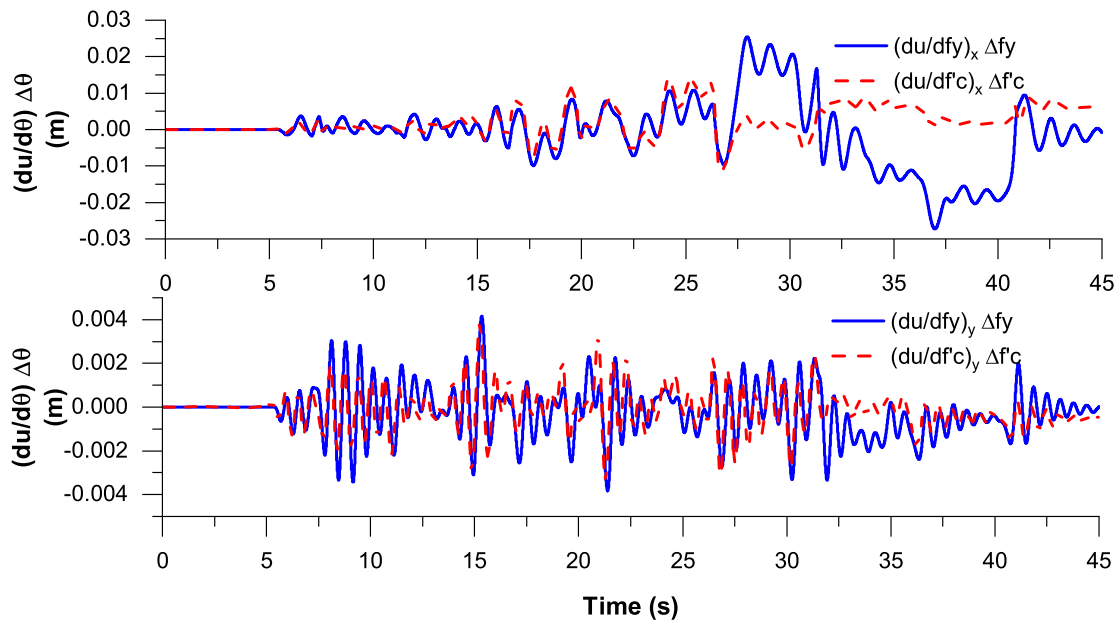
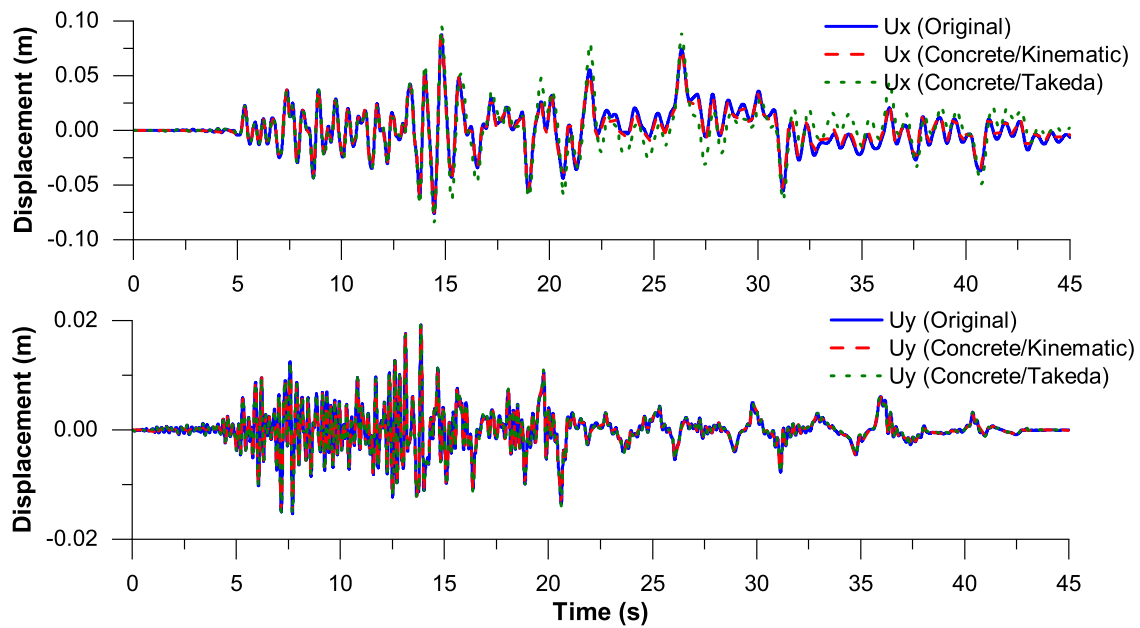(a) Structure Sensitivity.



(b) Abutment Sensitivity.

Figure 3.3: OSB1-MO Properties Sensitivity.

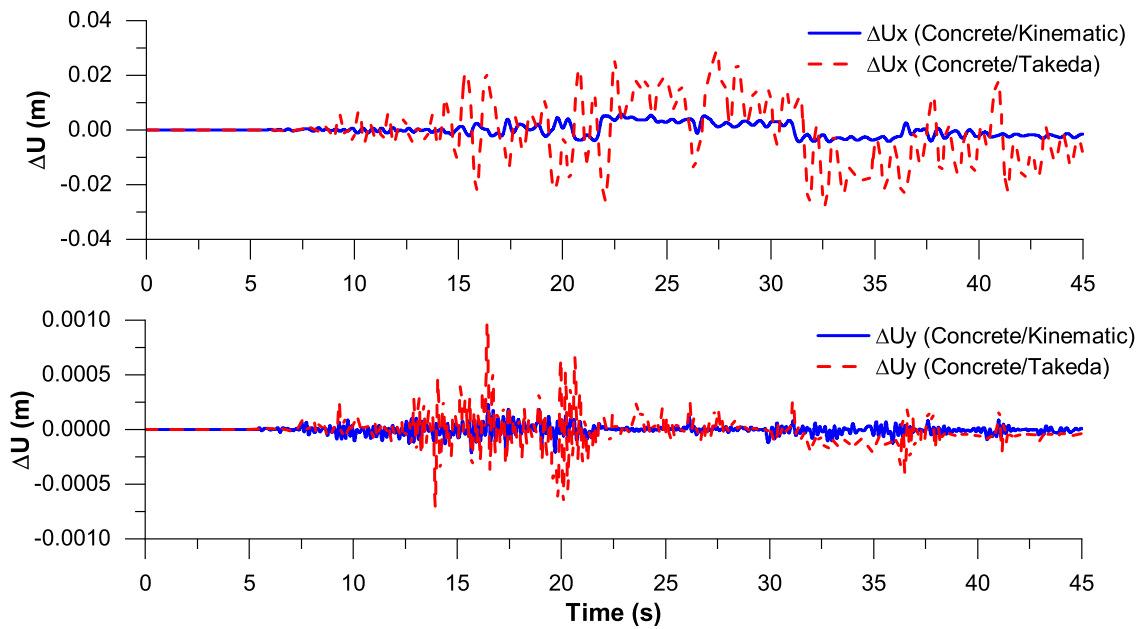Table 3.5: OSB2-MO Peak sensitivity results for hysteresis type.

| Hysteresis type | Longitudinal | | | Transversal | | |
|---|---|---|---|---|---|---|
| | $\Delta u$ (m) | $\Delta u$ (%) | t (sec) | $\Delta u$ (m) | $\Delta u$ (%) | t (sec) |
| Concrete/Kinematic | 0.0058 | 6.6 | 22.80 | 0.0002 | 1.2 | 16.48 |
| Concrete/Takeda | 0.0282 | 32.3 | 27.37 | 0.001 | 5.0 | 16.43 |

steel reinforcement hysteresis type assumptions, while changes in the concrete nonlinear behavior have less impact in the displacement response. Table 3.5 summarize the maximum values achieved during the sensitivity analysis for the hysteresis types.

The Figure 3.5 describes the displacement sensitivity to the modification of each parameter under the seismic load by separately. The model describes an insensitive response to changes in the columns and superstructure parameters during the first 5 seconds of the imposed seismic load, while changes in the displacement values start to appear after 13 seconds when we modify the abutment parameters. The bridge showed a highly sensitive response in the longitudinal direction between 14 to 16 seconds when the columns, superstructure, and abutment parameters are modified. The changes done over the concrete strength concluded in a peak difference of -0.0082m which represents a 7.2% of the maximum displacement obtained in the original NTHA. After perturbing the longitudinal abutment strength, the peak difference obtained in the deck longitudinal displacement was -0.001452m, which is near to a 5.9% of the maximum peak displacement of the bridge center of mass in the unperturbed model. On the other hand, the bridge shows an insensitive behavior in the transversal direction, resulting in a low variation of the displacement, except for the superstructure elastic modulus, which seems to be very sensitive to changes. Table 3.6 contains the peak values obtained during the analysis.
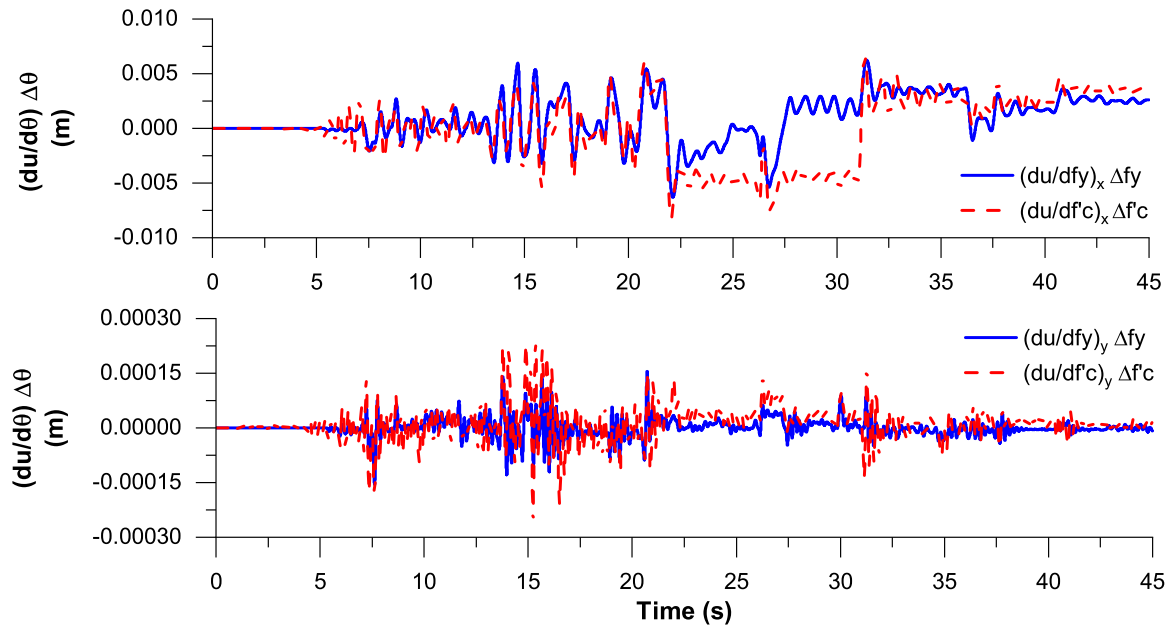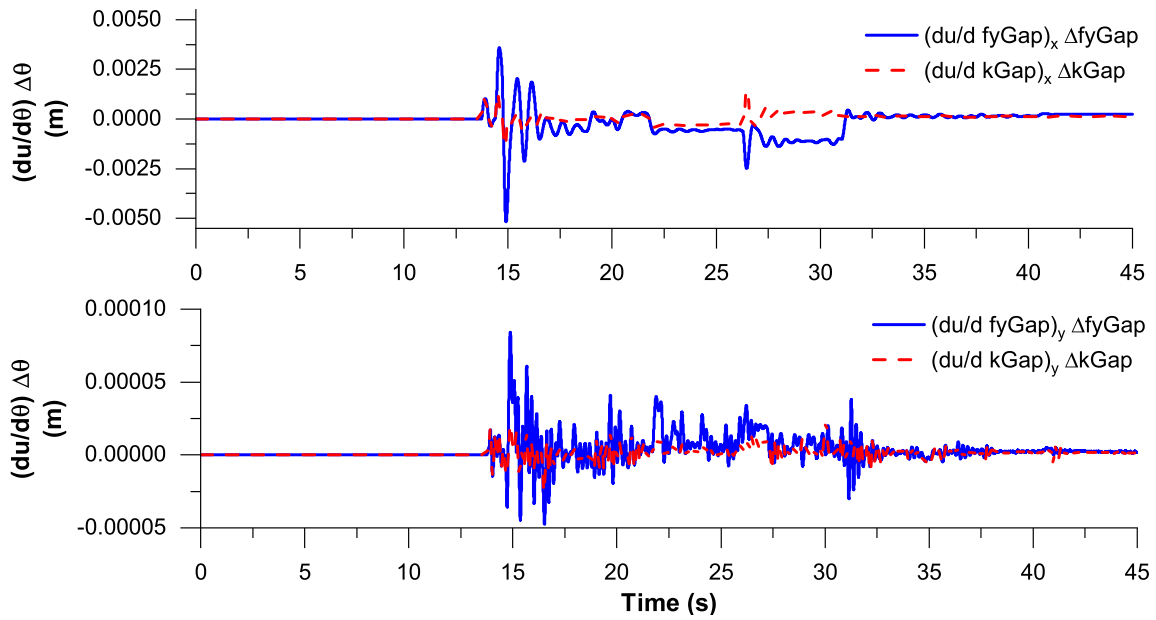
(a) Hysteresis type NTHA.



(b) Sensitivity for hysteresis type.

Figure 3.4: OSB2-MO Sensitivity response for hysteresis type.

(a) Structure Sensitivity.



(b) Abutment Sensitivity.

Figure 3.5: OSB2-MO Properties Sensitivity.

Table 3.6: OSB2-MO peak sensitivity results for bridge nonlinear parameters.

| Hysteresis type | Longitudinal | | | Transversal | | |
|---|---|---|---|---|---|---|
| | $\Delta$u (m) | $\Delta$u (%) | t (sec) | $\Delta$u (m) | $\Delta$u (%) | t (sec) |
| Column Diameter | -0.0077 | 8.8 | 22.03 | -0.00046 | 2.4 | 7.61 |
| Concrete Strength | -0.0082 | 9.3 | 22.03 | -0.00026 | 1.3 | 15.22 |
| Steel Yield Strength | -0.0063 | 7.2 | 22.11 | 0.00015 | 0.8 | 20.71 |
| Longitudinal Abutment Effective Stiffness | 0.0014 | 1.6 | 26.47 | -0.00003 | 0.1 | 16.51 |
| Longitudinal Abutment Strength | -0.0052 | 5.9 | 14.89 | 0.00008 | 0.4 | 14.87 |
| Superstructure Elastic Modulus | 0.0248 | 28.3 | 15.44 | 0.00739 | 38.4 | 7.75 |

## 3.2    Sensitivity Analysis summary

The research described the different properties and conditions employed to define Caltrans OSB1-MO and OSB2-MO models in SAP2000 according to the benchmark bridges. A deterministic Pushover analysis and NTHA were achieved and compared with the response obtained using the same properties and considerations in OpenSees, obtaining an excellent agreement between programs. The FDM was applied over the previous calibrated model, perturbing forward and backward specific nonlinear parameters with an established $\Delta\theta$ to obtain the bridge sensitivity to the change of each main property. The results show that OSB1-MO is much more sensitive than OSB2-MO to changes in the nonlinear parameters when is subjected to seismic loads. Both bridges concluded in high sensitivities responses in the longitudinal direction.

# CHAPTER 4: HYSTERETIC BEHAVIORS AND THEIR IMPACT IN THE RESPONSES

In this chapter, the study was focused on the analysis of the hysteretic behavior and their impact in the responses of single degree of freedom models under different ground motions. Based on different natural vibration periods ($Tn$) some linear elastic, elastoplastic, and softening models were developed to conform a constant-ductility response spectrum. An statistical analysis based on probability density function was conducted to obtain the bias in the responses after considering different hysteretic rules. Finally, a fast Fourier transform analysis is done to establish effect of the hysteretic considerations o the linear elastic natural vibration period.

## 4.1  Ground motions

The time history analysis was performed using CLAYN1N1000, CLAYN1N1090, ROCK N1N1000, and SANDN1N1000 ground motion accelerations (Lu et al., 2015). The strong motion duration was obtained based on the standard Arias 5-95 bounds (Mackie et al., 2017). Each lateral component of excitation was applied to the SDOF to obtain the corresponding peak displacements for the linear elastic consideration. The ground motion acceleration properties components are shown in Table 4.1, while the recorded ground motions are illustrated in the Appendix A.

Table 4.1: Ground motion acceleration time history properties.

| Component | SMD (s) | PGA (g) | PGV (cm/s) | PGD (cm) |
|---|---|---|---|---|
| CLAYN1N1000 | 30.4 | 0.706 | 108 | 95.9 |
| CLAYN1N1090 | 29.1 | 0.788 | 104 | 57.7 |
| ROCKN1N1000 | 15.0 | 0.399 | 59.2 | 25.7 |
| SANDN1N1000 | 37.0 | 0.784 | 86.3 | 33.3 |

## 4.2 Linear responses

An elastic model was defined to compare the peak deformation caused by the earthquake ground motions and the maximum response obtained on an elastoplaticity SDOF system under the same excitation. The stiffness ($k$) were obtained considering a constant mass of 175.12 kN-s$^2$/m (1 kip-s$^2$/in) and natural periods ($T_n$) between 0.10 s and 10.00 s using the equation for periodic motion. The damping was assumed equals to 1%.

The responses obtained for the linear elastic systems under CLAYN1N1000 ground motion are described in the Figure 4.2 for different values of $Tn$ and stiffness ($k$). Values were obtained using Newmark iteration method, considering $\beta$ and $\gamma$ coefficients equals to 0.25 and 0.5, respectively.

## 4.3 Single degree of freedom constitutive models

Using the linear elastic responses, the elastoplastic and softening SDOF systems were conformed for different ductility factors, natural periods, and stiffness. The SDOF models were defined with the same stiffness during the initial loading path obtained for the linear elastic models. The same mass and damping used to define the linear elastic systems were assumed for both, elastoplastic and softening model. Therefore, under small oscillations, all the models had the same natural vibration period Tn. The Figure 4.1 illustrates the SDOF models for $T_n$ = 0.9 s and $\mu$ = 1, 2, 4, 8, and 10 under specific ground motion.

## 4.4 Constant ductility response spectrum

A response spectrum was done based on the elastoplastic systems previously described for specified levels of ductility factor, using a $\zeta$ = 1%, under CLAYN1N1000 ground motion, and Kinematic hysteretic rule. For different values of $T_n$, the exact response $u(t)$ of the linear elastic systems were obtained. Using those values, the peak deformations ($u_o$) and the peak force ($f_o$)
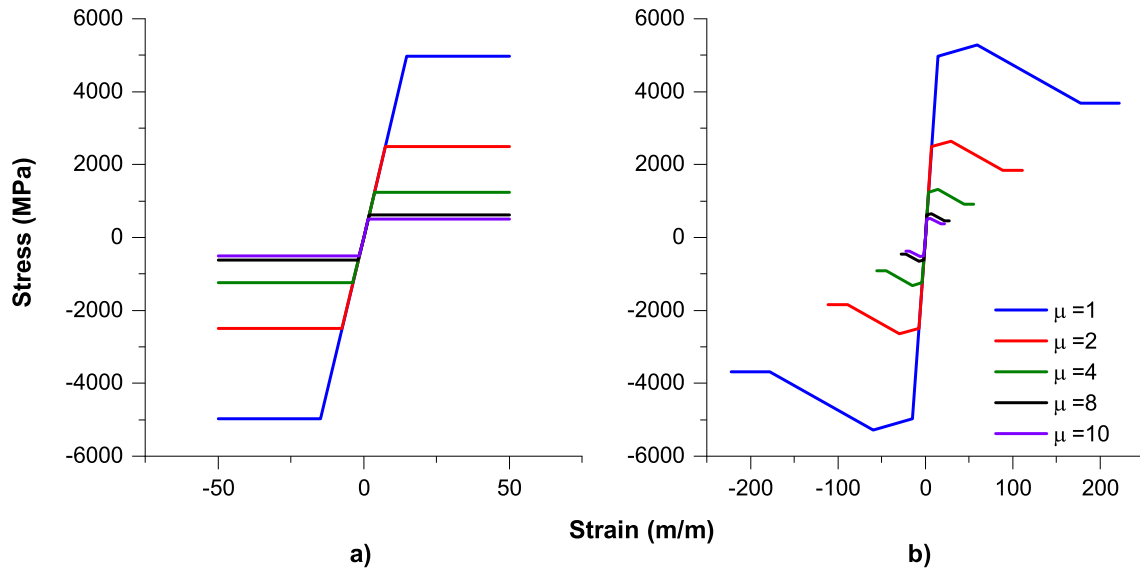
Figure 4.1: SDOF Material definition for $\mu$ = 1, 2, 4, 8, and 10 under CLAYN1N1000 ground motions, and Tn = 0.9s: a) Elastoplasticity; b) Softening.

were achieved for each case. The same values were obtained for the corresponding yielding forces associated to different ductility factors (Chopra, 2012). The Figure 4.2 shows the constant ductility response spectrum obtained. The Appendix C contains the normalized strength ($fy'$) vs ductility factor $\mu$ and reduction factor ($R_y$) plots used to achieve the response spectrum.

### 4.5   Predictions based on constant ductility response spectrum

Using the constant ductility response spectrum described in The Figure 4.2, some responses were predicted for different values of natural vibration periods and were compared with their corresponding SDOF system under the same hysteretic behavior. The analysis done describes a bias under 10% for 0.3s $\leq$ Tn $\leq$ 4.0s and 1 $\leq$ $\mu$ $\leq$ 4, while the bias for ranges outside of these boundaries tends to be over 20%. The Table 4.2 describes the resulting bias for different periods under CLAYN1N1000 ground motion and kinematic hysteretic rule.
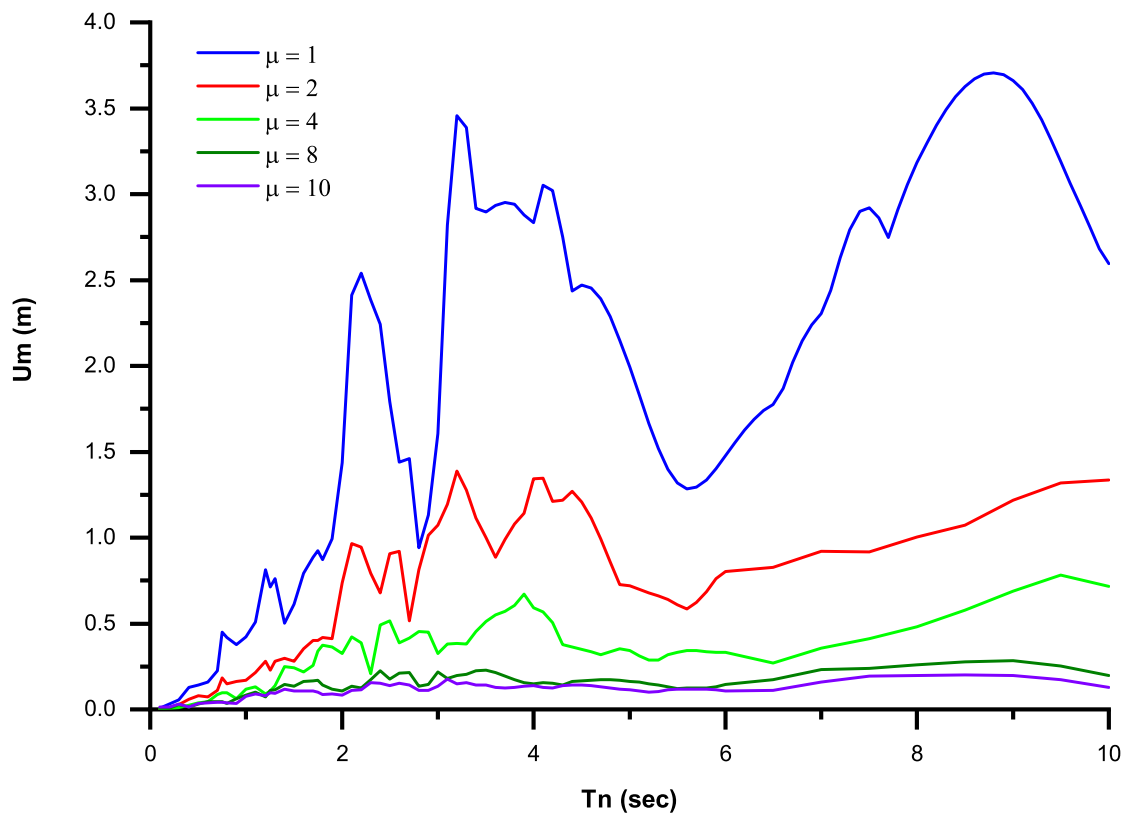
58

Figure 4.2: Constant-ductility response spectrum for elastoplastic systems and CLAY1N1000 ground motion; $\mu$ = 1, 2, 4, 8, and 10; $\zeta$ = 1%.

Table 4.2: Prediction bias for elastoplasticity systems under CLAYN1N1000 ground motion and Kinematic hysteretic rule

| $\mu$ | Tn (s) | | | | | | | |
|---|---|---|---|---|---|---|---|---|
| | 0.20 | 0.50 | 0.75 | 1.00 | 2.00 | 3.00 | 4.00 | 5.00 |
| 1 | 0.00% | 0.00% | 0.00% | 0.00% | 0.00% | 0.00% | 0.00% | 0.00% |
| 2 | -10.7% | -3.1% | -1.2% | -1.1% | -1.2% | 8.6% | 0.6% | -21.7% |
| 4 | -10.2% | -9.2% | 1.3% | 0.6% | 9.8% | -7.1% | 37.4% | -21.1% |
| 8 | 21.0% | 18.1% | -5.3% | 10.8% | -0.2% | 0.9% | -17.0% | 7.2% |
| 10 | 67.1% | 30.3% | -1.1% | 15.9% | 5.0% | -18.1% | 10.1% | 17.2% |

59

Table 4.3: Elastoplastic SDOF model peak displacements for $\mu = 2$ and Tn = 0.9s

| Hysteretic type | Peak displacements (m) | | | |
|---|---|---|---|---|
| | CLAYN1N1000 | CLAYN1N1090 | ROCKN1N1000 | SANDN1N1000 |
| Linear Elastic | 0.37 | 0.36 | 0.26 | 0.40 |
| Kinematic | 0.32 | 0.25 | 0.24 | 0.41 |
| Takeda | 0.29 | 0.28 | 0.21 | 0.32 |
| Isotropic | 0.32 | 0.25 | 0.24 | 0.41 |
| Degrading | 0.32 | 0.25 | 0.24 | 0.41 |
| BRB Hardening | 0.32 | 0.25 | 0.24 | 0.41 |
| Pivot | 0.28 | 0.27 | 0.20 | 0.33 |
| Elastic | 0.79 | 0.86 | 0.27 | 1.38 |
| Concrete | 0.75 | 1.13 | 0.25 | 0.79 |

## 4.6  Single degree of freedom peak values

The prediction was extended to analyze the effects of the hysterectic considerations over the elastoplastic and softening SDOF models under different ground motions. The elastoplastic models were analyzed assuming ductility factors equal to 2 and 8, while the softening model contemplated a $\mu$ equals to 2. The The Figures 4.3, 4.4, 4.5, and 4.6 show the responses obtained for the elastoplasticity SDOF system with a $\mu$ equals to 2 under a CLAYN1N1000, CLAYN1N1090, ROCKN1N1000, and SANDN1N1000 ground motions, while Tables 4.3, 4.4, and 4.5 summarize the peak displacements obtained for the models. The high bias presented in the Concrete and Elastic hysteretic types is attributed to their hysteresis loop definition, which allows more strain between the loading and unloading paths once the yielding occurs. Therefore, after the first substantial inelastic excursion is achieved (near to 15 seconds for figure 4.3), Concrete and Elastic hysteretic models describe more deformation compared with the other hysteretic rules. Figure 4.7 shows the hysteretic analysis at fiber level for each rule, using an elastoplastic SDOF model under CLAYN1N1000 ground motion.

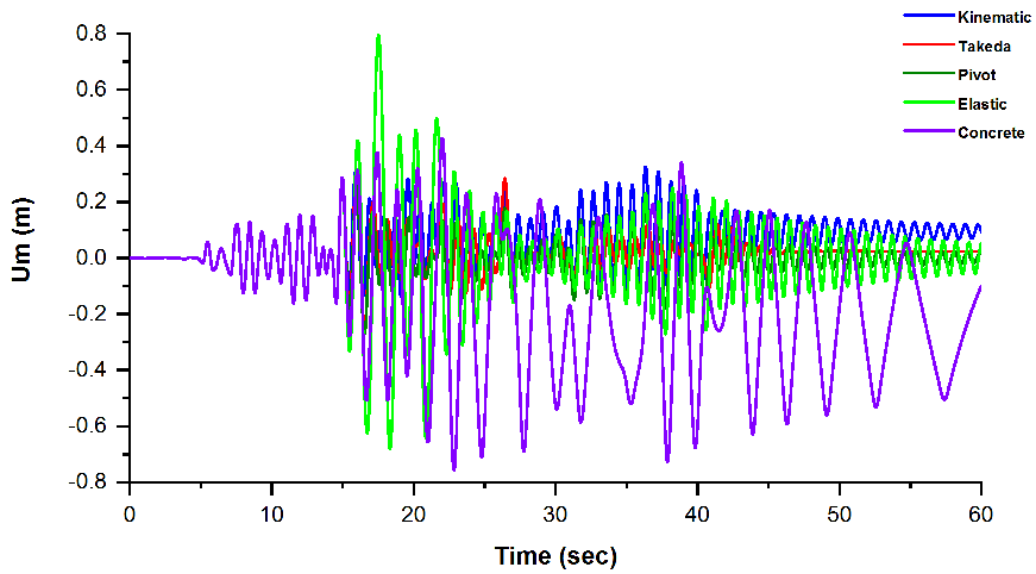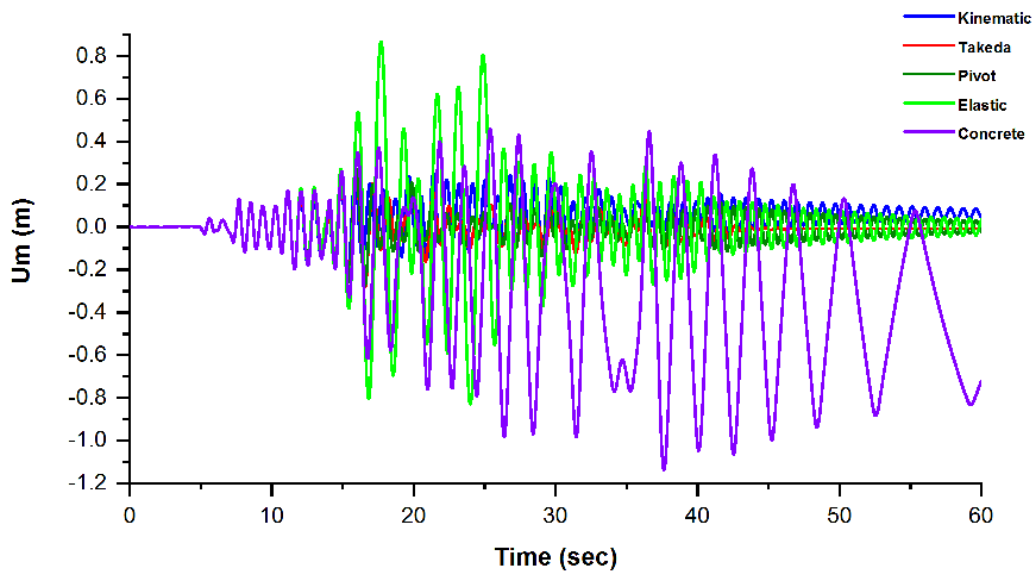The responses described were analyzed statistically under a probability density function

60

Figure 4.3: SDOF response spectrum with $\mu$=2 under CLAYN1N1000 ground motion for different hysteretic rules.



Figure 4.4: SDOF response spectrum with $\mu$=2 under CLAYN1N1090 ground motion for different hysteretic rules.
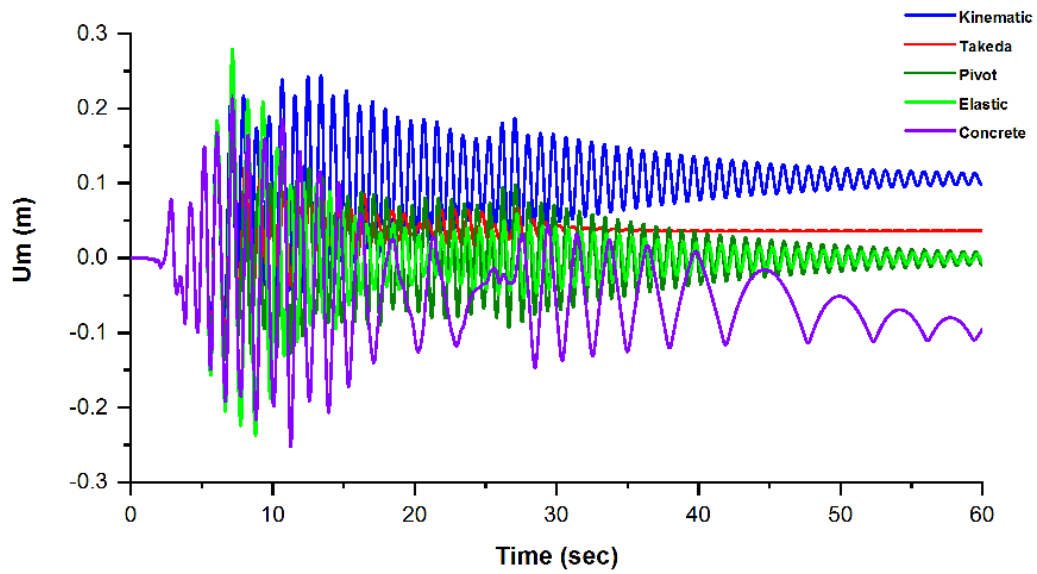
61

Figure 4.5: SDOF response spectrum with $\mu$=2 under ROCKN1N1000 ground motion for different hysteretic rules.
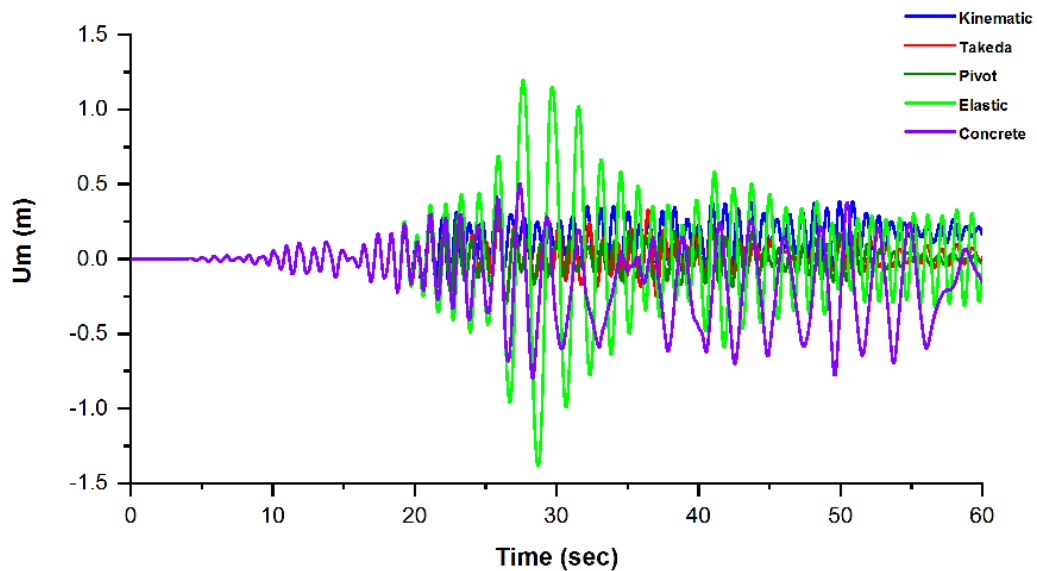


Figure 4.6: SDOF response spectrum with $\mu$=2 under SANDN1N1000 ground motion for different hysteretic rules.

Table 4.4: Elastoplastic SDOF model peak displacements for $\mu = 8$ and Tn = 0.9s

| Hysteretic type | Peak displacements (m) | | | |
| --- | --- | --- | --- | --- |
| | CLAYN1N1000 | CLAYN1N1090 | ROCKN1N1000 | SANDN1N1000 |
| Linear Elastic | 0.37 | 0.36 | 0.26 | 0.40 |
| Kinematic | 0.50 | 0.42 | 0.31 | 0.67 |
| Takeda | 0.86 | 0.71 | 0.41 | 0.40 |
| Isotropic | 0.50 | 0.42 | 0.31 | 0.67 |
| Degrading | 0.50 | 0.42 | 0.31 | 0.67 |
| BRB Hardening | 0.50 | 0.42 | 0.31 | 0.67 |
| Pivot | 0.57 | 0.58 | 0.44 | 0.35 |
| Elastic | 2.33 | 1.87 | 1.01 | 1.20 |
| Concrete | 1.64 | 0.97 | 0.75 | 1.44 |

Table 4.5: Softening SDOF model peak displacements for $\mu = 2$ and Tn = 0.9s

| Hysteretic type | Peak displacements (m) | | | |
| --- | --- | --- | --- | --- |
| | CLAYN1N1000 | CLAYN1N1090 | ROCKN1N1000 | SANDN1N1000 |
| Linear Elastic | 0.37 | 0.36 | 0.26 | 0.40 |
| Kinematic | 0.30 | 0.25 | 0.23 | 0.41 |
| Takeda | 0.30 | 0.28 | 0.21 | 0.32 |
| Isotropic | 0.30 | 0.25 | 0.23 | 0.41 |
| Degrading | 0.30 | 0.25 | 0.23 | 0.41 |
| BRB Hardening | 0.30 | 0.25 | 0.23 | 0.41 |
| Pivot | 0.29 | 0.27 | 0.21 | 0.34 |
| Elastic | 0.78 | 0.94 | 0.28 | 1.29 |
| Concrete | 0.87 | 1.06 | 0.24 | 0.73 |

(PDF) to study the effects of the hysteretic considerations over the SDOF systems. The Figure 4.8 and 4.10 show the corresponding PDF graphs for the peak displacement values of Elastoplastic $\mu$ = 2 and Elastoplastic $\mu = 8$, while the Figure 4.9 and 4.11 illustrate the PDF for the peak displacement normalized by the peak elastic response. The analysis shows that hysteretic assumption such as Concrete and Elastic behavior has a strong impact in the standard deviation of the responses. While the standard deviation in SDOF systems with a ductility factor of 2 and considering all the hysteretic behaviors was estimated between 10% to 70%, excluding from the analysis the Concrete
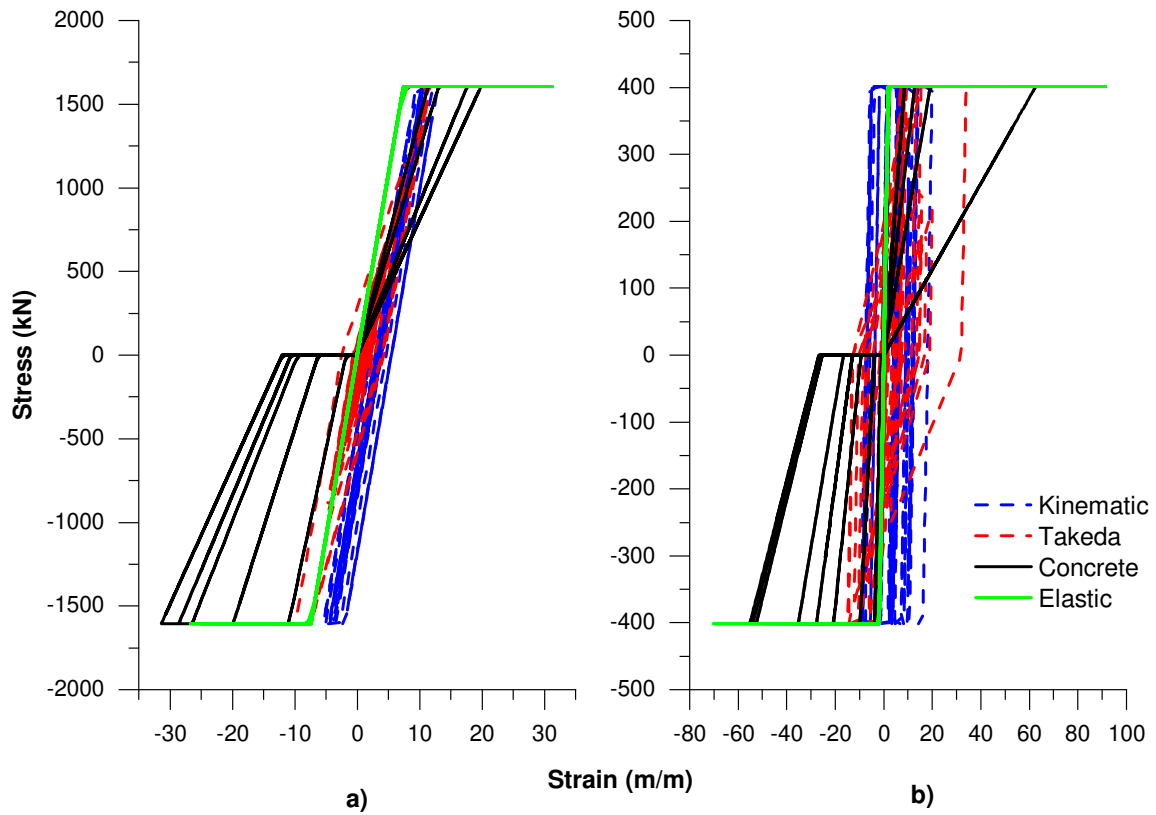
63

Figure 4.7: Fiber hysteretic analysis for SDOF system under CLAYN1N1000 ground motion: a) Elastoplastic model $\mu$=2; b) Elastoplastic model $\mu$=8.

and Elastic hysteretic rules concluded in a standard deviation around 5% to 10%. In addition, systems with high ductility tend to have a similar standard deviation (between 40% to 70%) when the analysis includes all the hysteretic types, but this is higher than low ductility factor systems when Concrete and Elastic hysteretic rules are excluded (15% to 25%). The Tables 4.6 and 4.7 show the values obtained for the statistical analysis.
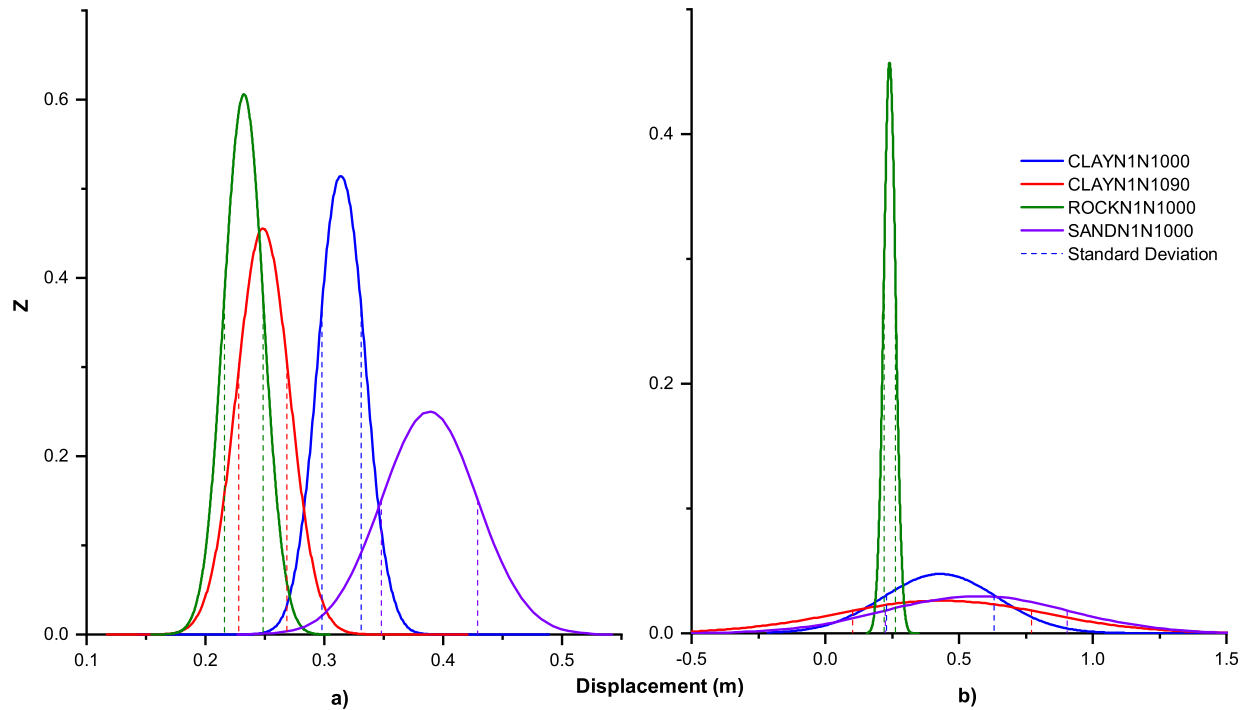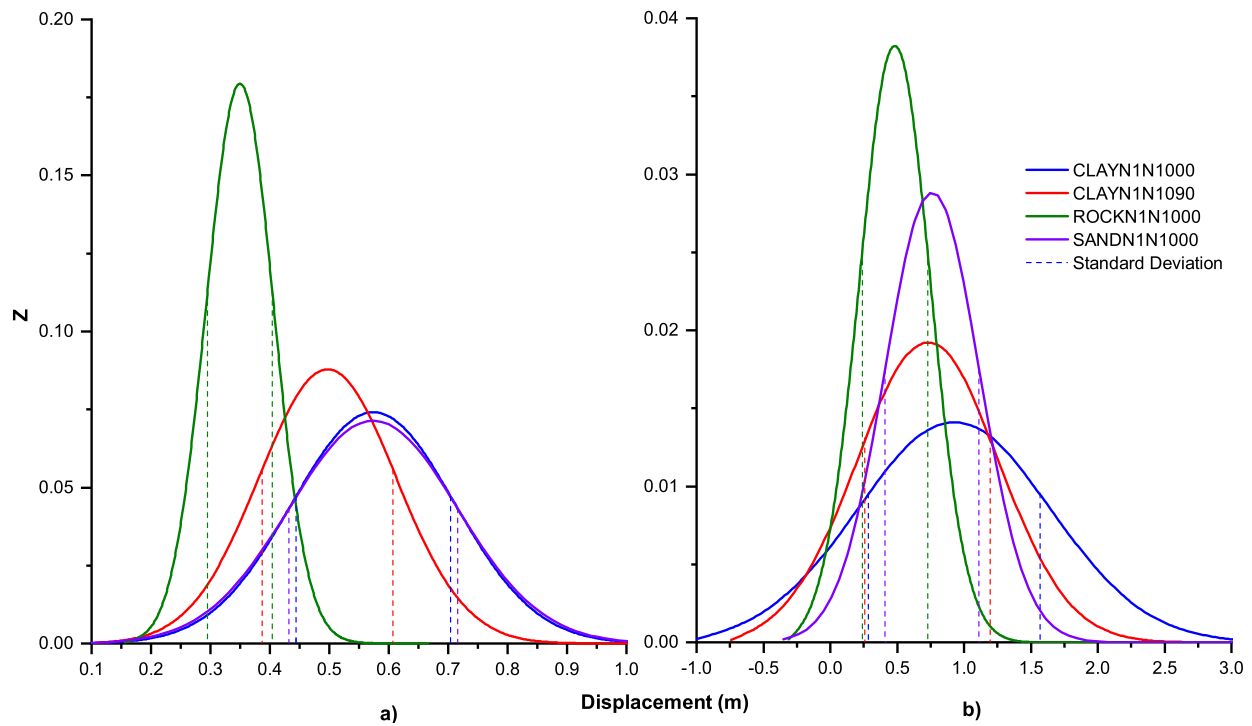
Figure 4.8: PDFs for Elastoplasticity SDOF with $\mu$=2: a) Excluding Concrete and Elastic hysteretic rules; b) Including all hysteretic rules.

Table 4.6: Mean value and standard deviation for Elastoplastic and Softening systems under different ground motions and considering all hysteretic rules.

| SDOF Systems | CLAYN1N1000 | | CLAYN1N1090 | | ROCKN1N1000 | | SANDN1N1000 | |
|---|---|---|---|---|---|---|---|---|
| | Mean | $\sigma$ | Mean | $\sigma$ | Mean | $\sigma$ | Mean | $\sigma$ |
| | (m) | (%). | (m) | (%) | (m) | (%) | (m) | (%) |
| Elastoplastic $\mu$ =2 | 0.43 | 46.7% | 0.44 | 76.4% | 0.24 | 8.9% | 0.56 | 60.2% |
| Elastoplastic $\mu$ =8 | 0.93 | 69.5% | 0.73 | 64.4% | 0.48 | 50.6% | 0.76 | 46.1% |
| Softening $\mu$ =2 | 0.43 | 53.3% | 0.44 | 73.1% | 0.23 | 8.8% | 0.54 | 56.8% |

## 4.7   Benchmark column

The research was broadened to analyze the impacts of the hysteretic variation in higher level models such as columns. Therefore, a benchmark column was defined assuming a diameter
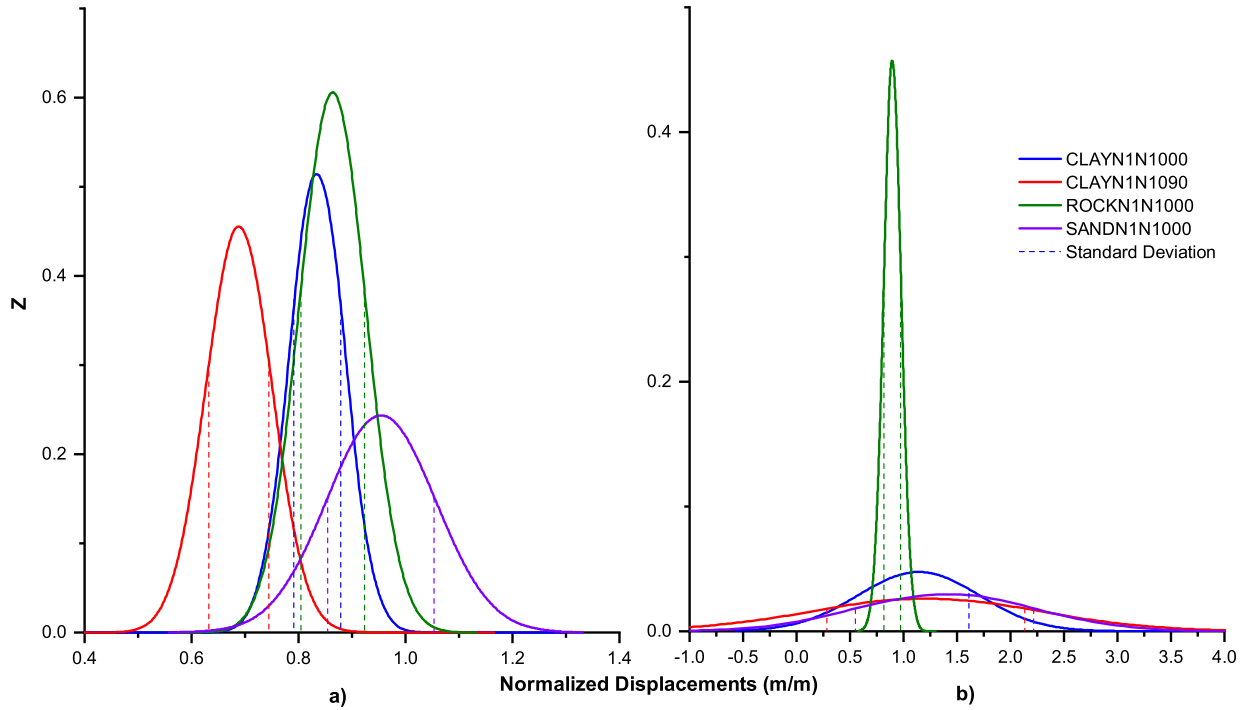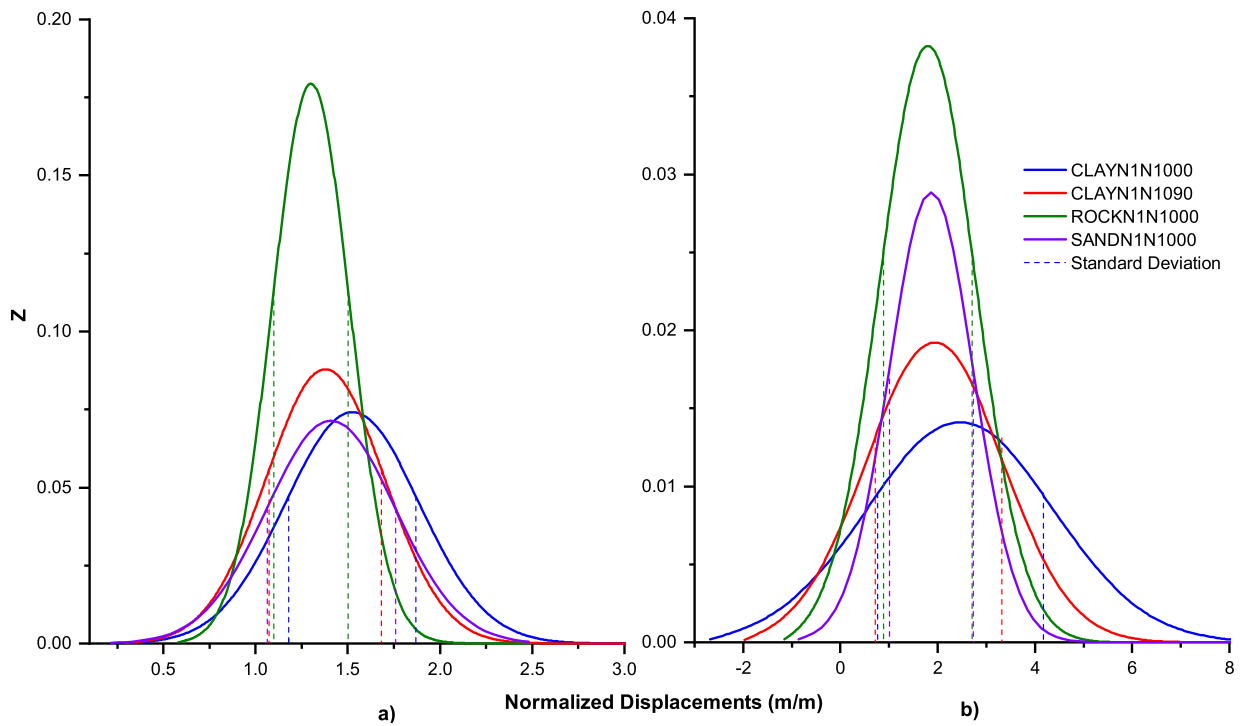
Figure 4.9: PDFs with normalized peak displacement for Elastoplasticity SDOF with $\mu$=2: a) Excluding Concrete and Elastic hysteretic rules; b) Including all hysteretic rules.

Table 4.7: Mean value and standard deviation for Elastoplastic and Softening systems under different ground motions excluding Concrete and Elastic hysteretic rules.

| SDOF Systems | CLAYN1N1000 | | CLAYN1N1090 | | ROCKN1N1000 | | SANDN1N1000 | |
|---|---|---|---|---|---|---|---|---|
| | Mean | $\sigma$ | Mean | $\sigma$ | Mean | $\sigma$ | Mean | $\sigma$ |
| | (m) | (%). | (m) | (%) | (m) | (%) | (m) | (%) |
| Elastoplastic $\mu$ =2 | 0.31 | 5.2% | 0.25 | 8.1% | 0.23 | 6.9% | 0.39 | 10.4% |
| Elastoplastic $\mu$ =8 | 0.57 | 22.6% | 0.50 | 22.1% | 0.35 | 15.5% | 0.57 | 24.7% |
| Softening $\mu$ =2 | 0.30 | 1.7% | 0.26 | 6.0% | 0.22 | 4.4% | 0.38 | 9.8% |

of 0.50 m and a high of 6.10m. The analysis considered a plastic hinge at the base of the column, with a length $l_{ph}$ = 0.678 m, and an integration point located at the center of the hinge ($x_h$ = 0.339 m). The effective moment of inertia of the column was $0.60I_g$ to assume an appropriated softening of the cracked elastic properties. The values assumed were taken according to the CP3

Figure 4.10: PDFs for Elastoplasticity SDOF with $\mu=8$: a) Excluding Concrete and Elastic hysteretic rules; b) Including all hysteretic rules.

case (Mackie & Scott, 2019). Similar values can be obtained using ACI-318 (ACI, 2014), Caltrans Seismic Design Criteria (Caltrans, 2013), and Paulay and Priestly (1992), where the recommended effective inertias are $0.70I_g$, $0.53I_g$, and $0.50 - 0.70I_g$, respectively.

A vertical load of $P$ = -1,718 KN was applied at the top of the column. The lateral ground motions imposed were CLAYN1N1000, CLAYN1N1090, ROCKN1N1000, and SANDN1N1000 synthetic accelerations (Lu et al., 2015) for x-axis. A damping equals to 1% and no P-Delta effects were considered in the dynamic analysis, and the time integration method used was Hilber-Hughes-Taylor with $\gamma = 0.5$, $\beta = 0.25$, and $\alpha = 0$. The material was assumed under an elastoplasticity behavior, with a Young's modulus of 200 GPa, yielding force equals to 345 MPa and mass of 175.12 kN. Therefore, a natural period of 0.89 sec was obtained using the equation for periodic motion.

Figure 4.11: PDFs with normalized peak displacement for Elastoplasticity SDOF with $\mu=8$: a) Excluding Concrete and Elastic hysteretic rules; b) Including all hysteretic rules.

The column was analyzed assuming the same hysteretic rules used for the SDOF analysis. The peak displacement obtained for each hysteretic rule under CLAYN1N1000 ground motion are described in the Table 4.8. The values were compared with the predicted peak displacement using the response spectrum obtained before, with $Tn = 0.89$ sec and $\mu = 2.64$. This ductility factor was calculated based on the elastic peak displacement of the column ($u_0$), the elastic peak force ($f_0 = ku_0$), the elastic peak moment ($My = f_0h$), the yielding strength of the system ($fy_{sys} = My/S$), and the yielding strength of the material ($fy_{mat} = 345$ MPa). The Figure 4.12 shows the column's responses for different hysteretic rules under CLAYN1N1000 ground motion, while the Table 4.8 illustrates the bias obtained with the predicted value. A high bias was achieved in the prediction of the peak displacement values for Concrete and Elastic hyteretic rules (near 60%), while the other hysteretic case concluded in a bias under 15%. Therefore, the assumptions done over the hysteretic
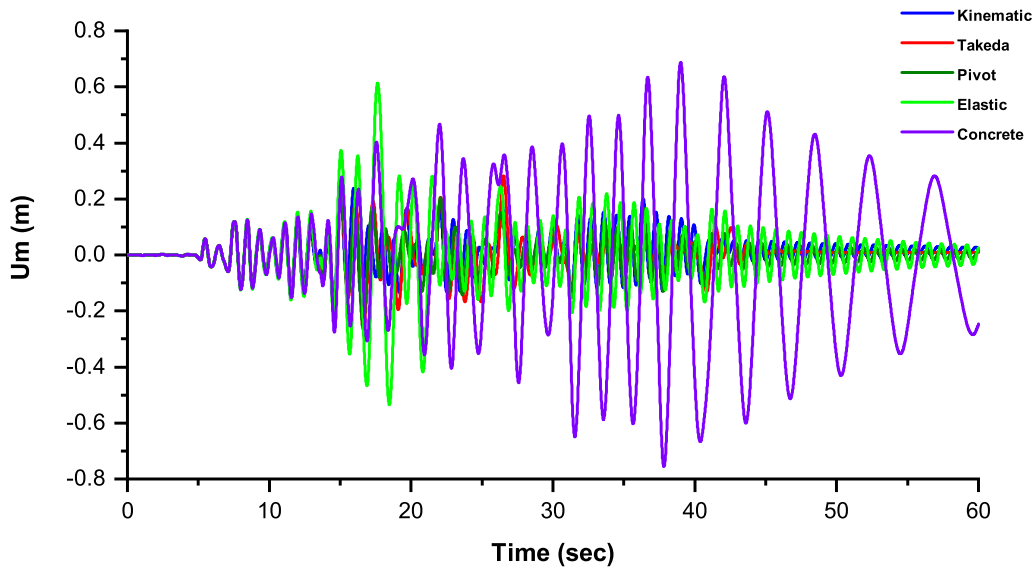
Figure 4.12: Column response spectrum with $\mu$=2.64 under CLAYN1N1000 ground motion for different hysteretic rules.

rules have an important effect over the column responses when comparing the results obtained with common hysteretic considerations such as Concrete and Kinematic or Takeda.

The column's peak displacements were analyzed statistically under a probability density function (PDF) to study the incidence of the hysteretic considerations over the systems. The Figure 4.13 shows the corresponding PDF graphs for the peak displacement values of the column, while the Figure 4.14 illustrates the PDF for the peak displacement normalized by the peak elastic response. The analysis shows that similar results as SDOF systems, where hysteretic assumptions such as Concrete and Elastic behavior have a strong impact in the standard deviation of the responses. While the standard deviation in column with a ductility factor of 2 and considering all the hysteretic behaviors had a huge variation (between 10% to 110%), excluding Concrete and Elastic hysteretic rules from the analysis concluded in standard deviations between 4% and 13%. PDF's analysis describes the same conclusions obtained during the column peak displacement predic-

Table 4.8: Peak displacement and prediction bias for benchmark column with a $\mu = 2.64$ and under CLAYN1N1000 ground motion.

| Hysteretic Rule | Um (m) | Um Prediction (m) | Bias (%) |
|---|---|---|---|
| Kinematic | 0.239 | 0.245 | -2.74% |
| Takeda | 0.283 | 0.245 | 13.31% |
| Isotropic | 0.239 | 0.245 | -2.74% |
| Degrading | 0.239 | 0.245 | -2.74% |
| BRB Hardening | 0.239 | 0.245 | -2.74% |
| Pivot | 0.257 | 0.245 | 4.78% |
| Elastic | 0.613 | 0.245 | 60.00% |
| Concrete | 0.755 | 0.245 | 67.55% |

tions, where the hysteretic assumption has an important effect on the responses when considering a Concrete or Elastic hysteretic rules instead of Takeda, Kinematic, or Pivot.

## 4.8    Fast Fourier Transform Analysis

The Fast Fourier Transform (FFT) and Transfer function (TF) of the acceleration responses of the SDOF and column were analyzed under different ground motions and hysteretic rules. Therefore, the impact on the behavior of the systems was studied after converting the responses to their representation in the frequency domain. The FFT and TF analysis of the SDOF time history can describe the different hysteretic behaviors of the systems and the impact in the responses. FFT is only applicable to time history response of linear systems. For the nonlinear responses considered, it was assumed that response was approximately stationary when averaged over the complete time history of response, and therefore only appropriate for cases of small ductility such as $\mu=2$. Therefore, it is not representative for nonlinear models with high ductility factors, such as $\mu=8$, which is used in just an approximate sense to establish if there is any trends. The Figure 4.15 and 4.16 illustrate the FFT power spectrum for the ground motions used and the FFT power spectrum for the elastoplastic SDOF considering $\mu=2$, respectively.

70
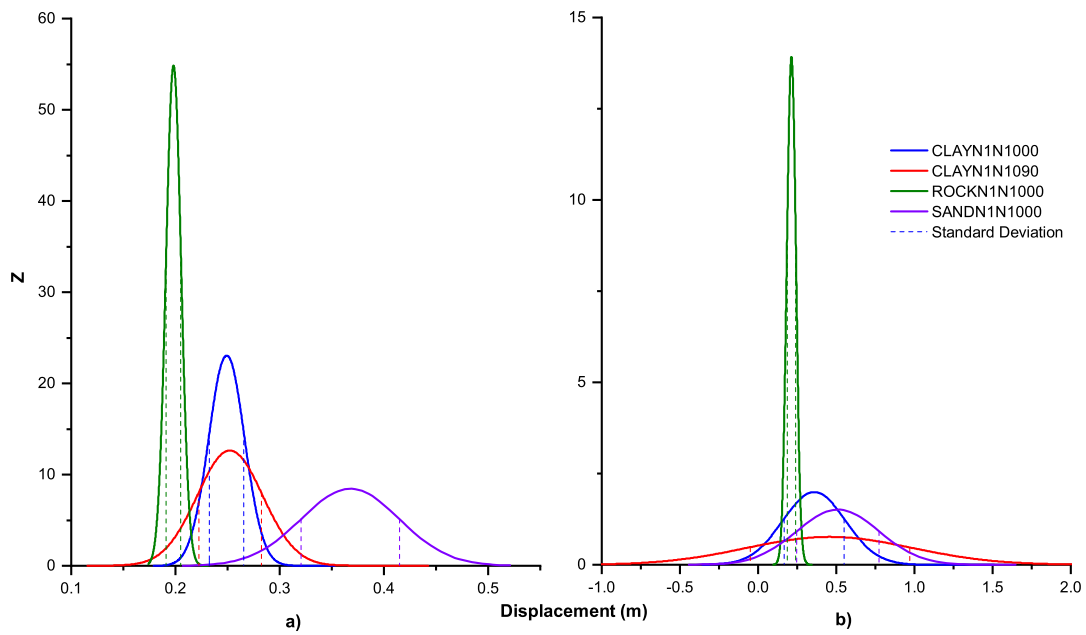
Figure 4.13: PDFs for elastoplasticity column with $\mu$=2.64: a) Excluding Concrete and Elastic hysteretic rules; b) Including all hysteretic rules.
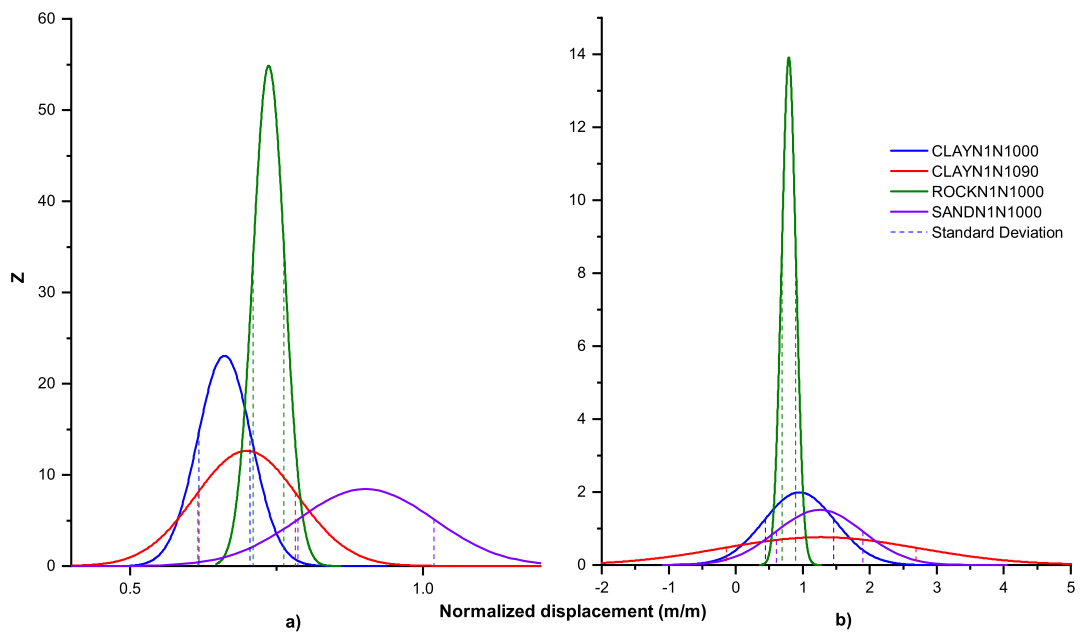


Figure 4.14: PDFs with normalized peak displacement for Elastoplasticity column with $\mu$=2.64: a) Excluding Concrete and Elastic hysteretic rules; b) Including all hysteretic rules.
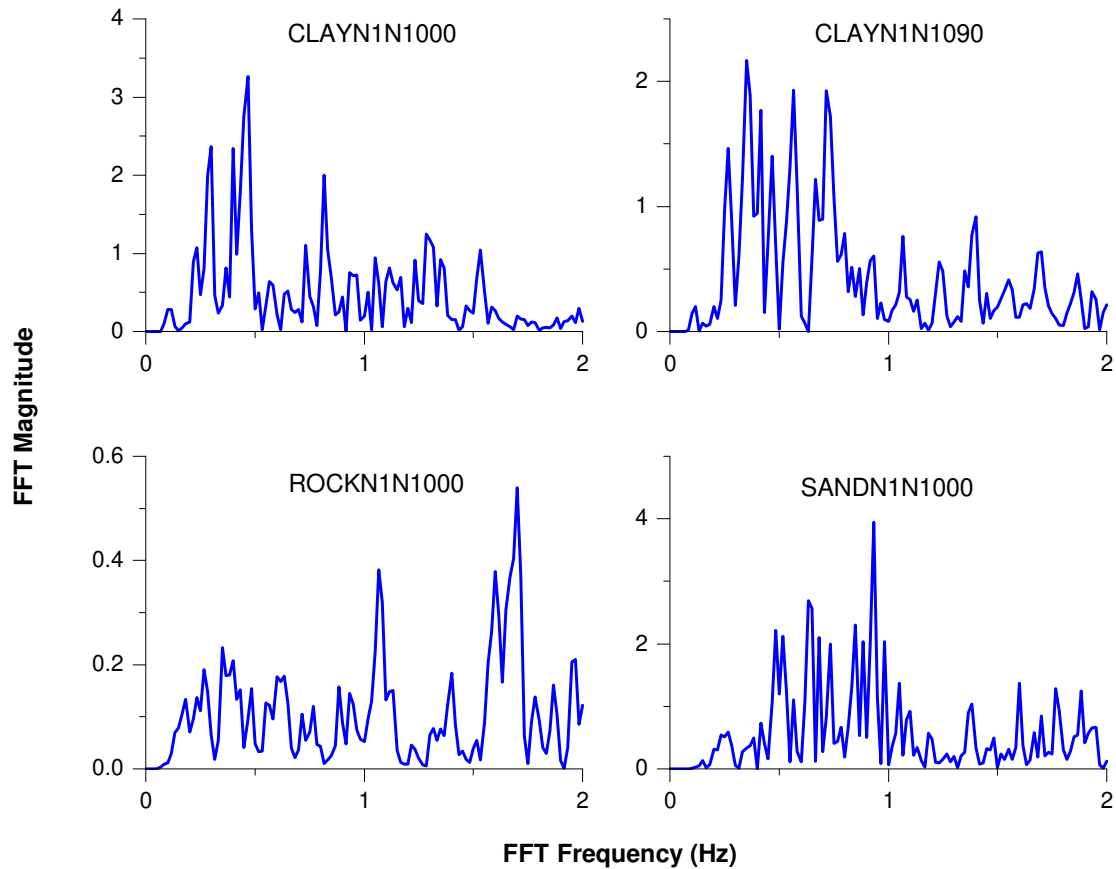
Figure 4.15: FFT ground motion power spectrum for CLAYN1N1000, CLAYN1N1090, ROCKN1N1000, and SANDN1N1000

The Figure 4.17 to 4.19 show the transfer function and natural period analysis done over the acceleration responses of the SDOF systems under CLAYN1N1000 ground motion. Similar results were obtained for the elastoplastic and softening materials under the same ductility factor. The analysis shows important variations in the linear elastic natural period when Concrete and Elastic hysteretic rules are assumed. This variations tend to increase for high values of ductility factor such as $\mu$=8. Therefore, the effects of the hysteretic behavior over the systems tend to increase when high ductility factors are considered and the impact of material nonlinear backbone consideration is very small when the same ductility factor is assumed.
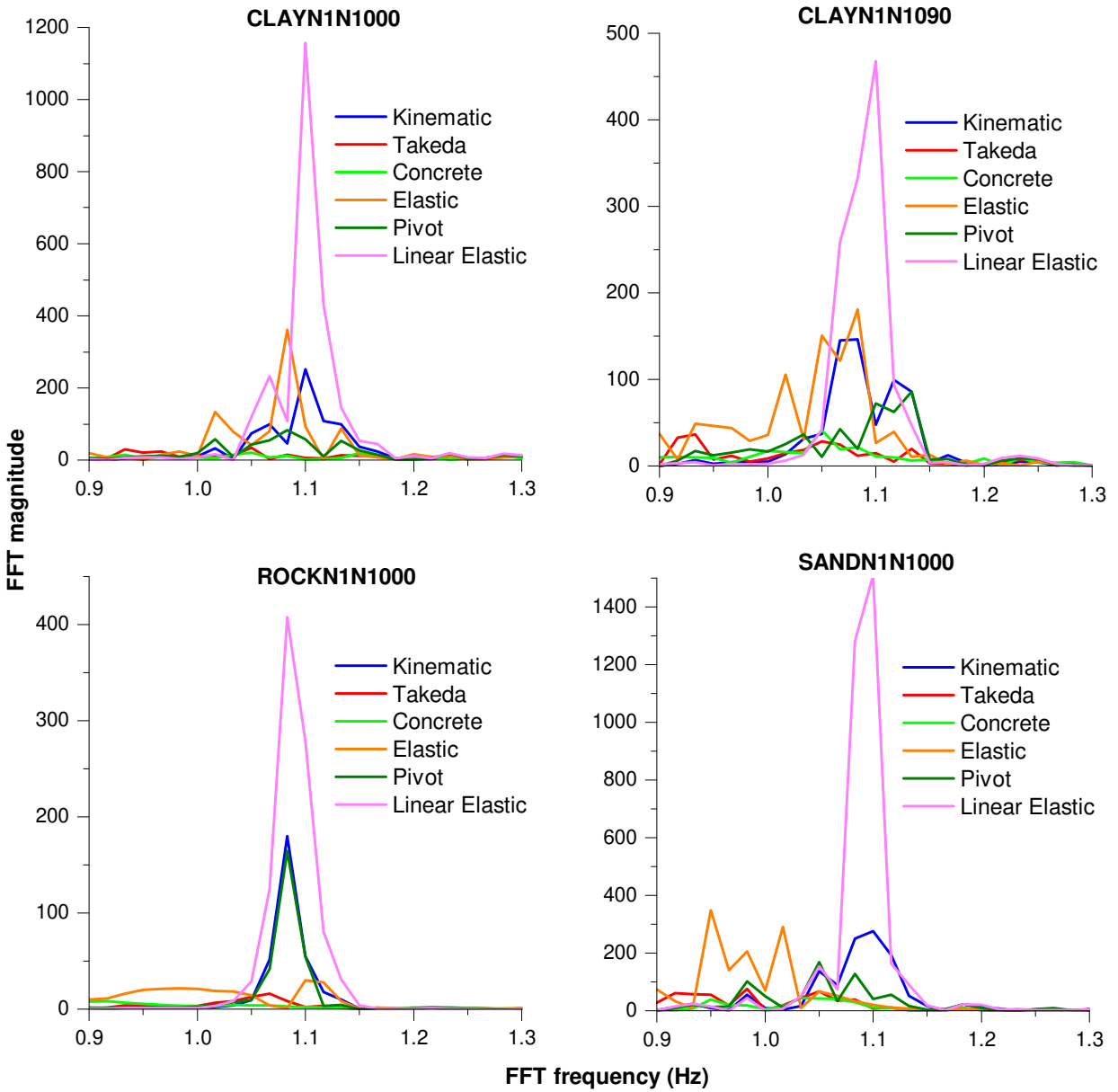
Figure 4.16: FFT ground motion power spectrum for elastoplastic SDOF with $\mu$=2 and different hysteretic rules
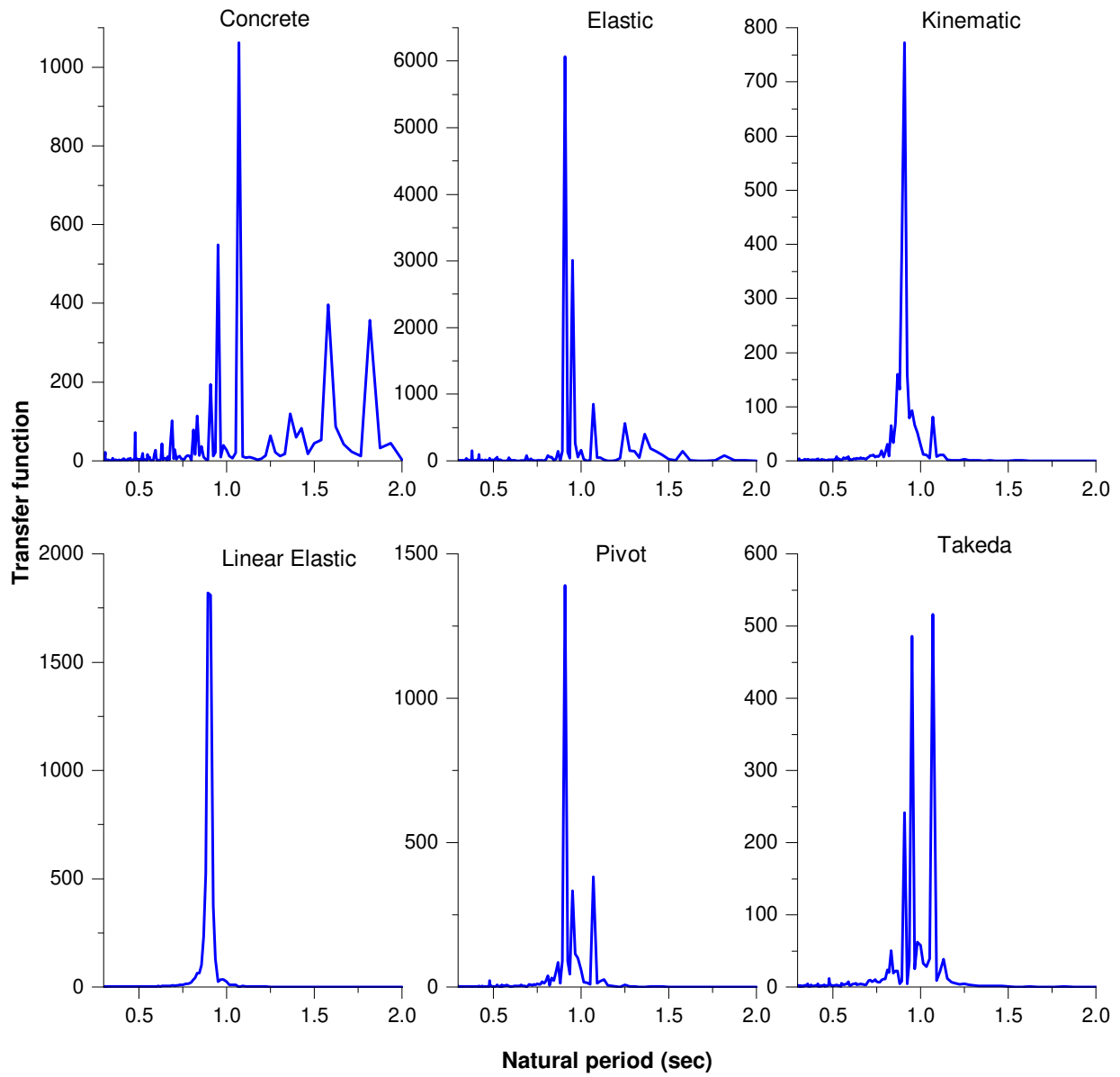
Figure 4.17: Transfer functions for elastoplastic SDOF with $\mu$=2 under CLAYN1N1000 ground motion.

74
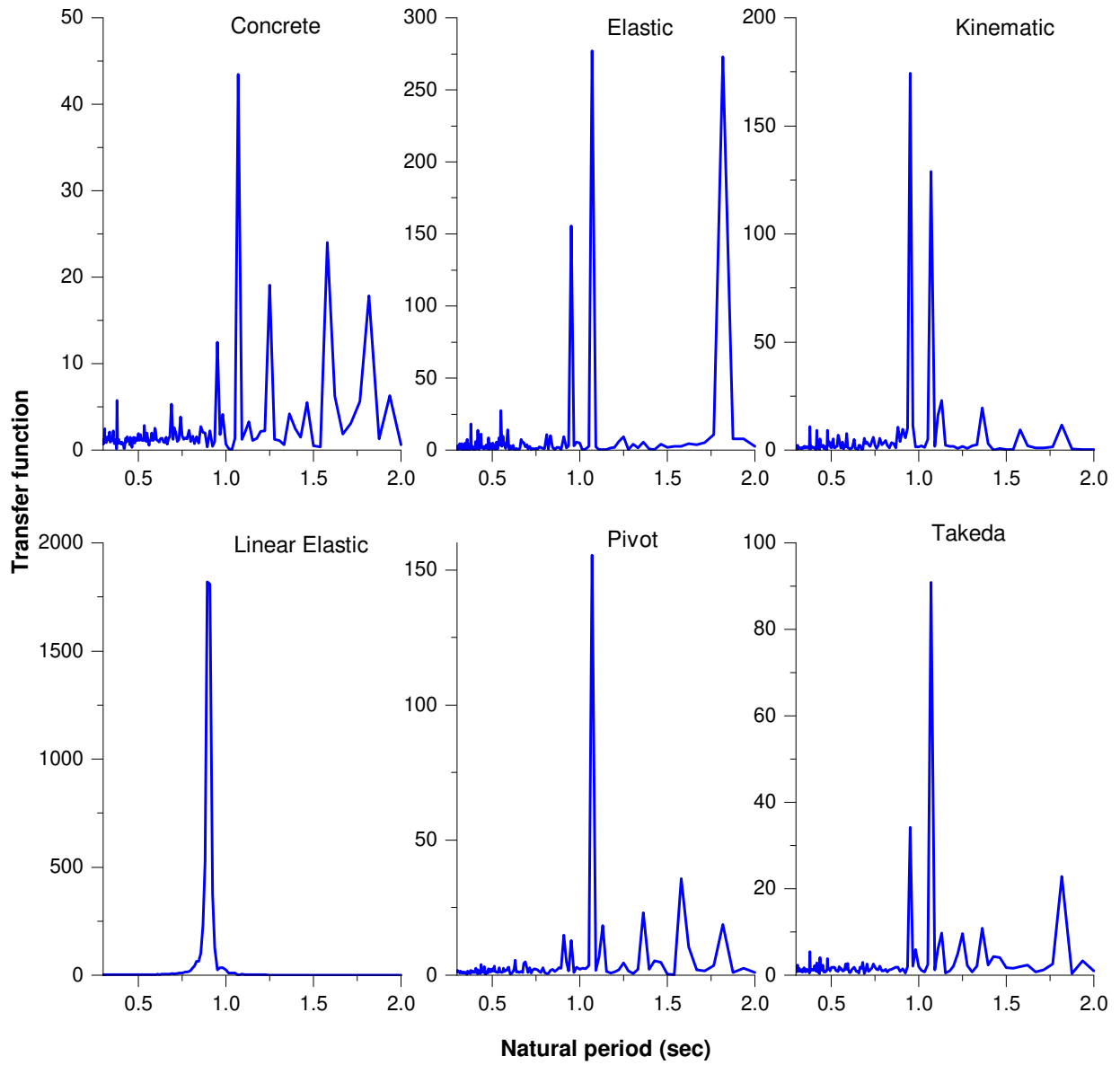
Figure 4.18: Transfer functions for elastoplastic SDOF with $\mu=8$ under CLAYN1N1000 ground motion.
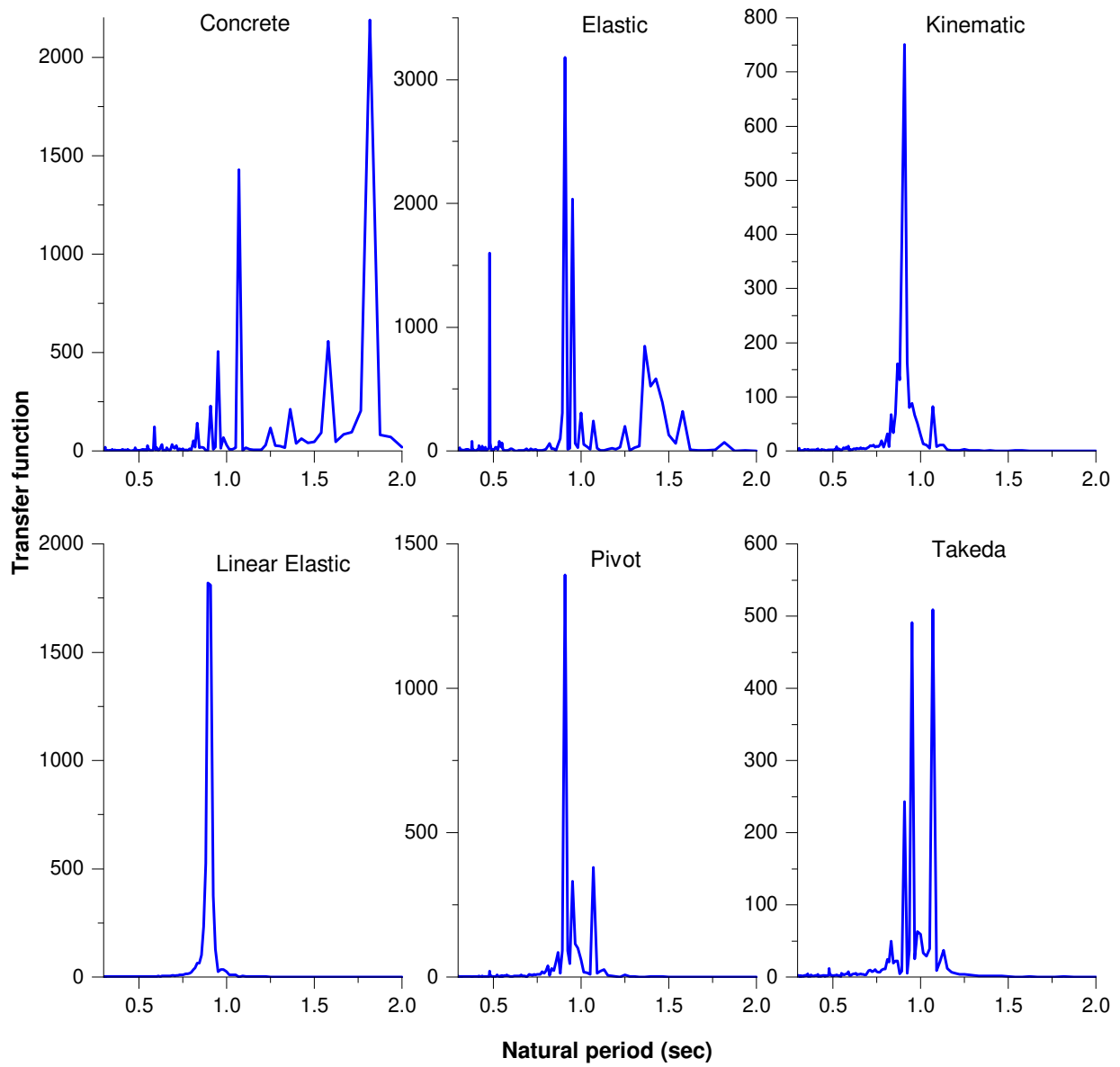
Figure 4.19: Transfer functions for softening SDOF with $\mu$=2 under CLAYN1N1000 ground motion.

The TF area was obtained for each system and was correlated with their corresponding peak displacement to analyze the variation in the natural period of the systems due to the hysteretic assumption. The nonlinear TF areas and peak displacements were normalized by their corresponding linear elastic values to generate dimensionless values. The values were correlated with the PDF probability density ($Z$) for both, normalized peak displacement and normalized TF area. The assumption in hysteretic rules such as Concrete and Elastic generates an important impact in the behavior of the systems. The Figure 4.20 a) illustrates the high dispersion of the normalized peak displacement and normalized TF area relationship for SDOF systems with $\mu$=2 and $\mu$=8, considering all the hystertic rules under different ground motions. The standard deviation of the peak displacement PDF was estimated in 57%. Accurate results can be achieved for normalized TF areas between 0.25 and 0.70, while the prediction tends to generate a strong bias when the normalized TF area is over 0.75 and below 0.20. After removing Concrete hyteretic rule from the analysis, the bias in the response decreases considerable, reducing the standard deviation of the PDF to 34%. The Figure 4.20 b) shows the distribution of the peak displacements and TF areas after excluding Concrete hysteretic rule from the analysis. On the other hand, the effect of the high ductility of the systems can be observed in the Figure 4.21, which after removing Concrete hysteretic rule and the responses of the SDOF systems with $\mu$=8, the standard deviation was reduced to 17%.

## 4.9   Summary and Discussion

The research developed elastoplastic and softening SDOF models based on different natural periods. The systems were analyzed under different ground motions accelerations, considering a damping equals to 1%. The linear elastic peak response under the ground motions was achieved for each model using their initial stiffness. Based on the linear elastic results and yielding force, the nonlinear models were modified for different values of ductility factor, concluding in the construction of a constant-ductility response spectrum for a specific ground motion. By linear interpolation
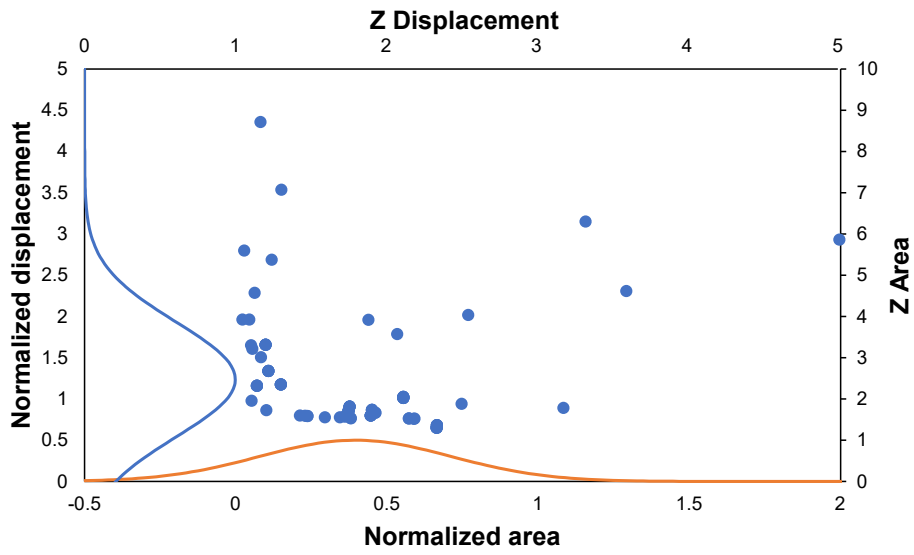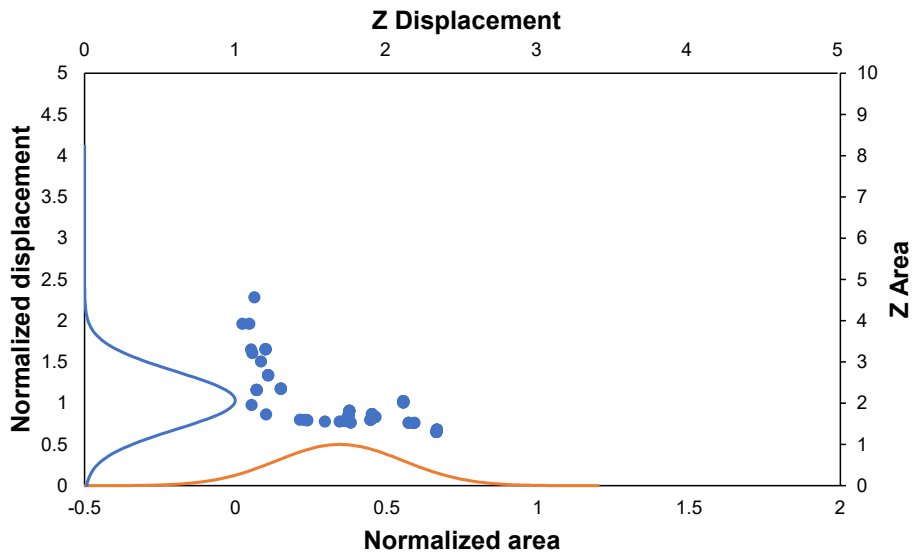
Figure 4.20: Normalized area and normalized displacement relationship for all SDOF systems: a) All hysteretic rules; b) Excluding Concrete hysteretic rule.
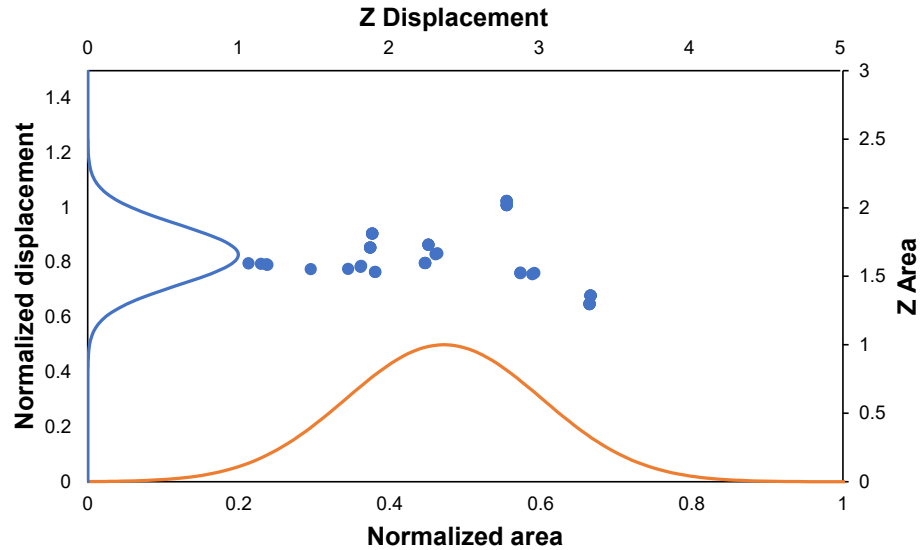
78

Figure 4.21: Normalized area and normalized displacement relationship for SDOF systems with $\mu$=2 and excluding Concrete hysteretic rule.

on the constant-ductility response spectrum, some peak displacements were predicted for different hysteretic rule assumptions and their corresponding bias was obtained to understand the effects of the hysteretic considerations on the SDOF systems. A statistical analysis was conducted using probability density function to study the variation in the standard deviation caused by the assumptions in the hysteretic rule of the material behavior, after imposing dynamic loads. A benchmark column using the same elastoplastic material was considered to conduct the same research done over the SDOF systems. The acceleration responses of the models were converted to a representation of the frequency domain for each ground motion and hysteretic type by using fast Fourier transformation, obtaining a series of FFT and TF graphical representations. The impact of the hysteretic behavior in the responses was analyzed using the TF plots by comparing the perturbation on period in the linear elastic system after a hysteretic assumption is considered.

# CHAPTER 5: CONCLUSIONS

The research demonstrated the constitutive models, element formulations, and modeling parameters necessary to achieve comparable nonlinear dynamic behavior of two OSBs in OpenSees and SAP2000. During the calibration process, both software showed close results for steel constitutive model under dynamic loads. The hysteresis type considered for SAP2000 in the model was Kinematic. On the other hand, concrete behavior had a different shape under Takeda hysteresis type (which was considered for SAP2000 models). An additional comparison was done using Concrete hysteresis type for SAP2000 concrete constitutive model and the results obtained were similar than OpenSees' concrete model. Concrete hysteresis type started to be available in SAP2000 recent versions. Thus, the Caltrans models only considered Takeda hysteresis type. The model was also calibrated using columns constitutive models. The values assumed were taken according to the concentrated plasticity case 3, CP3 (Mackie & Scott, 2019). The results obtained for SAP2000 and OpenSees described excellent agreement in phasing and peaks values, even the concrete constitutive model had disagreements in shape.

In the first bridge nonlinear analysis, OpenSees models were adapted to match Caltrans files, while SAP2000 remained the same. The results obtained for OSB1-O concluded in an acceptable agreement between both programs, while OSB2-O presented several differences due to issues in the hinge length considerations. A roller abutment analysis (S models) was developed to determinate the root of the differences between programs, confirming that OSB2-O incongruences were due to the inadvertent hinge length choice, while OSB1-O discrepancies were related to the concrete constitutive models and the nonlinear behavior of the abutments in the longitudinal direction.

The second bridge nonlinear analysis was focused to improve the issues found in Caltrans models. Important modifications were done over the elements of the columns in the models and the OSB2-O hinge length was improved to a more realistic one. The nonlinear time history anal-

ysis concluded in an excellent agreement between SAP2000 and OpenSees. Shape, phasing, and peaks values were almost identical for OSB1-MO and OSB2-MO. The improvement done over the models induced a more accurate response after applying dynamics loads to the Caltrans bridges. The results achieved with SAP2000 and OpenSees were almost the same, however concrete material constitutive model had several differences in its nonlinear dynamic behavior. The hinge, the fiber discretization in the hinge cross section, and the abutments nonlinear characterization clearly defined the main dynamic behavior of the bridge models.

The FDM was applied over the previous calibrated model, perturbing forward and backward specific nonlinear parameters with an established $\Delta\theta$ to obtain the bridge sensitivity to the change of each main property. The results show that OSB1-MO is much more sensitive than OSB2-MO to changes in the nonlinear parameters when is subjected to seismic loads. Both bridges concluded in high sensitivities responses in the longitudinal direction. Parameters such as steel yield strength for the column reinforcement and longitudinal abutment strength for the links have the highest sensitivities values for OSB1-MO, while the concrete strength in columns and the superstructure elastic modulus describe the most relevant perturbation in the displacement response for OSB2-MO. The displacement response in the transversal direction seems to be insensitive to changes for both bridges, except for the superstructure elastic modulus in OSB2-MO, which shows a high impact in the bridge response after its perturbation.

In addition, the bridge sensitivity to the hysteresis governing rule for concrete and reinforcement steel was analyzed. The deterministic response was obtained using the SAP2000 default hysteretic types (Takeda for concrete and Kinematic for steel). The change in the hysteresis behavior of the materials concluded in high sensitivity responses. The analysis concluded that OSB1-MO is much more sensitive that OSB2-MO to changes in the hysteresis rules assumption, especially in the steel reinforcement when is changed from Kinematic to Takeda. It is important to note that changing the concrete hysteresis rule from Takeda to Concrete generate in both bridges (specially OSB1-MO) an important perturbation in displacement of the deck and the Concrete hysteretic rule

was not available in the SAP2000 old versions. Therefore, a change in the concrete hysteretic assumption to a more realistic behavior could not be done until the latest SAP2000 versions.

The impact of the different hysteretic consideration over the responses of the SDOF systems under specific ground motion was demonstrated in the current study. The peak response predictions bias for Concrete and Elastic hysteretic rules was very high compared with the other hysteretic behaviors. Therefore, the hysteretic assumption will strongly affect the estimation of the peak displacement in SDOF systems. The research achieved similar conclusion after analyzing the results obtained in the probability density function. The PDF figures described steep slopes and small standard deviation when the Concrete and Elastic hysteretic rules were excluded from the analysis, while the values tend to be dispersed when the calculations included all the hysteretic behavior. The hysteretic effect on the responses tends to be higher when the ductility factor is increased. This is the case of the analysis done over the elastoplastic material with $\mu = 8$ and the comparison with the same material assuming a $\mu = 2$. The increment in the standard deviation is considerable when the ductility factor is changed from 2 to 8. On the other hand, the impact of material nonlinear backbone consideration (elastoplastic vs softening) is very small when the same ductility factor is assumed for them. The results achieved for both, elastoplastic and softening material using $\mu = 2$ where very similar. The TF analysis was focused to study the perturbations on the average peak displacement over the time history after applying ground motion accelerations, assuming a stationary response and considering different hysteretic rules. The TF plots showed an important variation in the behavior of the SDOF systems when Concrete and Elastic hysteretic rules are assumed, while the perturbation was small for the remaining hysteretic types. Similar to the PDF analysis, the perturbation tends to increase for high values of ductility factor such as $\mu = 8$. The bias and the standard deviation were considerably reduced after excluding the high ductility systems and Concrete hysteretic rule responses from the PDF analysis. Therefore, the responses in a SDOF system are highly affected by the hysteretic assumption and the ductility factor.

A similar nonlinear time history analysis and sensitivity study could be extended to dif-

ferent Caltrans ordinary standard bridges, such as OSB3 and OSB4. Also, the sensitivity analysis could be extended to compare the results with different softwares and the variation using the direct differentiation method. Finally, the bias analysis can be broadened to composite materials implemented in different type of structures such as concrete reinforced columns and bridges.

# APPENDIX A: OSB1-S PUSHOVER ANALYSIS
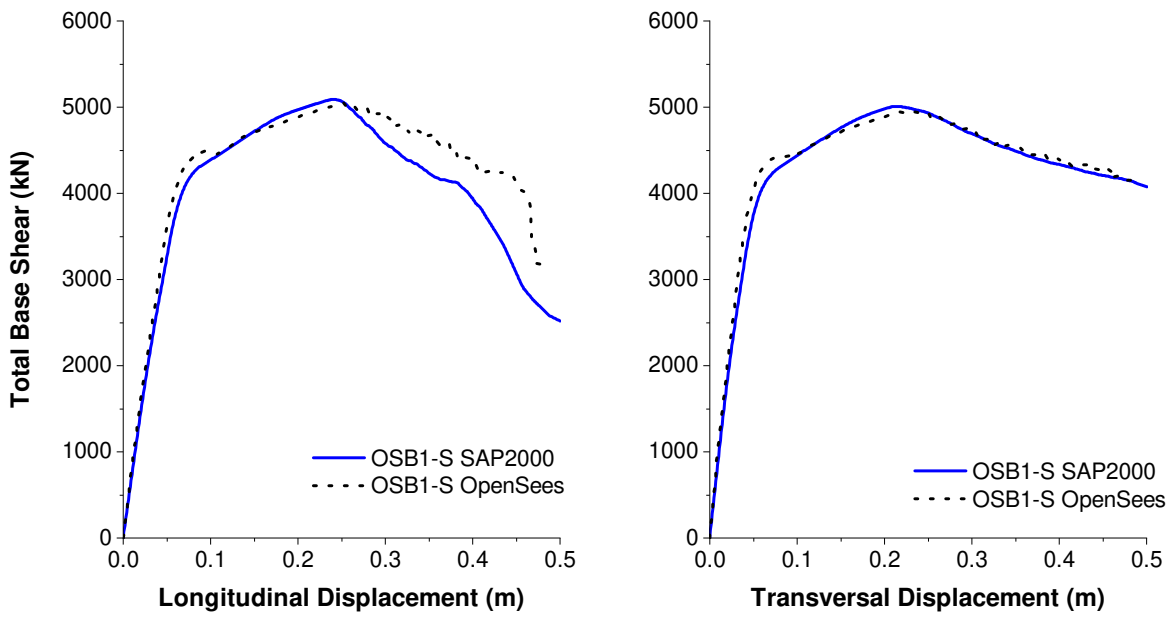
Figure A.1: OSB1-S Pushover analysis using concrete constitutive model dropping to zero stress at crushing in SAP2000

# APPENDIX B: GROUND MOTIONS
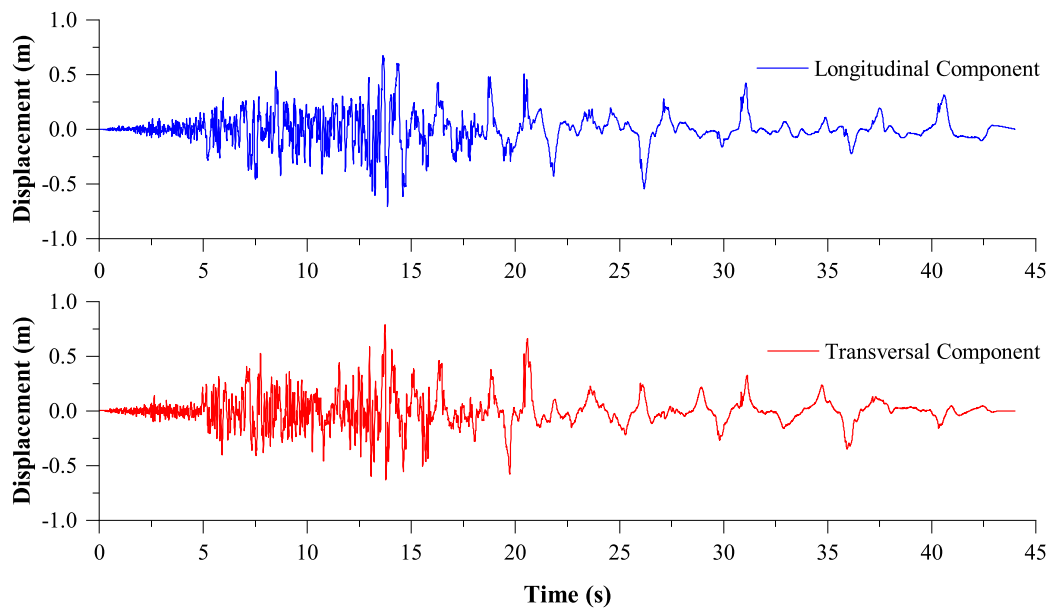
Figure B.1: CLAYN1N1 Recorded Ground Motion.
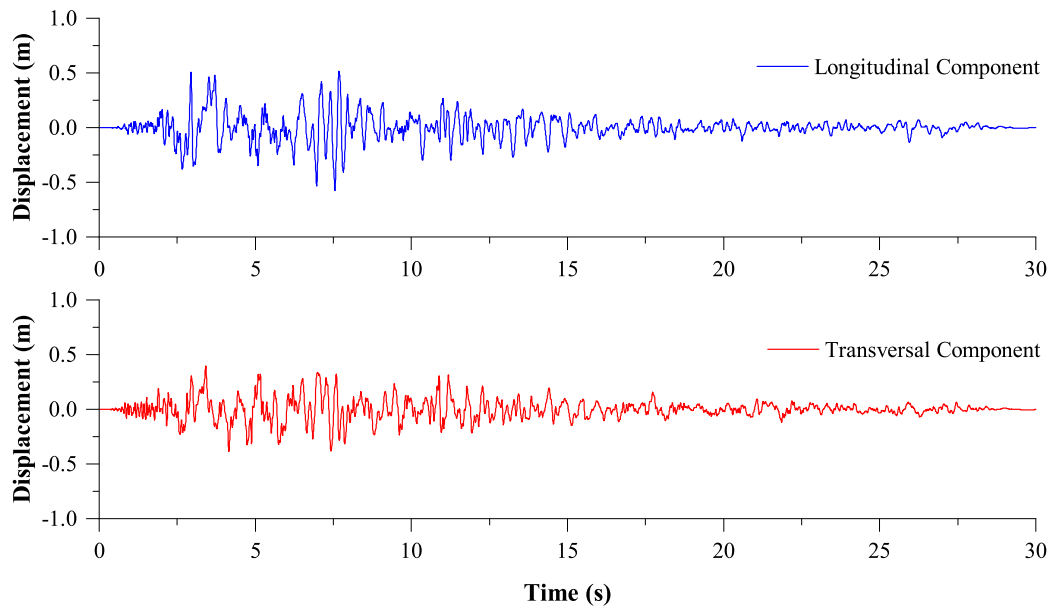


Figure B.2: ROCKN1N1 Recorded Ground Motion.
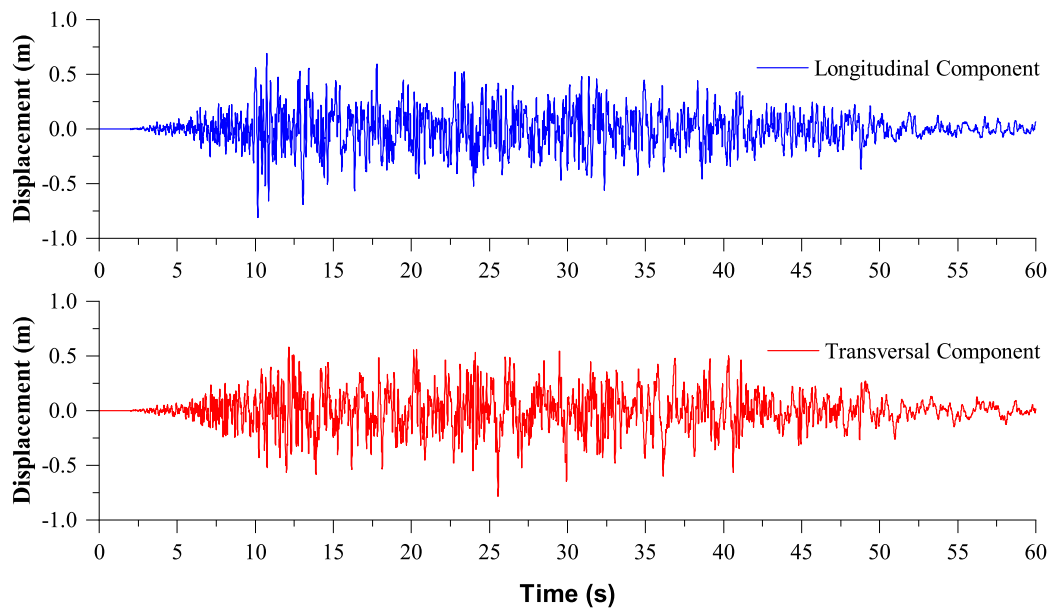
Figure B.3: SANDN1N1 Recorded Ground Motion.

# APPENDIX C: CENTER OF MASS DISPLACEMENTS
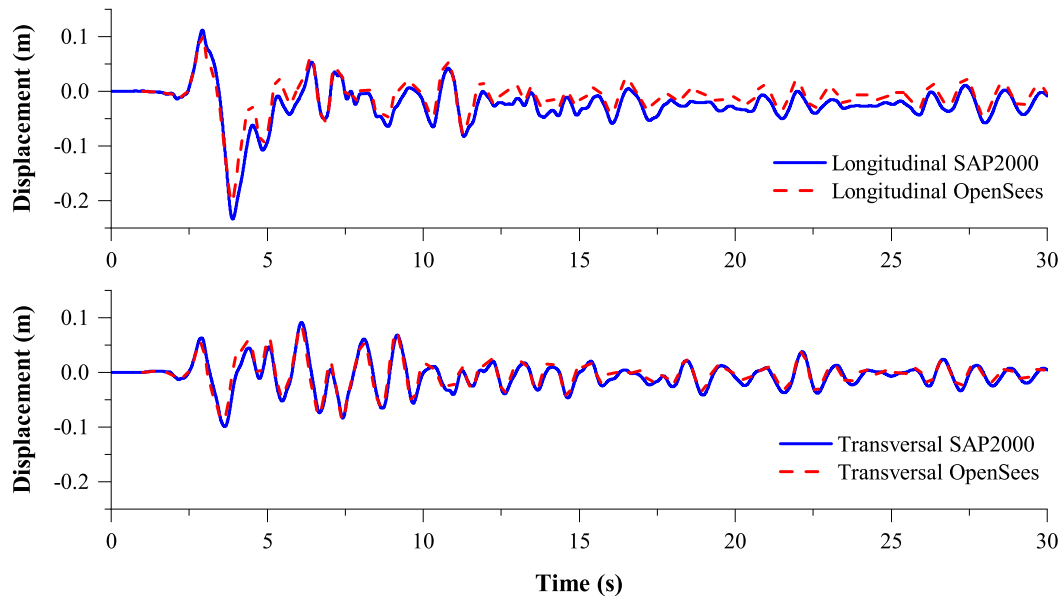
Figure C.1: OSB1-S center of mass displacement time history for ROCKN1N1 recorded ground motion.
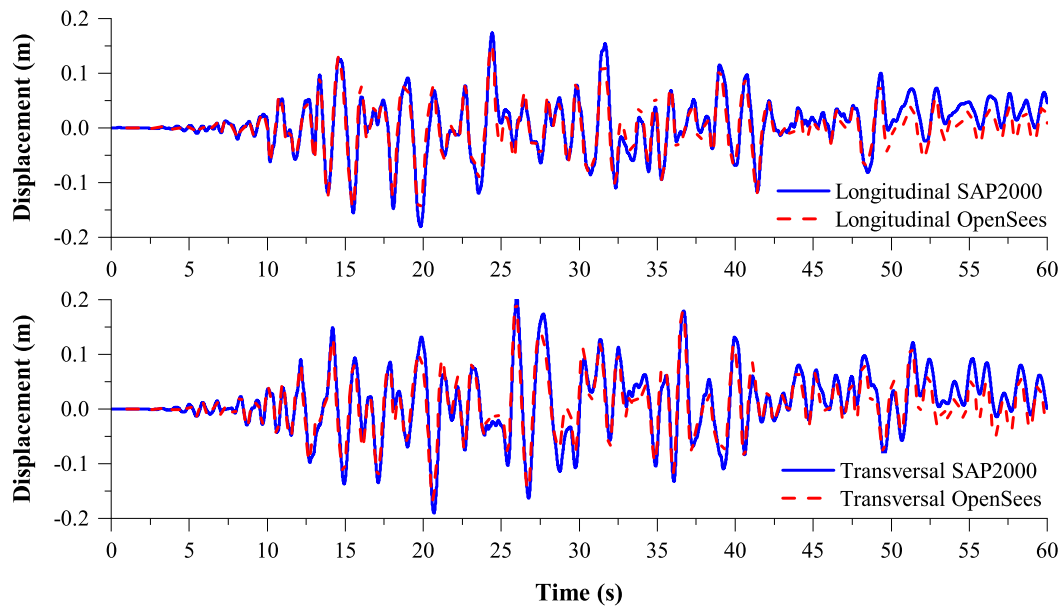


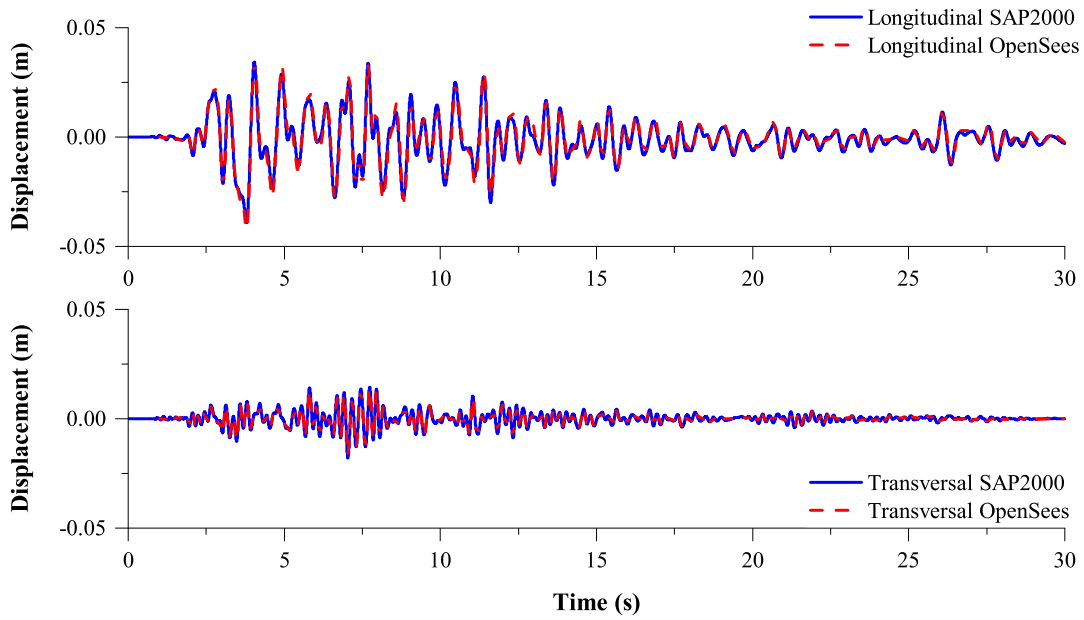Figure C.2: OSB1-S center of mass displacement time history for SANDN1N1 recorded ground motion.
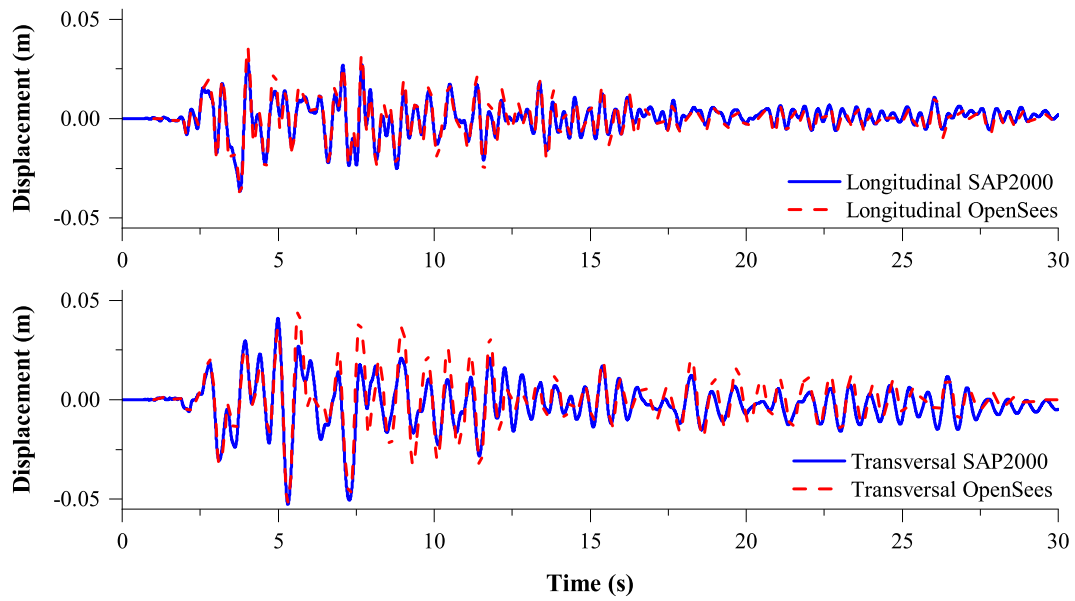
Figure C.3: OSB2-S center of mass displacement time history for ROCKN1N1 recorded ground motion.
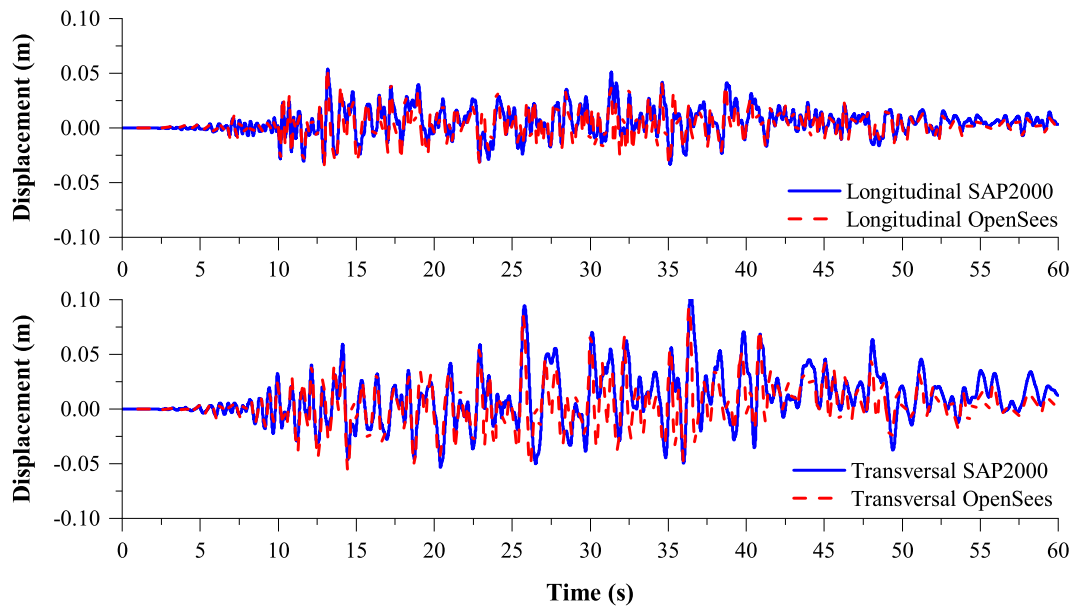


Figure C.4: OSB2-S center of mass displacement time history for SANDN1N1 recorded ground motion.
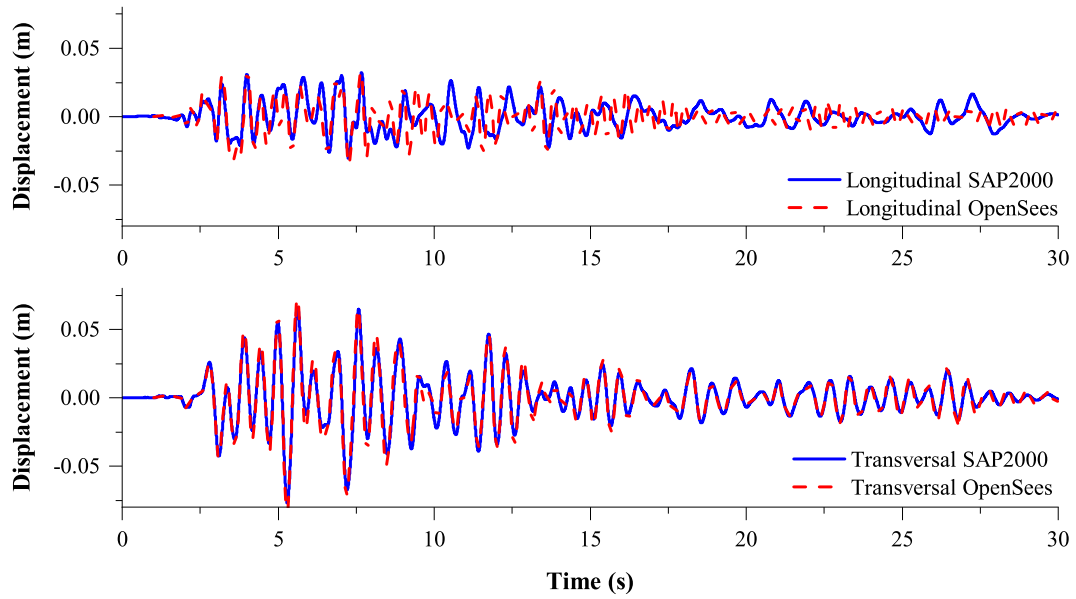
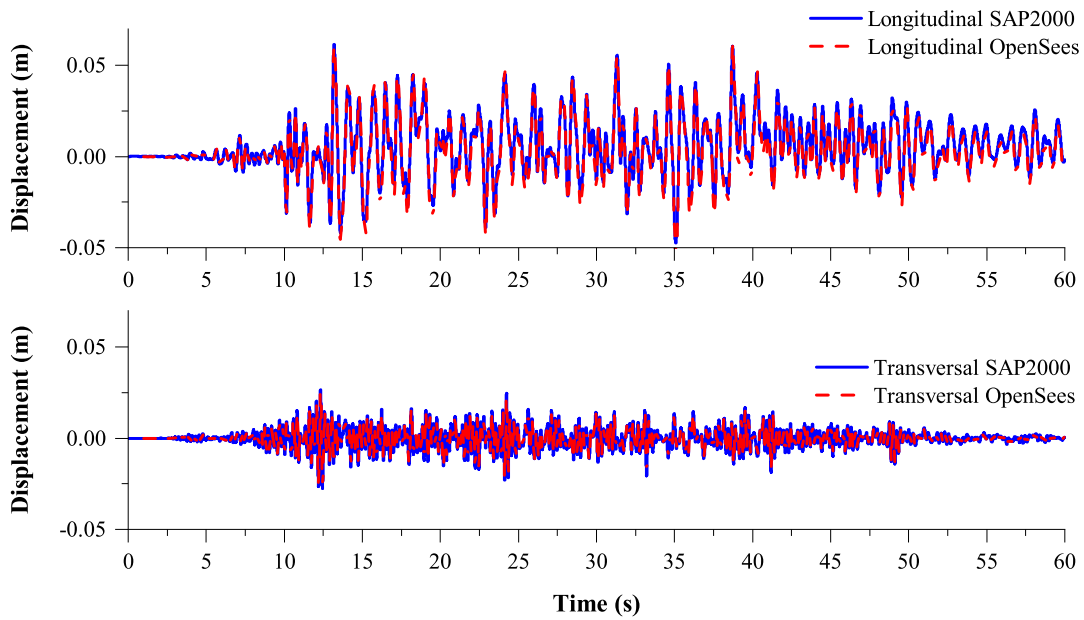Figure C.5: OSB1-O center of mass displacement time history for ROCKN1N1 recorded ground motion.
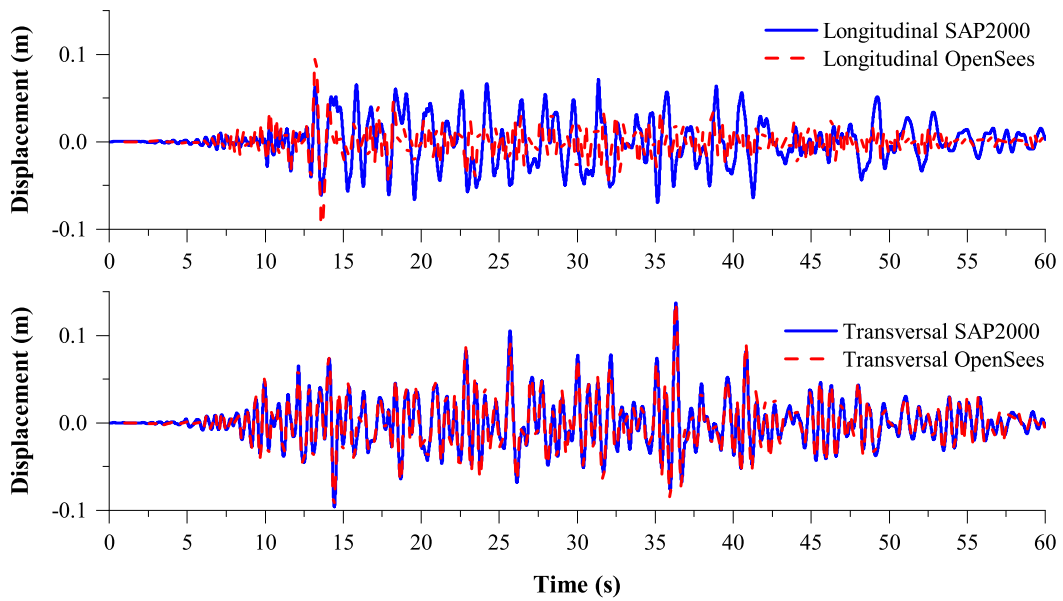


Figure C.6: OSB1-O center of mass displacement time history for SANDN1N1 recorded ground motion.
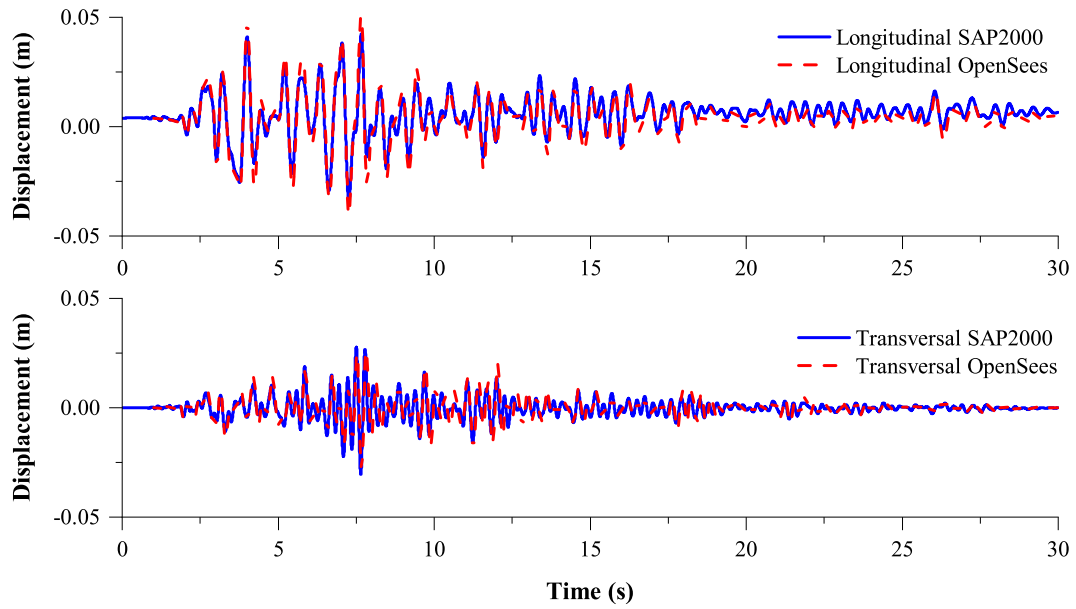
Figure C.7: OSB2-O center of mass displacement time history for ROCKN1N1 recorded ground motion.
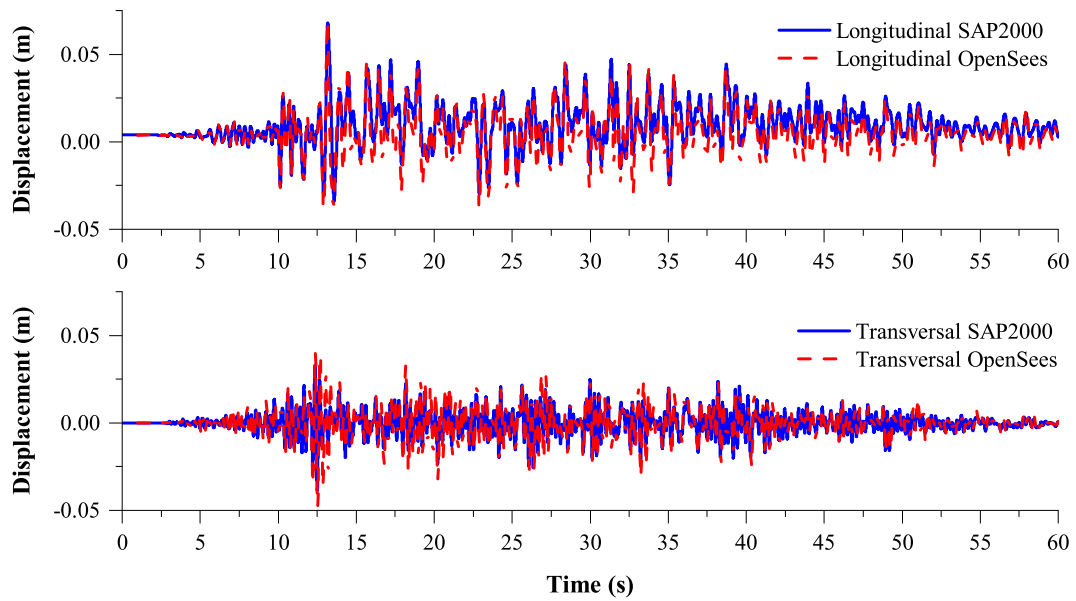


Figure C.8: OSB2-O center of mass displacement time history for SANDN1N1 recorded ground motion.
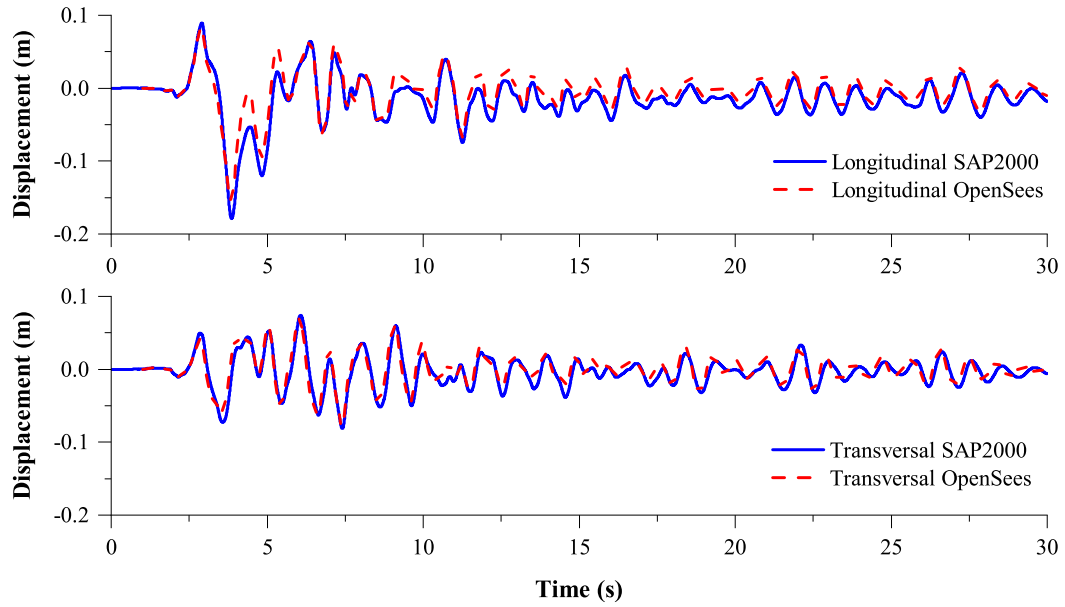
Figure C.9: OSB1-MS center of mass displacement time history for ROCKN1N1 recorded ground motion.
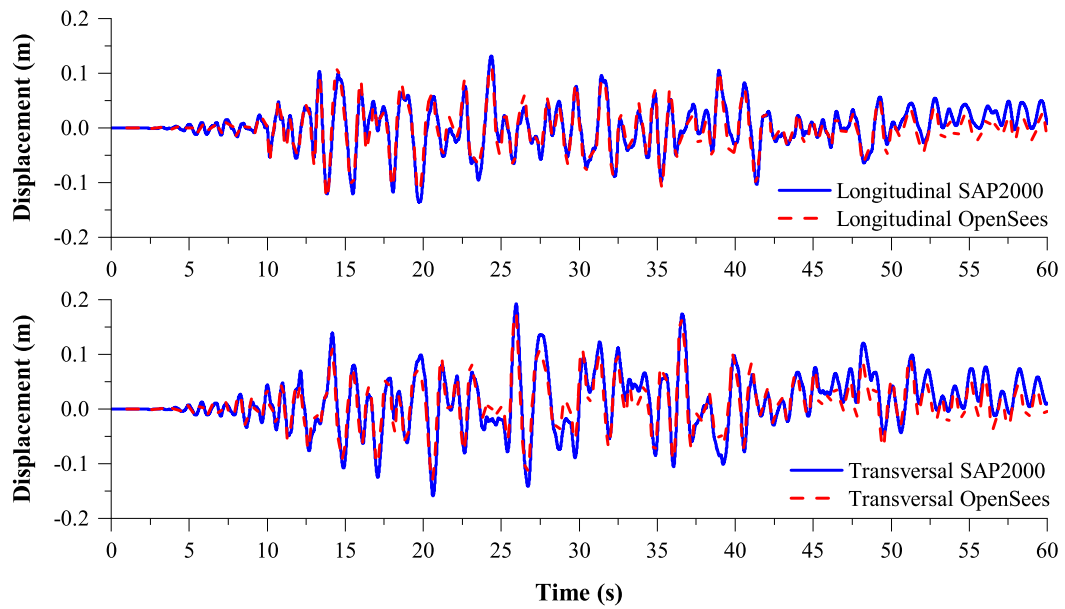


Figure C.10: OSB1-MS center of mass displacement time history for SANDN1N1 recorded ground motion.

94
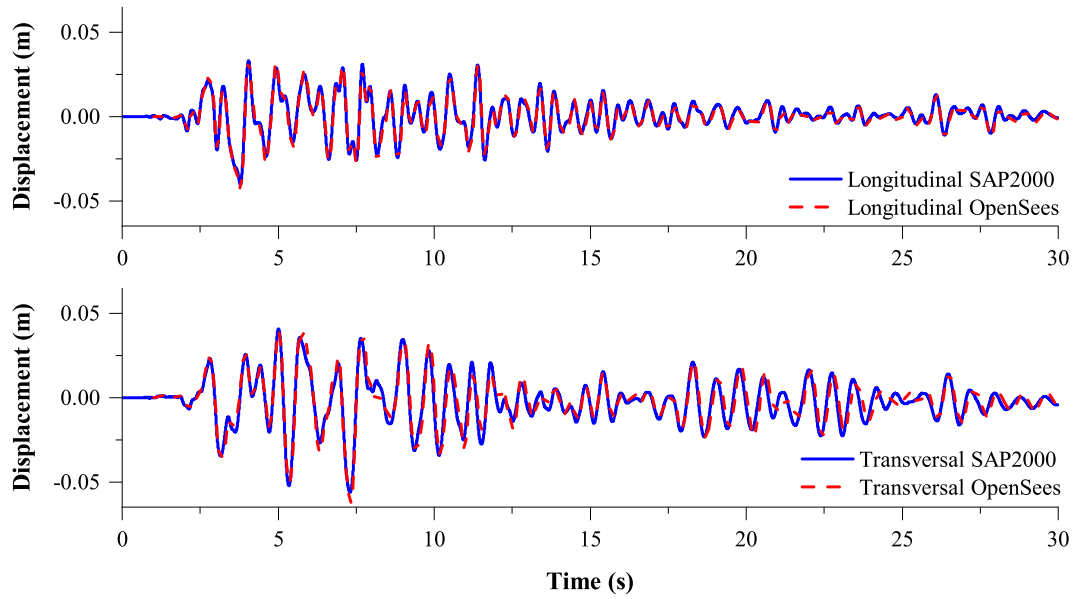
Figure C.11: OSB2-MS center of mass displacement time history for ROCKN1N1 recorded ground motion.
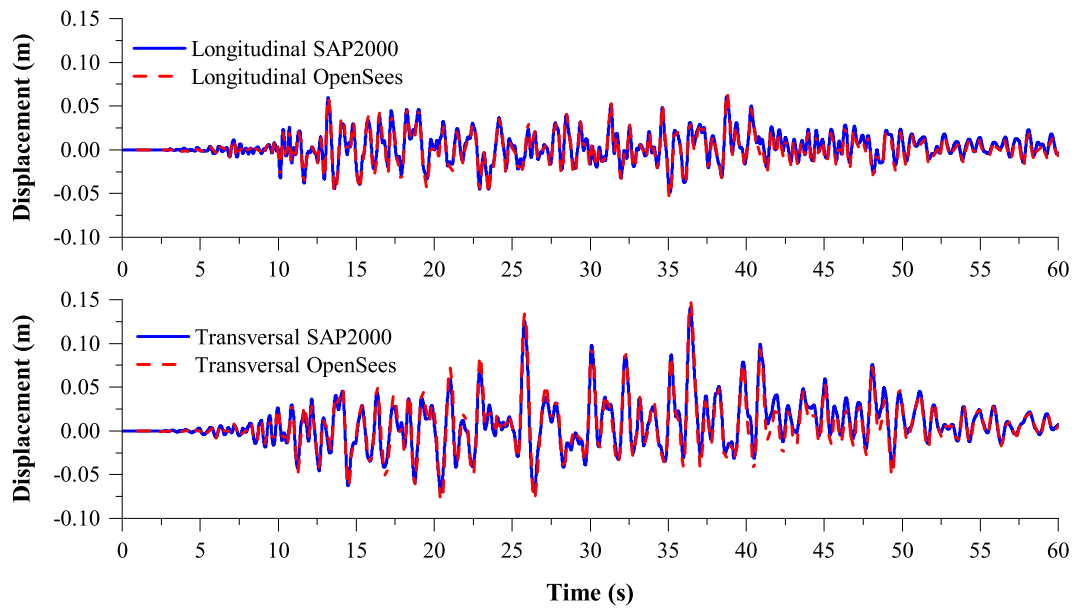


Figure C.12: OSB2-MS center of mass displacement time history for SANDN1N1 recorded ground motion.
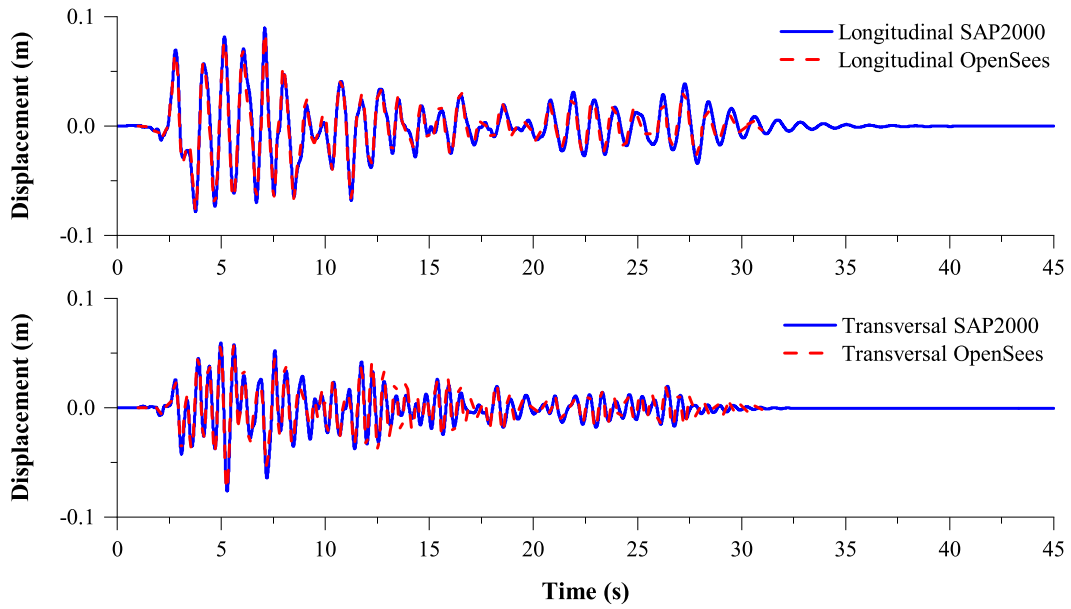
Figure C.13: OSB1-MO center of mass displacement time history for ROCKN1N1 recorded ground motion.
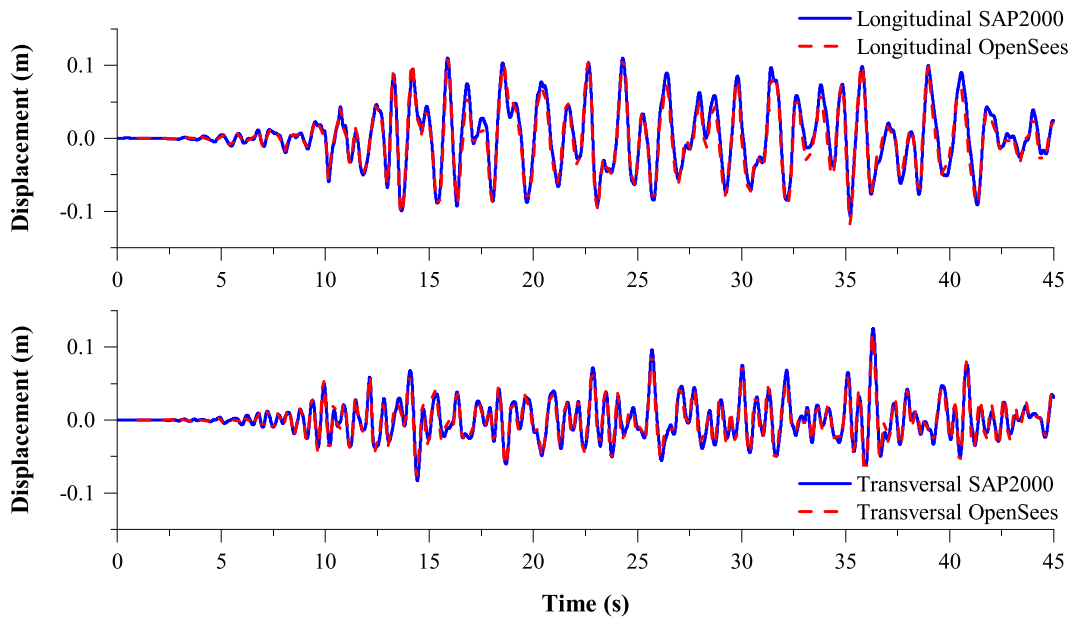


Figure C.14: OSB1-MO center of mass displacement time history for SANDN1N1 recorded ground motion.

Figure C.15: OSB2-MO center of mass displacement time history for ROCKN1N1 recorded ground motion.



Figure C.16: OSB2-MO center of mass displacement time history for SANDN1N1 recorded ground motion.

# APPENDIX D: CONSTANT DUCTILITY RESPONSE SPECTRUM
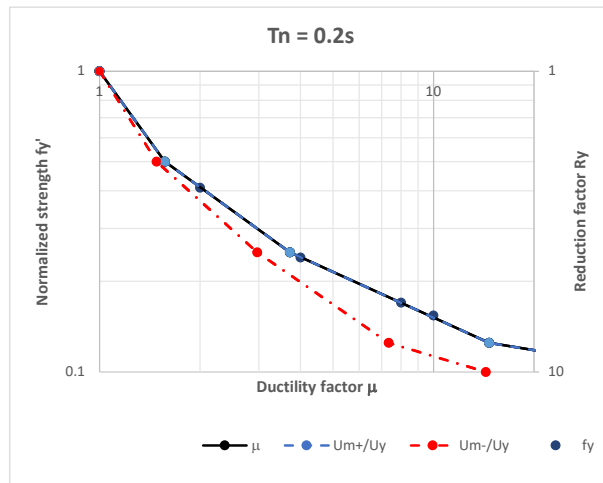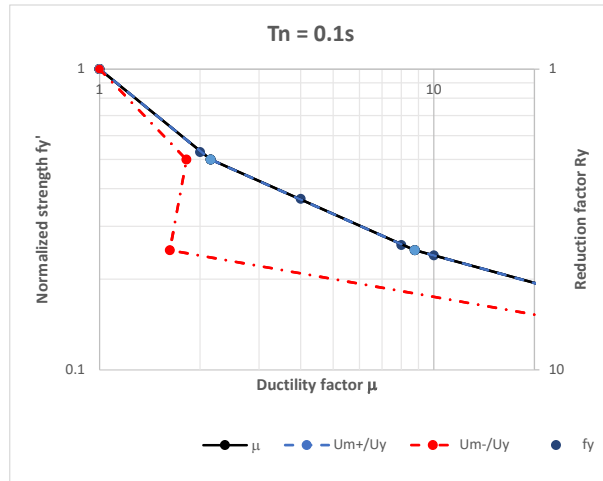
Figure D.1: Normalized strength vs ductility factor and reduction factor for $T_n$ = 0.1s and 0.2s under CLAYN1N1000 ground motion.
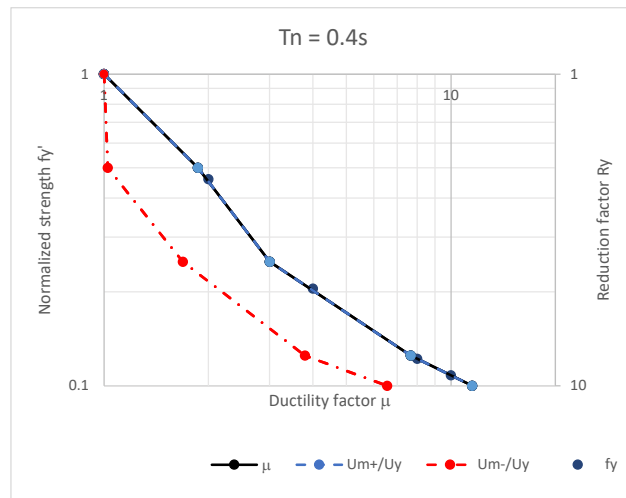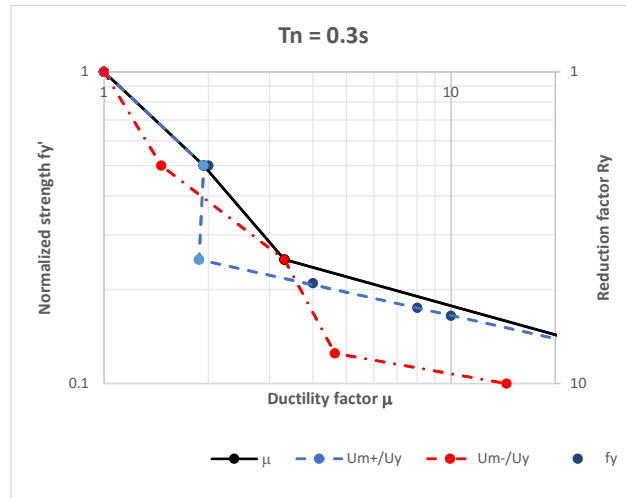
Figure D.2: Normalized strength vs ductility factor and reduction factor for $T_n$ = 0.3s and 0.4s under CLAYN1N1000 ground motion.
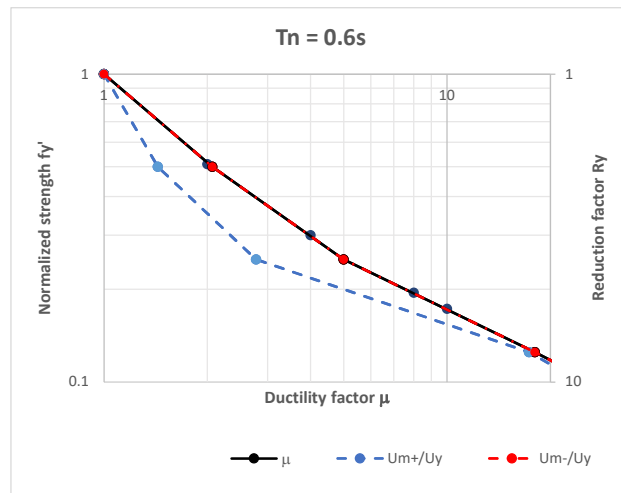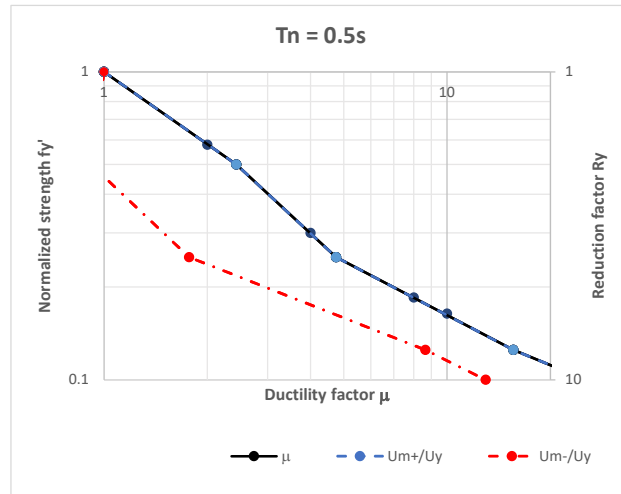
Figure D.3: Normalized strength vs ductility factor and reduction factor for $T_n$ = 0.5s and 0.6s under CLAYN1N1000 ground motion.
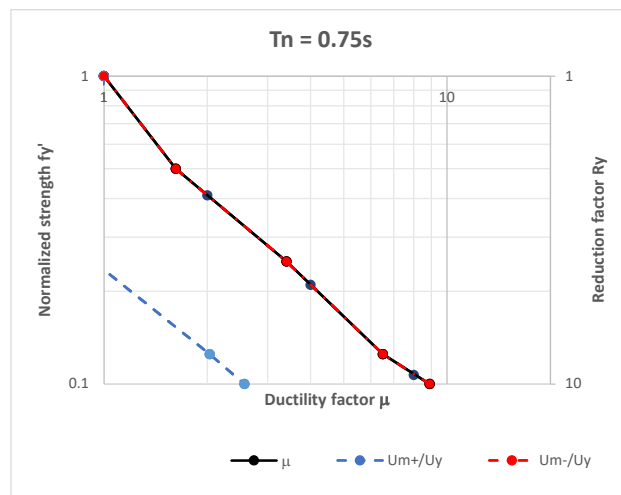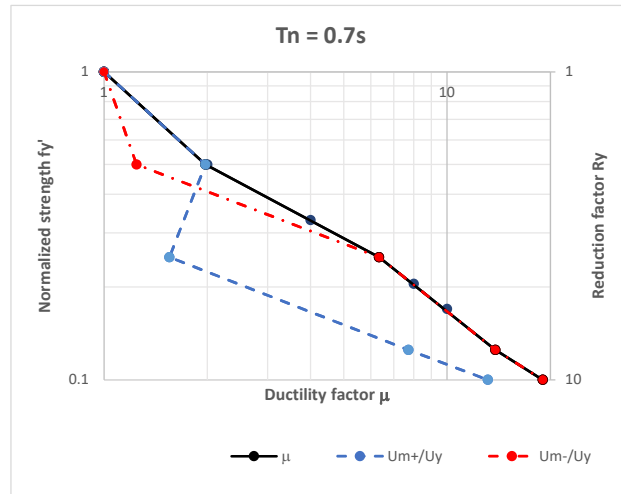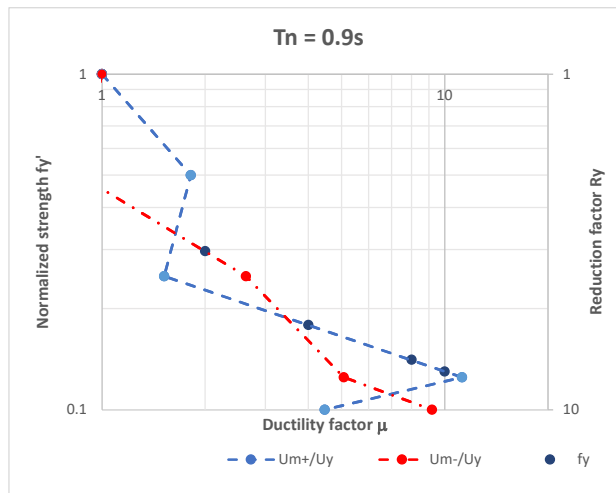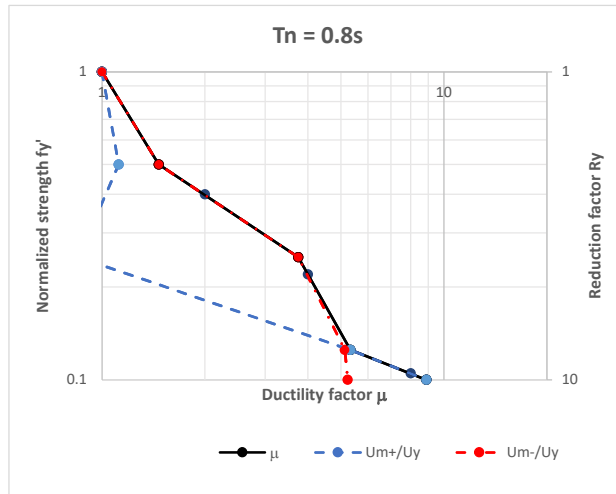
Figure D.4: Normalized strength vs ductility factor and reduction factor for $T_n$ = 0.7s and 0.75s under CLAYN1N1000 ground motion.

Figure D.5: Normalized strength vs ductility factor and reduction factor for $T_n$ = 0.8s and 0.9s under CLAYN1N1000 ground motion.
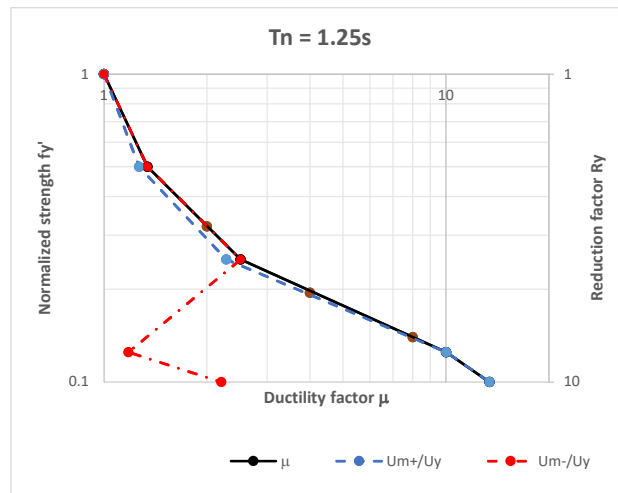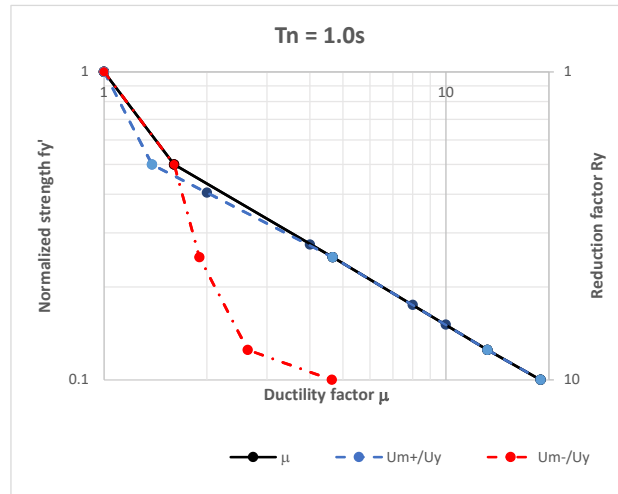
Figure D.6: Normalized strength vs ductility factor and reduction factor for $T_n$ = 1.0s and 1.25s under CLAYN1N1000 ground motion.
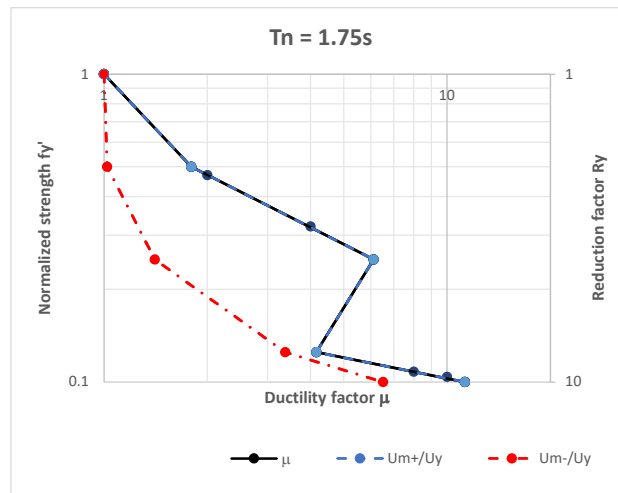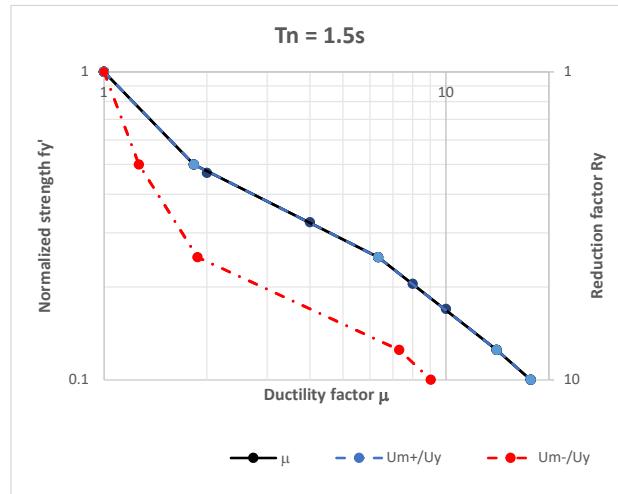
Figure D.7: Normalized strength vs ductility factor and reduction factor for $T_n$ = 1.5s and 1.75s under CLAYN1N1000 ground motion.

Figure D.8: Normalized strength vs ductility factor and reduction factor for $T_n$ = 2.0s and 2.5s under CLAYN1N1000 ground motion.

Figure D.9: Normalized strength vs ductility factor and reduction factor for $T_n$ = 3.0s and 4.0s under CLAYN1N1000 ground motion.

Figure D.10: Normalized strength vs ductility factor and reduction factor for $T_n$ = 5.0s and 10.0s under CLAYN1N1000 ground motion.
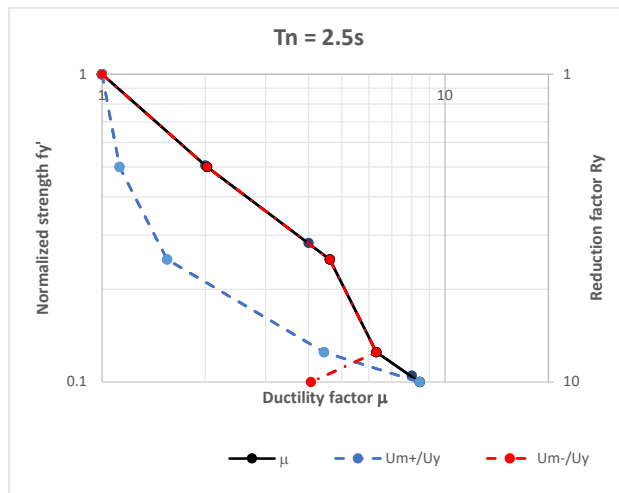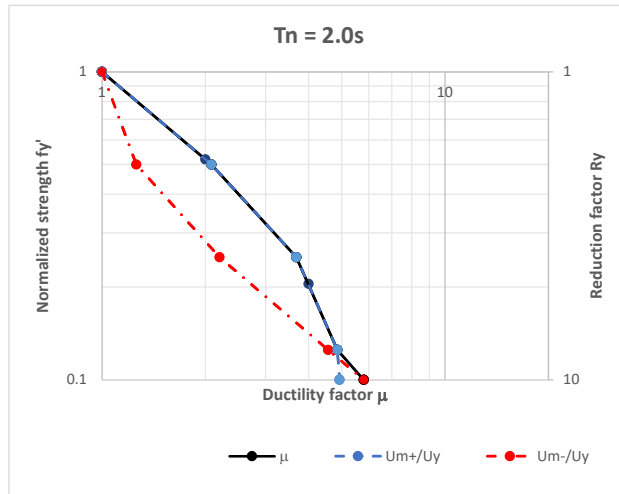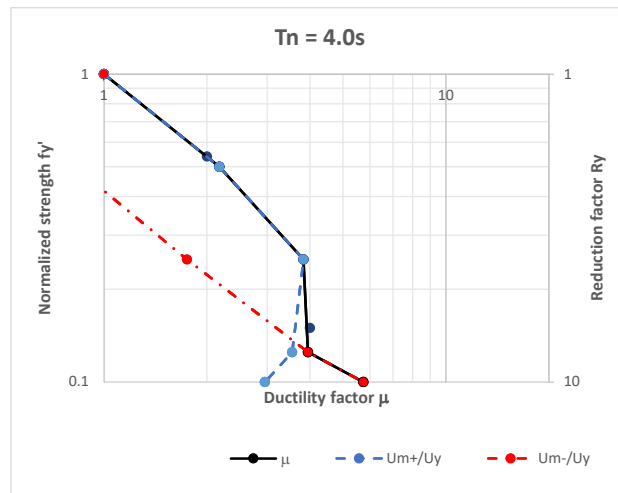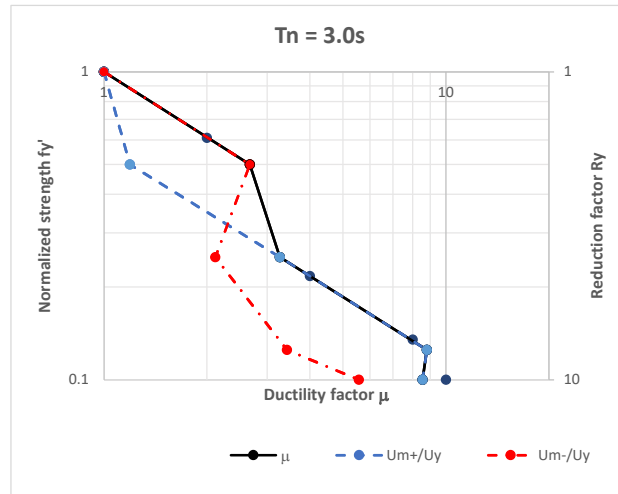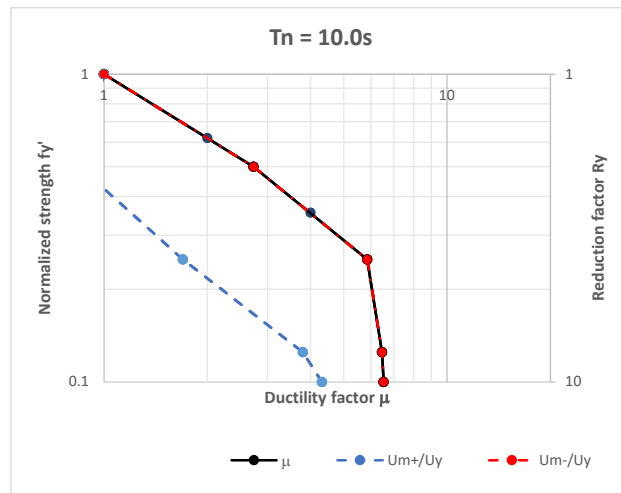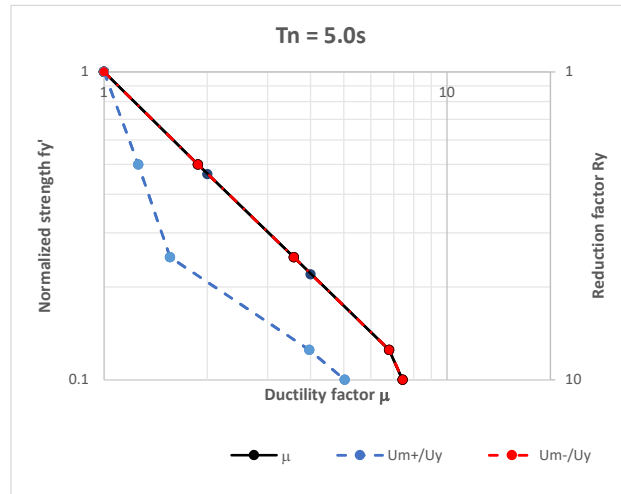
# LIST OF REFERENCES

Aviram, A., Mackie, K., & Stojadinovic, B. (2008). *Guidelines of Nonlinear Analysis of Bridge Structures in California* (tech. rep. August). Pacific Earthquake Engineering Research Center, University of Berkely. Berkeley, California.

Bolin, R., & Stanford, L. (2006). *The Northridge earthquake: Vulnerability and disaster*. https://doi.org/10.4324/9780203028070

Chopra, A. K. (2012). *DYNAMICS OF STRUCTURES Theory and Applications to Earthquake Engineering* (W. J. Hall, Ed.; Fourth Edi). Berkeley, California, Pearson.

CSI. (2017). *CSI analysis reference manual for SAP2000, ETAPS, SAFE, and CSIBridge*. Berkeley, California, Computer & Structures, Inc.

EERI. (1989). The Loma Prieta earthquake of October 17, 1989. *Earthquakes & Volcanoes (USGS)*, *21*(6), 216–237.

Fenves, G. L., & Ellery, M. (1998). *Behavior and failure analysis of a multiple-frame highway bridge in the 1994 Northridge earthquake* (tech. rep.). Pacific Earthquake Engineering Research Center, University of California. Berkeley, California.

Fung, G. G., Lebeau, E., Klein, J., Belverder, & Goldschmidt, A. (1971). *Field investigation of bridge damage in the San Fernando earthquake*. Sacramento, California, California Department of Transportation, bridge department, division of highways.

Ghotbi, A. R. (2014). Performance-based seismic assessment of skewed bridges with and without considering soil-foundation interaction effects for various site classes. *Earthquake Engineering and Engineering Vibration*, *13*(3), 357–373. https://doi.org/10.1007/s11803-014-0248-7

Haukaas, T., & Der Kiureghian, A. (2007). Methods and Object-Oriented Software for FE Reliability and Sensitivity Analysis with Application to a Bridge Structure. *Journal of Computing*

*in Civil Engineering*, *21*(3), 151–163. https://doi.org/10.1061/(ASCE)0887-3801(2007)21:
3(151)

Jeremić, B., Kunnath, S., & Xiong, F. (2004). Influence of soil-foundation-structure interaction
on seismic response of the I-880 viaduct. *Engineering Structures*, *26*(3), 391–402. https:
//doi.org/10.1016/j.engstruct.2003.10.011

Jurado, J.A., Hernadez, S., Nieto, F., & Mosquera, A. (2011). *Bridge aeroeslasticity, sensitivity
analysis and optimal desing*. Billerica, MA, USA, WIT Press.

Kappos, A. J., & Dimitrakopoulos, E. (2005). Analysis and assessment of a seismically isolated
bridge. *WIT Transactions on the Built Environment*, *81*, 625–635. https://doi.org/10.2495/
978-1-84564-672-1/13

Kawashima, K., Unjoh, S., Hoshikuma, J. I., & Kosa, K. (2011). Damage of bridges due to the
2010 Maule, Chile, earthquake. *Journal of Earthquake Engineering*, *15*(7), 1036–1068.
https://doi.org/10.1080/13632469.2011.575531

Khan, M. A. (2015). *Accelerated bridge construction, best practices and techniques*. Waltham,
MA, USA, Butterworth-Heinemann.

Kleiber, M., Antunez, H., Hien, T. D., & Kowalczyk, P. (1997). *Parameter sensitivity in nonlinear
mechanics. Theory and finite element computations*. New York, John Wiley & Sons, Inc.
https://doi.org/10.1016/s0997-7538(99)80031-x

Kunnath, S. K. (2007). *Application of the PEER PBEE methodology to the I-880 viaduct.* (tech.
rep.). Pacific Earthquake Engineering Research Center, University of California. Berkeley,
California.

Kwon, O. S., & Elnashai, A. S. (2008). Seismic analysis of meloland road overcrossing using mul-
tiplatform simulation software including SSI. *Journal of Structural Engineering*, *134*(4),
651–660. https://doi.org/10.1061/(ASCE)0733-9445(2008)134:4(651)

Lu, J., Elgamal, A., & Mackie, K. R. (2015). *Parametric Study of Ordinary Standard Bridges using OpenSees and CSiBridge* (tech. rep. No. 2). California Department of Transportation, University of California. La Jolla, California.

Mackie, K. R. (2008). Integrated Probabilistic Performance-Based Evaluation of Benchmark Reinforced Concrete Bridges. *Pacific Earthquake Engineering Research Center*, (PEER Report 2007/09).

Mackie, K. R., & Scott, M. H. (2019). Implementation of Nonlinear Elements for Seismic Response Analysis of Bridges. *Practice Periodical on Structural Design and Construction*, *24*(3), 1–14. https://doi.org/10.1061/(ASCE)SC.1943-5576.0000420

Mackie, K. R., Scott, M. H., Johnsohn, K., Al-Ramahee, M., & Steijlen, M. (2017). *Nonlinear Time History Analysis of Ordinary Standard Bridges* (tech. rep.). California Department of Transportation (Caltrans). Sacramento, California. https://rosap.ntl.bts.gov/view/dot/37382

Mackie, K. R., & Stojadinović, B. (2003). *Seismic demands for performance based design of bridges* (tech. rep. August). Pacific Earthquake Engineering Research Center, University of California. Berkeley, California.

Mackie, K. R., & Stojadinović, B. (2005). *Fragility basis for California highway overpass brige seismic decision making* (tech. rep. June). Pacific Earthquake Engineering Research Center, University of California. Berkeley, California.

Mander, J., Priestley, M., & Park, R. (1988). Theoretical stress-strain model for confined concrete. Journal of Structural Engineering. *Journal of Structural Engineering*, 114(8): 1804–1826.

Nielson, B. G., & DesRoches, R. (2007). Analytical seismic fragility curves for typical bridges in the central and southeastern United States. *Earthquake Spectra*, *23*(3), 615–633. https://doi.org/10.1193/1.2756815

NIST. (1996). *The January 17, 1995 Hyogoken-Nanbu (Kobe) earthquake. Performance of structures, lifelines, and fire protection systems. NIST SP 901* (tech. rep.). National Institute of Standards and Technology. Gaithersburg, MD.

Omrani, R., Mobasher, B., Liang, X., Gunay, S., Mosalam, K. M., Zareian, F., & Taciroglu, E. (2015). *Guidelines for Nonlinear Seismic Analysis of Ordinary Bridges: Version 2.0* (tech. rep. December). California Department of Transportation (Caltrans). Sacramento, California. https://doi.org/10.13140/RG.2.1.4946.6648

Pan, Y., Agrawal, A. K., Ghosn, M., & Alampalli, S. (2010). Seismic Fragility of Multispan Simply Supported Steel Highway Bridges in New York State. I: Bridge Modeling, Parametric Analysis, and Retrofit Design. *Journal of Bridge Engineering*, *15*(5), 448–461. https://doi.org/10.1061/(ASCE)BE.1943-5592.0000085

Pinto, P. E., & Franchin, P. (2010). Open Issues in the Seismic Design and Assessment of Bridges, In *Geotechnical, earthquake engineering in europe (vol. 17)*. Rome, Italy, Springer. https://doi.org/10.1007/978-90-481-9544-2_13

Priestly, N. M. J., Seible, F., & Calvi, G. M. (1996). *Seismic Design and Retrofit of Bridges*. New York, John Wiley & Sons, Inc.

Sullivan, I., & Nielson, B. G. (2010). Sensitivity Analysis of Seismic Fragility Curves for Skewed Multi-Span Simply Supported Steel Girder Bridges, In *Structures congress 2010*, Reston, VA, American Society of Civil Engineers. https://doi.org/10.1061/41131(370)19

Zhang, Y., Acero, G., Conte, J., Yang, Z., & Elgamal, A. (2004). Seismic Reliability Assessment of a Bridge Ground System. *13th World Conference on Earthquake Engineering*, Paper No. 2978.

Zhao, Q., Vasheghani-Farahani, R., & Burdette, E. G. (2011). Seismic Analysis of Integral Abutment Bridges Including Soil-Structure Interaction, In *Structures congress 2011*, Reston, VA, American Society of Civil Engineers. https://doi.org/10.1061/41171(401)26

Zona, A., Barbato, M., & Conte, J. P. (2006). Finite element response sensitivity analysis of continuous steel-concrete composite girders. *Steel and Composite Structures*, *6*(3), 183–202. https://doi.org/10.12989/scs.2006.6.3.183